

DESIGN DATA BOOK

FOR

PHASE A/B STUDY FOR A PRESSURE FED ENGINE
ON A REUSABLE SPACE SHUTTLE BOOSTER
NASA-MSFC REPORT SE-019-010-2H

Prepared For

NATIONAL AERONAUTICS AND SPACE ADMINISTRATION

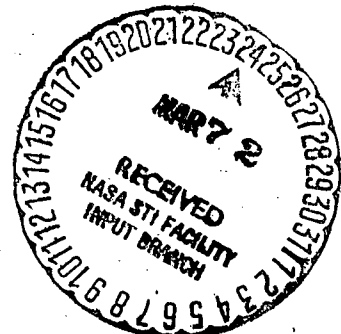
George C. Marshall Space Flight Center

Huntsville, Alabama 35812

Contract NAS 8-28217
DPD 303; DR SE-01

9755-72-3
15 March 1972

CR-123639



AEROJET LIQUID ROCKET COMPANY

A DIVISION OF AEROJET-GENERAL

SACRAMENTO, CALIFORNIA

N72-25701

Unclas
21H G3/28 15428

(NASA-CR-123639) DESIGN DATA BOOK PHASE
A/B STUDY FOR A PRESSURE FED ENGINE ON A
REUSABLE SPACE SHUTTLE BOOSTER (Aerojet
Liquid Rocket Co.) 15 Mar. 1972 63 p CSCI

Report SE-019-010-2H

FOREWORD

This report provides preliminary engineering definition information for a liquid pressure-fed reusable booster engine. Enclosed are: Volume I, Program and Baseline Data; Volume II, Critical Trade Studies Summary and Volume III, Methodology.

These data are presented in accordance with the Data Procurement Document (DPD) No. 303, dated October 1971, which specifies the Data Requirement (DR) No. SE-01 for Contract NAS 8-28217.

TABLE OF CONTENTS

	<u>Page</u>
A. <u>INTRODUCTION</u>	1
B. <u>SUMMARY</u>	1
C. <u>TECHNICAL DISCUSSION</u>	4
Volume I - Program and System Baseline	4
Volume II - Critical Trade Studies Summary	7
Volume III - Methodology	12

TABLE LIST

<u>Table No.</u>	<u>Title</u>	<u>Page</u>
I	Acoustic Modal Frequencies	25
II	Thermal Analysis Nomenclature	37
III	Regenerative Coolant Flow Schemes - Advantages and Disadvantages	40

FIGURE LIST

<u>Figure No.</u>	<u>Title</u>
1	Baseline Program Schedule
2	Baseline Development Program Schedule
3	Baseline Development Test Program
4	Baseline Hardware Demand
5	Baseline Deliverable Engine Hardware
6	NASA-MSFC Pressure-Fed Engine Need Dates
7	Space Shuttle Vehicle Flight Schedule
8	NASA Pressure-Fed Booster Engine Characteristics
9	Flow Schematic
10	Pressure-Fed Engine Design (2 pages)

FIGURE LIST (cont.)

<u>Figure No.</u>	<u>Title</u>
11	Summary of Key Design Parameters
12	Summary of Design Features (2 pages)
13	Modular Injector Design
14	Modular Injector Construction
15	Modular Combustor
16	Modular Injector/Thrust Chamber Interface
17	Regenerative Thrust Chamber
18	Tube Bundle Thermal Design (2 pages)
19	Thrust Chamber Tube Design Details
20	Gimbaling Characteristics
21	Pressure Schedule
22	Performance and Weight Summary
23	Performance Summary
24	Vehicle Exchange Ratios (1-19-72)
25	Vehicle Exchange Ratios (3-3-72)
26	Chamber Pressure Optimization
27	Specific Impulse vs MR for LOX/RP-1
28	Mixture Ratio Optimization
29	Chamber Length Optimization (Chrysler/MDAC)
30	Chamber Length Optimization (GDC, MMC and TBC)
31	Nozzle Separation Data
32	Nozzle Exit Pressure Variation with Area Ratio
33	Area Ratio for Nozzle Separation as a Function of Throttling Capability
34	Nozzle Area Ratio Impact on Gross Liftoff Weight
35	Nozzle Contour Length Optimization
36	Variation in Specific Impulse with Nozzle Area Ratio
37	Variation in Engine Weight with Nozzle Area Ratio

FIGURE LIST (cont.)

<u>Figure No.</u>	<u>Title</u>
38	Stage Diameter Variation with Nozzle Area Ratio
39	Chamber Pressure Drop due to Combustion
40	Variation in Inlet Pressure with Contraction Ratio
41	Engine Weight Variation with Contraction Ratio
42	Contraction Ratio Optimization
43	Propellant Line Velocity Effect on Vehicle Liftoff Weight
44	Propellant Line Velocity Optimization
45	Pressure-Fed Regenerative-Cooled Chamber Study
46	Hydraulic Load Influence on Engine Weight
47	Effect of Vehicle Recovery Impact on Engine and Actuator
48	Design Conditions Correlated with Vaporization Model
49	Performance Loss Evaluation
50	JANNAF Procedure
51	Sensitive Time Lag Characteristics
52	Pressure-Fed Engine (Stability) Relationship
53	Block Diagram of Low-Frequency Combustion Stability
54	Nyquist Diagram for Typical Engine with Feed System Resonances
55	Feed System Coupled Stability Gain Stabilizing Pressure Drops for LOX and RP-1
56	Equivalent Circuit for Engine/Feed System
57	RP-1 Burnout Characteristics
58	Soot Characteristics
59	Radiation Heat Transfer Effect

A. INTRODUCTION

Currently NASA-MSFC is investigating the design and program characteristics of using a pressure-fed propulsion system for the first-stage booster of the future Space Shuttle Vehicle. Contract NAS 8-28217 was issued to Aerojet Liquid Rocket Company (ALRC), on 24 November 1971, to investigate the design and program requirements of a pressure-fed engine to support this booster study.

As part of this study, ALRC is responsible for providing a Design Data Book in accordance with the Data Requirement (DR) Number SE-01 which is specified in the Data Procurement Document (DPD) Number 303, dated October 1971. Therefore, summary data for Program and System Baseline, Critical Trade Studies, and Methodology used during this study are provided herein. This report is issued at the completion of the contract in accordance with an agreement with the NASA-MSFC Engine Program Office.

B. SUMMARY

1. Program and System Baseline

The pressure-fed engine baseline development program is 54 months long. This includes the delivery of 28 engines to be used as follows: 7 ground test engines, 7 unmanned flight test engines, 7 first manned orbiting flight engines, and 7 dummy engines for a dynamic test vehicle. Production and delivery of 77 engines for 10 Space Shuttle booster vehicles would be completed by 1981. Total engine deliveries are, hence, 105 engines.

The engine system baseline features include: the use of oxygen and RP-1 propellants; a head-end gimbal using the Saturn 1C gimbal actuator which has an RP-1 hydraulic actuation source; articulating fuel and oxidizer lines to accommodate engine movement; two fuel and two oxidizer right-angle

B, 1, Program and System Baseline (cont.)

poppet valves which are identical in size and use RP-1 hydraulic actuation; a hypergolic ignition system using 85% TEB plus 15% TEA; a modular injector using 55 modules, each with a thrust of 21,820 lbf to provide a total thrust of 1.2M lb at a thrust chamber pressure of 250 psia, a nozzle area ratio of 5 and an engine mixture ratio of 2.4; and a two-pass RP-1 regenerative-cooled combustion chamber and nozzle.

2. Critical Trade Studies Summary

The initial Phase A level of the study contract was primarily involved with the selection of an engine concept based upon design analyses and trade studies. These trade studies included the consideration of cost, state of development, producibility, reliability and safety, and operational reusability. These considerations were evaluated on a relative basis for the candidate design concepts in addition to the design considerations of size, weight, and performance. The results of these trade studies were reported in the Phase A effort Final Report, Volume II - Technical, dated 18 January 1972. A general engine design concept was selected for further design definition in the Phase B level of the study.

The Phase B level of the study has provided a design optimization of the selected engine concept. Due to the strong influence of the vehicle design characteristics on engine design, vehicle exchange ratios were requested from each of the 5 vehicle contractors. Optimization of engine thrust chamber pressure, chamber length, mixture ratio, nozzle area ratio, nozzle contour length, chamber contraction ratio, injector thrust-per-element, chamber cooling design, line and valve sizes, and design approaches were then accomplished using the vehicle exchange ratios and engine influence data. Therefore, the resulting selected pressure-fed booster engine design results from both the current NASA requirements and the vehicle data provided to ALRC during the tradeoff analysis phase of this contract.

B, Summary (cont.)

3. Methodology

The analytical methods used for the critical thermal, performance and dynamic analyses studies are presented in Volume III of this report. The dynamic analyses includes high frequency and low frequency engine combustion stability as well as POGO.

C. TECHNICAL DISCUSSION

The following paragraphs discuss the specific data requested by the DR SE-01 of the NASA DPD 303.

VOLUME I - PROGRAM AND SYSTEM BASELINE

1. Program

The baseline program considered the development, production, flight, and refurbishment of a pressure-fed engine. The overall program is shown by Figure 1. The total development program is 54 months from authority to proceed (ATP) to completion of engine certification. During development 7 ground test engines (PTA), 7 unmanned flight test engines, 7 first manned orbiting flight (FMOF) engines, and 7 dynamic test vehicle dummy engines are delivered to NASA (Figure 2). A total of 363 development firing tests would be conducted which includes 50 PFC and FFC certification tests (Figure 3). Component tests would not only develop each major component but also establish manifold and line hydrodynamic transient and steady state characteristics, compatibility with the environmental requirements, life capabilities, etc. The hardware demand for development tests and deliveries is summarized in Figure 4.

A total of 77 production engines are delivered for 10 flight vehicles. The hardware demand, acceptance test, and delivery date (on the dock at ALRC) schedule are shown by Figure 5. Deliveries are in accordance with the NASA-MSFC need dates (Figure 6). A possible vehicle use schedule for the 445 flights from 1978 to 1988 is shown Figure 7. This schedule provides for a total of 40 flights per engine with the first engine deliveries being phased out of the shuttle program to allow the use of the latest improved hardware for the major missions.

C, Volume I - Program and System Baseline (cont.)

2. System Baseline

The engine design baseline selected for the NASA Pressure-Fed Space Shuttle Booster is shown by Figure 8. A simplified flow schematic of the engine is illustrated by Figure 9 and the major components are summarized in the layout drawings of Figure 10.

The design characteristics of the ALRC pressure-fed engine include: 2 LOX valves and 2 fuel valves all having a 13.5-in. inlet diameter to provide a cost-effective valve development program. Equal valve sizes also results in a lower ΔP on the fuel side which is a critical circuit because of the ΔP required by the regenerative-cooled combustion chamber and nozzle design; articulating propellant lines are used in conjunction with the head-end gimbal thrust vector control system. The existing NASA-developed Saturn 1C gimbal actuator which utilizes fuel (RP-1) as a hydraulic actuation source is used; the injector is a modular design featuring 55 modules with a thrust per module of 21,820 lb to provide a total engine thrust of 1.2M lb. This injector approach permits development of a state-of-the-art low thrust module which is then clustered in a common chamber to provide the total thrust required for the booster engine design. This approach reduces not only problems associated with combustion stability but also in hardware fabrication and performance projections; the ignition system is hypergolic utilizing 85% TEB and 15% TEA. This ignition system is operated by the fuel pressure provided to the engine which discharges the hypergol into each injector module to insure ignition of the nonhypergolic LOX/RP-1 propellants; the regenerative chamber, nozzle and modules are cooled in series during engine operation. A two-pass regenerative design is employed. Although this design approach requires a 40 lb pressure drop for cooling the thrust chamber, it allows reusing the thrust chamber for a cost-effective booster design. A cylindrical structure is provided between the injector and the nozzle to transmit thrust loads from the

C, Volume I, 2, System Baseline (cont.)

nozzle to the injector during engine operation and support the nozzle during splashdown prior to water retrieval.

A summary of the design parameters is presented for the pressure-fed engine on Figure 11. The key design features of the baseline engine design are presented on Figure 12 (2 pages). The modular injector design is illustrated by Figures 13 and 14. The injector design utilizes 55 modules. The module design includes an injector with a thrust of 21,820 lb at a chamber pressure of 250 psia and a thrust of 1,090 lb per element. An illustration of the module design is shown by Figure 15. The integration of the module into the total injector assembly is shown on Figure 16. This design allows oxidizer to be delivered to the injector without any common welds between the oxidizer and the fuel which returns from the regenerative chamber and nozzle coolant jacket and then regeneratively cools the module.

The regeneratively-cooled thrust chamber parameters are summarized by Figure 17 which includes a contraction ratio of 1.8, a chamber length of 70-in. and an equivalent bell nozzle contour length of 86%. The thermal design data for the 2-pass cooling jacket at both the rated chamber pressure of 250 psia and at a chamber pressure of 150 psia for a thrust modulation to 60% of maximum thrust is summarized by Figure 18. The details of the tube design for the regenerative combustion chamber are summarized by Figure 19. The candidate material for the tubes is Inconel 625.

The gimbal characteristics of the proposed engine are summarized by Figure 20. The gimbal angle is $\pm 6^\circ$ and the engine moment of inertia about the gimbal point is 43,150 slug/ft².

The engine pressure schedule, a performance and weight summary and a performance loss analysis are shown on Figures 21, 22 and 23, respectively.

C, Volume I, 2, System Baseline (cont.)

The ALRC performance analysis has been correlated to LOX/RP-1 Titan I experience and indicates that a sea-level specific impulse of 237.8 sec is possible with the proposed engine design. This performance value is 95% of theoretical and provides a 10.8 sec contingency over the NASA baseline nominal specific impulse value of 227.0 sec. Therefore, a potential performance growth is possible if the vehicle is designed around the NASA baseline requirements. It should be emphasized that the 95% of theory value is a predicted nominal development goal. The ALRC guaranteed minimum sea-level specific impulse is 93% of theoretical which results in the following performance values for a chamber pressure of 250 psia, area ratio of 5.0 and MR of 2.4.

	<u>Guaranteed Minimum</u>	<u>Predicted Nominal</u>
I_s , Sea-Level, sec	232.6	237.8
I_s , Vacuum, sec	283.9	289.8

C, Technical Discussion (cont.)

VOLUME II - CRITICAL TRADE STUDIES SUMMARY

During the Phase A/B pressure-fed engine study, trade studies were conducted to optimize engine design parameters which resulted in the engine design which is discussed in Volume I of this report. Due to the strong influence of vehicle design characteristics on engine design, vehicle exchange ratios were requested from each of the five vehicle contractors. These exchange ratios were used in conjunction with engine weight, performance, geometry and pressure drop requirement data to establish the optimum engine design.

The vehicle exchange ratios received during the tradeoff study phase of the contract are summarized by Figure 24. These vehicle exchange ratios have been revised by the vehicle contractors since the tradeoff studies were conducted and are shown by Figure 25. Comparative analysis have shown that the decisions made using the original exchange ratios are valid and the modified values do not affect the trends discussed herein. By comparing the values shown on Figures 24 and 25, it should be noted that 3 out of 5 sets of the current exchange ratio data are very nearly the same as the original GDC values. Hence, the GDC analyses would approximate current trends and the selected pressure-fed engine design best meets the NASA and vehicle requirements.

The tradeoffs conducted for the major engine design parameters are presented in the sections which follow.

1. Chamber Pressure Optimization

Evaluation of the changes in vehicle gross liftoff weight as a function of chamber pressure were investigated using GDC and TBC exchange ratio data (Figure 26). Data from other contractors was not available when

C, Volume II, 1, Chamber Pressure Optimization (cont.)

this tradeoff was performed. This analysis trades off the effects of engine performance, engine weight, tank weight and engine geometry effects upon the vehicle boattail. These data indicate that chamber pressures higher than 250 psia reduce the vehicle gross liftoff weight. A chamber pressure of approximately 275 psia is optimum but the reduction in GLOW compared to the 250 psia design point is insignificant.

2. Mixture Ratio Optimization

The variation in specific impulse and bulk density with mixture ratio were considered during the engine study. The selected mixture ratio of 2.4 provides the maximum specific impulse (Figure 27), however, increased bulk density can be achieved by increasing the mixture ratio. Vehicle data received during this study did not justify this mixture ratio increase which thus resulted in an optimum mixture of 2.4 (Figure 28).

3. Chamber Length Optimization

Tradeoffs between chamber length, engine weight and engine geometry effects upon the vehicle were conducted to establish an optimum combustion chamber length. These studies also considered the effect of thrust per element on system performance. The effects of chamber length on gross liftoff weight for values typical of the current Chrysler and MDAC exchange ratios are shown on Figure 29 and for values typical of the current GDC, MMC, and TBC exchange ratios on Figure 30. A chamber length of 70-in. was selected from this study. The data also shows that further reductions in GLOW can be obtained by reducing the thrust/element of the injector to 500. However, the thrust/element was not reduced below 1000 to keep the number of elements to be machined to a minimum and to provide larger diameter injector holes to facilitate cleaning.

C, Volume II - Critical Trade Studies Summary (cont.)

4. Nozzle Optimization

The nozzle design was evaluated for effects of separation at sea-level with the candidate chamber pressures. A comparison of empirical separation data with model data is shown by Figure 31 and nozzle exit pressure variation with area ratio is shown by Figure 32. The possible requirements for the engine to throttle to provide reduced thrust to maintain the maximum acceleration of 3G's and a maximum dynamic pressure of 650 lb per sq ft required that area ratio for nozzle separation as a function of throttling be considered (Figure 33). With the NASA requirements for 70% throttling capability this analysis indicated that a 5:1 area ratio was the maximum that could be utilized without separation occurring.

The effect of nozzle area ratio upon GLOW was investigated by trading off the impact of performance, envelope and weight for various nozzle designs (Figure 34). This figure shows that an area ratio of 6 is optimum although the curve is relatively flat between area ratios of 5 and 6. This data along with the separation criteria leads to the selection of an area ratio equal to 5.

The nozzle contour length effect upon GLOW is shown on Figure 35 for the original TBC and GDC exchange ratios. Based upon this figure, an 86% length bell nozzle was selected.

The variations of specific impulse with nozzle area ratio and contour length used in this study are shown on Figure 36 in conjunction with variations in engine weight with contour length and nozzle area ratio as shown on Figure 37. Geometry data effects as shown by the stage diameter variations with nozzle area ratio on Figure 38 were also included in the study.

C, Volume II - Critical Trade Studies Summary (cont.)

5. Combustion Chamber Contraction Ratio Optimization

Tradeoffs were conducted to evaluate the effects of combustion chamber contraction ratio (A_{Inj}/A_T), on pressure drop from the injector face to the plenum, injector and chamber weight, and tank weight. A theoretical curve showing the impact of contraction ratio on this pressure drop is presented on Figure 39. The current NASA F-1 engine value is also compared to the theoretical value. The effects of this combustion chamber contraction ratio on engine inlet pressures was then investigated (Figure 40) and the variation in engine weight (Figure 41) with contraction ratio was traded off against the variation in vehicle tank weight. The resulting tradeoffs conducted using TBC and GDC data indicated that the optimum contraction ratio was about 1.8 for the selected pressure-fed engine design (Figure 42). The figure shows that the variation in GLOW with contraction ratio is minor and the contraction ratio selection is dictated by pressure drop limitations for a 380 psia engine inlet pressure and physical design constraints.

6. Propellant Line Velocity Optimization

The effect of the engine line velocities upon the line and valve pressure drops and attendant variations in required vehicle tank pressures were traded-off against the line and valve wet weight variations. Figure 43 shows the variation of GLOW with propellant velocity for both the fuel and oxidizer. This figure shows that a propellant velocity of approximately 22 ft/sec is optimum for each circuit which results in different valve and line sizes.

Consideration of utilizing the same size oxidizer and fuel valves to reduce fabrication and development costs was also evaluated. Figure 44 shows that this results in an optimum LOX velocity of 25 ft/sec which

C, Volume II, 6, Propellant Line Velocity Optimization (cont.)

corresponds to a fuel velocity of 15 ft/sec. Although the common size criteria results in an engine wet weight penalty of approximately 900 lb, the minor increase in GLOW was considered acceptable to obtain commonality benefits.

The corresponding pressure drops resulting from this tradeoff are a line ΔP of 10 psi in the oxidizer circuit and 3 psi in the fuel circuit and a valve ΔP of 6 psi in the oxidizer circuit and 3 psi in the fuel circuit.

7. Cooling Tradeoffs

The regenerative-cooled combustion chamber selected for the pressure-fed engine design was evaluated for optimum cooling fabrication and ΔP characteristics. The analysis indicated that a coolant pressure drop of 40 psi was obtainable with a chamber design utilizing 230 tubes. This results in a bulk temperature rise of approximately 90°F (Figure 45).

8. Water Impact Considerations

As a result of the pressure-fed booster being water-recovered and impacting in the ocean at approximately 150 ft/sec, an analysis was conducted to investigate the effects of splashdown hydraulic loads on engine weight. This analysis considered the structural characteristics of the engine required to withstand impact loads for various boattail configurations. The effect of the impact loads on the engine weight is shown on Figure 46. The "% Engine Bell Protection" parameter on this figure refers to the axial length of the nozzle, measured from the throat, that is protected by the vehicle boattail.

The effect of the water impact loads upon the gimbals actuator were also considered. Figure 47 shows that the actuator can withstand an impact velocity of 150 ft/sec without modification and porting the actuator increases its impact capability to 200 ft/sec.

C, Technical Discussion (cont.)

VOLUME III - METHODOLOGY

Analytical methods used in the pressure-fed engine study are summarized in this volume for performance, thermal, and dynamic analysis. Existing ALRC computer programs were utilized to provide design data in a timely and cost-effective manner.

1. Performance

a. Delivered Performance

In order to meet the program objectives of a reliable high performance engine design, the analytical models used to predict performance are of primary importance. The performance evaluation techniques which are proposed have been successfully applied to many ALRC engine programs, including TRANSTAGE, APOLLO, and TITAN-GEMINI-624A. The model has been used as an analysis tool to define areas of excessive performance loss and as a design tool to correct the deficiency. These techniques, when applied to the proposed engine design, will ensure a high degree of confidence in the predicted performance values. Propellant combinations and injector design configurations correlated with the performance model are shown on Figure 44.

The performance model is the methodology recommended by the ICRPG Performance Standardization Working Group⁽¹⁾ modified to include performance loss interactions based upon liquid propellant vaporization theory.⁽²⁾ Vaporization-limited combustion properties are used to calculate those losses resulting from incomplete energy release, finite-rate limited gas expansion, and boundary layer shear drag and heat transfer. This modified program is termed the "Vaporization Interaction Performance Model".

(1) Pieper, J. L., ICRPG Liquid Propellant Thrust Chamber Performance Evaluation Manual, CPIA No. 178, September 1968

(2) Kors, D. L., and Bassham, L. B., and Walker, R. E., A Liquid Rocket Performance Model Based on Vaporization Interactions, AIAA 5th Propulsion Joint Specialist Conference, 9-13 June 1969

C, Volume III, 1, Performance (cont.)

The technique used for evaluation and prediction of performance considers the one-dimensional equilibrium (ODE) flow conditions to be the base case. As seen in the following equation, all performance losses are subtracted from this base:

$$I_{sp}(\text{delivered}) = I_{sp}(\text{ODE}) - I_{sp} \text{ losses} \quad \text{Eq. (1)}$$

One-dimensional equilibrium performance is evaluated using AGC computer program No. FD0068. This documented program computes one-dimensional flow in chemical equilibrium and is the basis for all % I_{sp} and % c^* quotations.

The losses which are considered during performance analysis of the engine are shown schematically on Figure 49 and are described below along with the basic relationships that incorporate the vaporized propellant parameters into each performance loss definition. Each loss is defined independently from the other performance losses to more clearly show how the vaporized propellant parameters influence the loss analysis. The loss derivations are developed without reference to any particular evaluation program; however, both the ICRPG Standard and Simplified Reference Computer Programs can be utilized with the final derived performance loss formulations. A list of abbreviations and symbols for the performance model is included as the last page in this section.

For the PFE study the engine designs are based on a sea level thrust. Therefore, the sea level specific impulse is an output. The performance computer model bases performance on the vacuum conditions and as a final step conversion to sea level performance is made, as shown on Figure 50. The computer model iterates on weight flow rate, engine geometry, and the performance losses to obtain a sea level thrust consistent with the required value. The individual losses considered in the performance model are described in the following paragraphs.

C, Volume III, 1, Performance (cont.)

(1) The Energy Release Loss (ERL)

This loss accounts for the performance reduction as a result of incomplete vaporization, mixing, and chemical reaction. ERL is evaluated by determining the mass defect caused by unvaporized propellant and the effect of the vaporized mixture ratio upon the thermochemical performance output. Using one-dimensional equilibrium (ODE) conditions as the baseline or maximum achievable performance, the energy release loss at any nozzle expansion ratio is found by subtracting the product of the total percent mass of propellant vaporization and the ODE specific impulse at the vaporized mixture ratio from the ODE specific impulse at the liquid propellant mixture ratio. That is, in ODE notation;

$$\text{ERL} = I_{\text{sp ODE}}(O/F) - I_{\text{sp ODE}}(O/F)_v \frac{\dot{m}_v}{\dot{m}_T} \quad \text{Eq. (2)}$$

For an engine with several "stream tubes" of different mixture ratios or atomization/vaporization characteristics, this process is used for each stream tube and the results are mass flow rate weight summed to give the total loss. Therefore, Equation (2) can be generalized to the following notation:

$$\text{ERL} = \sum_i^n \left[I_{\text{sp ODE}}(O/F)_i \dot{m}_i - I_{\text{sp ODE}}(O/F)_{vi} \dot{m}_{vi} \right] \frac{1}{\dot{m}_T} \quad \text{Eq. (3)}$$

ERL is evaluated using Priem's vaporization model (3) modified to account for ALRC test data correlations.

(2) The Mixture Ratio Maldistribution Loss (MRDL)

This loss accounts for the performance degradation attributable to non-homogeneous combustion products on a macroscopic scale.

(3) Priem, R. J. and Heidmann, M. F., Propellant Vaporization as a Design Criterion for Rocket Engine Combustion Chambers, NASA TR-R-67, 1960

C, Volume III, 1, Performance (cont.)

The loss can be intentionally induced, as with barrier cooling or may be unintentional as a result of non-uniform injector hydraulics. The mixture ratio maldistribution loss is calculated using a stream tube technique (4). The mass flow rate weighted sum of the ODE specific impulse for the individual stream tubes at the stream tube mixture ratios are subtracted from the ODE specific impulse at the over-all mixture ratio to define this loss. Again, using ODE as the reference condition, the MRDL is defined by the following relationship:

$$\text{MRDL} = I_{\text{sp ODE}} (O/F)_{O/A} - \sum_{i=1}^n (I_{\text{sp ODE}} (O/F)_i \cdot \frac{\dot{m}_i}{\dot{m}_T}) \quad \text{Eq. (4)}$$

where the "ith" stream tube refers to discrete zones of flow whose mixture ratios are calculable by known injector hydraulic parameters. For the Phase B PFE study this loss was estimated from data on a similar engine to be 1% of the sea level specific impulse.

(3) Coolant Performance Loss Model (FCL)

The coolant performance loss model described herein accounts for the performance penalty associated with the resultant nonuniform propellant distribution and the thermal energy transport from the high temperature core to the low temperature boundary flow. The basic assumptions are summarized as:

1. Film bulk temperature is obtained from existing heat transfer models.
2. Energy is assumed to be exchanged upstream of throat.
3. Energy is extracted uniformly from core.

(4) Pieper, J. L., Dean, L. E., Valentine, R. S., "Mixture Ratio Distribution - Its Impact on Rocket Thrust Chamber Performance, "Journal of Spacecraft and Rockets, Vol. 4, No. 6, June 1967

C, Volume III, 1, Performance (cont.)

$$\begin{aligned}
 4. \quad \Delta h_c &= \int_{T_{IN}}^{T_B} C_p (dT_c) \\
 5. \quad (\dot{m} \Delta h)_{core} &= (\dot{m} \Delta h_c)_{coolant} \\
 6. \quad I_{sp_{del}} &= f \left\{ \frac{\dot{m}_{core} (h - \Delta h)_{core}^{1/2} + \dot{m}_c (h + \Delta h)_{coolant}^{1/2}}{\dot{m}_T} \right\}
 \end{aligned}$$

where:

 Δh = enthalpy C_p = specific heat at constant pressure T_B = bulk film coolant temperature T_{IN} = inlet film coolant temperature

Computationally, the heat is removed from the core by reducing the propellant heat of formation in the ODK or TDK computer program by an amount which exactly compensates for the total enthalpy gained in the coolant stream tube when it is heated from its inlet temperature to the final bulk coolant temperature. Both stream tubes - the heated coolant and reduced enthalpy core are then expanded to the nozzle exit conditions using ODK/TKD computer program for the core and Thermocal for the film coolant. The coolant performance decrement $\Delta I_{sp_{coolant}}$ is then computed by using the following relationship:

$$\Delta I_{sp_{coolant}} = I_{sp_{O/F_{overall}}} - \left[\frac{\dot{m}_{core} I_{sp_{core O/F, h}} + \dot{m}_{coolant} I_{sp, hc}}{\dot{m}_T} \right]$$

The model assumes no species transport between the core and coolant stream tubes, which may limit its general application. However, extensive correlation of this model with experimental test data has indicated its basic validity for the type of thrust chamber designs proposed for this program. The other assumption requiring justification is the selection of the

C, Volume III, 1, Performance (cont.)

bulk temperature of the coolant flow after thermal transport from the core. The thermal models discussed elsewhere are used to estimate the bulk coolant temperature. The accuracy of this prediction is not critical since the sensitivity of the coolant performance loss to the assumed amount of thermal transport is quite low as shown in Figure 20.

In conclusion, it can be stated that the proposed coolant model is simple in concept and computational procedure, and correlates adequately the available film coolant performance data for design and operating variable that are presentative of the proposed thrust chamber.

(4) The Kinetic Loss (KL)

This loss accounts for performance reduction from the equilibrium condition resulting from finite time dependent chemical recombination of the species present in the exhaust gas during the nozzle expansion process. The kinetic loss is defined by considering the mass flow rate-summed ODE performance at the stream tube mixture ratio as the reference point. The one-dimensional kinetic (ODK) performance⁽⁵⁾ evaluated at the vaporized mixture ratio for each of the individual stream tubes, and then summed over the "n" stream tubes, is subtracted from the ODE performance to obtain the kinetic loss. Again, it is emphasized that both the kinetic and ODE performance must be evaluated at the vaporized mixture ratio and mass flow rate rather than at the liquid propellant mixture ratio because the vaporized parameters represent the actual composition of the exhaust gases.

Equation (5) is a mathematic representation of this definition of kinetic loss.

(5) Frey, H. M., et al, ICRPG One-Dimensional Kinetic Reference Program, Dynamic Science, July 1968.

C, Volume III, 1, Performance (cont.)

$$KL = \sum_i^n \left[I_{sp \text{ ODE } (O/F)_{vi}} - I_{sp \text{ ODK } (O/F)_{vi}} \right] \frac{\dot{m}_{vi}}{\dot{m}_T} \quad \text{Eq. (5)}$$

For the design - configuration and operating levels surveyed for the booster study this loss should be small, less than 0.2% of the ODE specific impulse.

(5) The Boundary Layer Loss (BLL)

This loss accounts for the degradation of performance from the shear drag and heat loss at the boundary of the thrust chamber. The boundary layer loss is evaluated using the vaporized performance combustion properties in the outer stream tube. Again, the vaporized composition is considered rather than the composition based upon over-all propellant flow rates. Using a suitable evaluation procedure⁽⁶⁾, ΔF_{BLL} is calculated and divided by the total propellant flow rate to determine the boundary layer loss.

$$BLL = \frac{(\Delta F_{BLL}) (O/F)_v}{\dot{m}_T} \quad \text{Eq. (6)}$$

(6) The Nozzle Divergence Loss (DL)

This loss accounts for the decrease in thrust attributable to non-axially directed momentum at the nozzle exit and the non-planar sonic surface. In most cases, this loss is not significantly affected by the variance of the vaporized mixture ratio from the over-all liquid flow mixture ratio. Therefore, no vaporized mixture ratio notation is included in the definition of the divergence loss. This performance loss, when evaluated by

(6) Weingold, H. D., The ICRPG Turbulent Boundary Layer Reference Program, Pratt and Whitney Aircraft, July 1968.

C, Volume III, 1, Performance (cont.)

itself, usually can be expressed in terms of a divergence efficiency, η_{DIV} , which modifies the delivered or actual thrust.

$$DL = \frac{I_{sp_{del}}}{\eta_{DIV}} - I_{sp_{del}} = I_{sp_{del}} \left[\frac{1 - \eta_{DIV}}{\eta_{DIV}} \right] \quad \text{Eq. (7)}$$

The analytically predicted specific impulse of a vaporization-limited rocket engine can be evaluated by subtracting the above defined performance losses from the ODE theoretical condition.

$$\begin{aligned} I_{sp_{del}} &= I_{sp_{ODE}} - \Sigma I_{sp} \text{ losses} \\ &= I_{sp_{ODE}} - (ERL + MRDL + KL + BLL + DL) \end{aligned} \quad \text{Eq. (8)}$$

Substituting Equations (2) through (7) for the five performance loss terms of Equation (8) and cancelling like terms, the following final formulation is obtained.

$$I_{sp_{del}} = \sum_i^n \left[I_{sp_{ODK(O/F)_{vi}}} \cdot \frac{\dot{m}_{vi}}{\dot{m}_T} \right] \eta_{DIV} - \frac{\Delta F_{BLL}}{\dot{m}_T} \quad \text{Eq. (9)}$$

A more detailed description of the performance model and its component losses, along with a discussion of the application of the model to other engine programs, is available in the existing literature.^{(7) (8)}

(7) Pieper, J. L., op. cit.

(8) Kors, Bassham, Walker, op. cit.

C, Volume III, 1, Performance (cont.)

LIST OF ABBREVIATIONS AND SYMBOLS FOR THE PERFORMANCE MODEL

BLL	=	Boundary layer loss, lbf-sec/lbm
DL	=	Divergence loss, lbf-sec/lbm
ERL	=	Energy release loss, lbf-sec/lbm
KL	=	Kinetic loss, lbf-sec/lbm
I_{sp}	=	Vacuum specific impulse, lbf-sec/lbm
\dot{m}	=	Mass flow rate, lbm/sec
MRDL	=	Mixture ratio maldistribution loss, lbf-sec/lbm
O/F	=	Mixture ratio
ΔF_{BLL}	=	Boundary layer thrust decrement, lbf
ϵ	=	Area ratio
η_{DIV}	=	Nozzle curvature-divergence efficiency
η	=	Enthalpy

Subscripts

del	=	delivered value
i	=	of "ith" stream tube
n	=	number of stream tubes
O/A	=	overall engine property
ODE	=	one dimensional equilibrium
ODK	=	one dimensional kinetic
T	=	total engine property
v	=	vaporized property
c	=	coolant property

C, Volume III - Methodology (cont.)

2. Engine Combustion Stability

Stability considerations for the pressure-fed engine system involve the evaluation of high frequency combustion stability, feed system coupled stability and the POGO coupling of the vehicle structural dynamics with the combustion process. Each of these three stability modes have been addressed in the preliminary design of the engine and in the evaluation of the vehicle feed system and structural dynamics.

The unique engine design provides a degree of conservatism in the suppression of high frequency combustion oscillations through the modular injector approach. The high frequency combustion stability modes are amenable to suppression using the modular design with absorbing cavities forward of the energy generation zone providing suppression in addition to the damping provided by the module "pocket" walls and the detuning of module frequencies from the injector pattern sensitive frequencies.

For the feed system coupled mode, two design features make solution of such potential instabilities a practical engineering problem. The first feature uses the basic flexibility of the injector manifold system which feeds the modules to allow tuning of the system to reject unwanted frequency response. The second feature uses the injector inertance to produce a fluid dynamic filter which attenuates energy transmission between the injector and the feed system. This blocking filter would be tuned at 50 Hz to be effective below the lowest possible chugging frequency and its effectiveness would increase with higher frequencies.

The analyses performed to evaluate the POGO mode of oscillation indicates that vehicle structure and engine oscillations do not exactly coincide at the same frequency. However, an analysis was performed which used representative PFE vehicle data and a mathematical vehicle representation which was artificially forced unstable and indicated that effective suppression of this

C, 2, Engine Combustion Stability (cont.)

induced instability may be achieved by terminating the oxidizer lines at the engine inlets with accumulators equivalent to 6 ft³ of Helium.

The following sections identify the methodology used in these analyses.

a. High Frequency

(1) Stability Evaluation

The Crocco sensitive time-lag model was used to evaluate engine combustion stability. The procedure for evaluating engine combustion stability involves three basic steps: (1) determining the injector response curve, (2) determination of the chamber response based on the type of chamber, and (3) determination of the acoustic modes of the chamber in the frequency range where the injector shows a high response.

The injector response curve is defined by the relationship

$$N_{\text{injector}} = n_o \left(1 - \cos \pi \frac{f}{f_s} \right)$$

f_s is the sensitive frequency

n_o is the injector response magnitude parameter

f is the frequency of interest

The assumed value for n_o is 0.60 based upon experimental information.

The value of f_s is dependent upon the type of injector orifice element and the operating conditions. Empirical relationships for the sensitive frequency is given by the data plotted in Figure 51 where

M_c is the chamber mach number at the injector face

P_c is the chamber pressure in psia

$\tau = \frac{1}{2f_s}$ is the sensitive time lag in milliseconds

C, Volume III, 2, Engine Combustion Stability (cont.)

The ALRC baseline configuration has $P_c = 250$ psia, chamber contraction ratio = 1.8, and mean orifice size $d_m = 0.21$ in. As a result, $M_c = 0.329$ and $\tau(M_c P_c)^{1/3} \approx 1.8$, which yields the sensitive frequency: $f_s = 1210$ Hz.

The injector response curve corresponding to $f_s = 1210$ Hz is shown in Figure 52.

The term N_{chamber} defines the minimum response required to establish an acoustic instability within the chamber. For cylindrical chambers the values of N_{chamber} range from 0.35 to 0.75 where the largest values are associated with large mach numbers (i.e., $M_c \geq 0.3$). Since $M_c = 0.329$ for the ALRC baseline configuration, a value of $N_{\text{chamber}} = 0.70$ was chosen for this study.

The combined injector and chamber response curves are shown in Figure 52 where the upper shaded region indicates the frequency range for a possible high frequency instability.

Chamber modal frequencies represent the various resonant frequencies which can exist in a particular chamber in the transverse and longitudinal directions.

For longitudinal modes, the characteristic length is the distance from the injector face to the nozzle throat. For a cylindrical chamber

$$l_{\text{eff}} = l_c + \frac{2}{3} l_n$$

C, Volume III, 2, Engine Combustion Stability (cont.)

where subscripts c and n refer to the cylindrical and converging conical nozzle portions, respectively.

The ALRC baseline configuration has

$$\begin{aligned} \ell_{\text{eff}} &= (40 + \frac{2}{3} \times 30) \text{ in.} \\ &= 60 \text{ in.} \end{aligned}$$

The nth longitudinal modal frequency is determined from the relationship:

$$f_L = \frac{n}{2} \frac{12c}{\ell_{\text{eff}}}, \quad n = 1, 2, 3, \dots$$

where c is the velocity of sound, f_{ps}

For the transverse modes, the characteristic length is the chamber diameter. The transverse modal frequencies are determined from the relationship:

$$f_T = \frac{c}{2\pi r} S_{\nu n}$$

where c is the velocity of sound, r is the radius, and $S_{\nu n}$ is the argument of a Bessel function. Separate Bessel functions are required for determining the frequencies of combined radial and tangential modes. The frequencies for combined longitudinal and transverse modes are the vectorial sum of the individual modal frequencies.

A listing of the acoustic modal frequencies for the ALRC baseline configuration is contained in Table I and is based upon the chamber radius of 46 in. and a velocity of sound, $c = 3600 f_{ps}$.

TABLE I

ACOUSTIC MODAL FREQUENCIES

<u>Acoustic Modes</u>	<u>Modal Frequencies (Hz)</u>
Longitudinal	
1	360
2	720
3	1,080
4	1,440
Tangential	
1	276
2	457
3	630
4	795
5	960
6	1,122
7	1,286
8	1,450
Radial	
1	572
2	1,050
3	1,520
Combined Tangential-Radial	
1T-1R	799
1T-2R	1,276
1T-3R	1,752
2T-1R	1,003
2T-2R	1,490
2T-3R	1,970
3T-1R	1,200
3R-2R	1,700
3T-3R	2,180
Combined Tangential-Longitudinal	
1T-1L	455

C, Volume III, 2, Engine Combustion Stability (cont.)

The acoustic modes whose frequencies correspond to the unstable zone frequencies are shown in Figure 52. Of prime significance are the second radial and sixth tangential modes. Note that the longitudinal modes have been ignored since they tend to be highly damped by the nozzle losses and the distribution of combustion along the chamber axis.

An additional consideration that is important are the maximum dimensions for which the first tangential and first radial modes are neutrally stable. Referring to the response curve of Figure 52, this corresponds to determining the radial dimensions which yield a modal frequency of 1750 Hz where:

$$r = \frac{c}{2\pi f} S$$

For the first tangential mode, $r_{1T} = 7.2$ inches.

For the first radial modes, $r_{1R} = 15$ inches.

(2) Modular Chamber

To achieve stability using a modular chamber design requires that the sensitive frequency, f_s , be sufficiently lower than the chamber acoustic modes. Calculations previously discussed at the end of the Stability Evaluation section indicate that a modular chamber should have a radial dimension no greater than 7.2 in. to prevent the occurrence of a first tangential mode of instability.

b. Feed System Coupled (Low Frequency)

(1) General Stability Model

Feed system coupled combustion instability is characteristically caused by the closed-loop dynamic interaction of the combustion

C, Volume III, 2, Engine Combustion Stability (cont.)

process and propellant feed system as shown in Figure 53. The forward loop and the feedback loop dynamics are associated with the combustion process and the feed system dynamics, respectively.

The open loop transfer function $G(\omega)$ of this system is given by the equation:

$$G(\omega) = Z_c(\omega) \frac{K_f}{Z_{ff}(\omega)} + \frac{K_o}{Z_{fo}(\omega)}$$

$Z_c(\omega)$ = combustion process impedance

$Z_{ff}(\omega)$ = fuel feed system impedance

$Z_{fo}(\omega)$ = oxidizer feed system impedance

K_f = fuel mixture ratio weighting factor

K_o = oxidizer mixture ratio weighting factor

ω = radian frequency

The combustion impedance is given by the expression

$$Z_c(\omega) = \frac{c^*}{A_t g} \frac{e^{-j\omega t_1}}{1 + j\omega t_2}$$

c^* = characteristic exhaust velocity

A_t = throat area

t_1 = injection-combustion transport delay

t_2 = chamber residence time

g = gravitational constant

C, Volume III, 2, Engine Combustion Stability (cont.)

K_o and K_f are constant weighting factors which account for mixture ratio perturbations:

$$K_f = \frac{A_t g}{c^*} \frac{\frac{\partial \bar{P}_c}{\partial \bar{W}_f}}{\bar{W}_f} = 1 - \frac{\bar{r}(\bar{r}+1)}{c^*} \frac{\partial c^*}{\partial \bar{r}}$$

$$K_o = \frac{A_t g}{c^*} \frac{\frac{\partial \bar{P}_c}{\partial \bar{W}_o}}{\bar{W}_o} = 1 + \frac{(\bar{r}+1)}{c^*} \frac{\partial c^*}{\partial \bar{r}}$$

where

\bar{r} = is the steady-state mixture ratio

$\frac{\partial c^*}{\partial \bar{r}}$ = is the slope of the c^* vs \bar{r} curve

System stability can be evaluated analytically by use of the foregoing math model. Specifically, the open loop gain and phase can be computed as a function of frequency and plotted in the complex plane as shown in Figure 54. Stability is then determined by the use of the Nyquist stability criterion.

(2) Gain Stabilizing Criterion

When applying the Nyquist stability criterion, it is noted that if the magnitude of the open loop transfer function, $|G(\omega)|$, is less than unity at a frequency corresponding to a 180° phase shift, then the system is said to be gain stabilized. Hence, a gain stabilizing criterion may be expressed by:

$$|G(\omega)| < 1$$

C, Volume III, 2, Engine Combustion Stability (cont.)

This equation can be rewritten in terms of the system parameters where:

$$K_f \left| \frac{Z_c}{Z_{ff}} \right|_{\min}^{\max} + K_o \left| \frac{Z_c}{Z_{fo}} \right|_{\min}^{\max} < 1$$

This equation is based on the assumption that the minimum feed system impedances occur simultaneously at the same frequency. This assumption is quite conservative since the destabilizing minimum values of impedance occur at the acoustic mode resonant frequencies of each feed system and these resonant frequencies are seldom coincident.

The minimum value of the feed system impedances is governed by the injector resistances, R_j , as defined by the following relations

$$|Z_{ff}|_{\min} = R_{fj} = \frac{2 \overline{\Delta P}_{fj}}{\overline{W}_f}$$

$$|Z_{fo}|_{\min} = R_{oj} = \frac{2 \overline{\Delta P}_{oj}}{\overline{W}_o}$$

$$\overline{\Delta P}_j = \text{steady state injector pressure drop}$$

$$\overline{W}_f = \text{steady state fuel weight flow}$$

$$\overline{W}_o = \text{steady state oxidizer weight flow}$$

The maximum value of Z_c is given by

$$|Z_c|_{\max} = \frac{c^*}{A_t g} = \frac{P_c}{\overline{W}_t}$$

$$\overline{P}_c = \text{steady state chamber pressure}$$

$$\overline{W}_t = \text{total weight flow}$$

C, Volume III, 2, Engine Combustion Stability (cont.)

Combining equations yields the following form of the conservative stability criterion:

$$1 - \frac{\bar{r}(\bar{r}+1)}{c^*} \frac{\partial c^*}{\partial \bar{r}} \frac{\bar{P}_c}{2 \Delta \bar{P}_{fj}} \frac{\bar{W}_f}{\bar{W}_t} + 1 + \frac{(\bar{r}+1)}{c^*} \frac{\partial c^*}{\partial \bar{r}} \frac{\bar{P}_c}{2 \Delta \bar{P}_{oj}} \frac{\bar{W}_o}{\bar{W}_t} < 1$$

At the stability boundary corresponding to neutral stability, the left hand side of the equation representing the conservative stability criterion is equal to unity. This equation can then be rearranged to yield:

$$\frac{\bar{P}_{jf}}{\bar{P}_c} = \frac{K_f}{2(\bar{r}+1)} \left(1 + \frac{K_o \bar{r}}{K_f} \frac{\Delta \bar{P}_{jf}}{\Delta \bar{P}_{jo}} \right)$$

Since c^* and $\partial c^*/\partial \bar{r}$ do not vary significantly for the range of P_c values under consideration, the foregoing equation can be used to generate a normalized map of the stability boundaries for feed system coupled stability.

Using the curves for characteristic velocity (c^*) versus mixture ratio (\bar{r}) for LOX/RP-1, a set of stability boundaries based solely on gain stabilization were obtained and are shown in Figure 55. The curves in Figure 55 represent the minimum pressure drops for absolute gain stabilization as a function of mixture ratio for LOX and RP-1 propellants. These curves can be interpreted in the following ways.

(1) At a given mixture ratio (\bar{r}) and a chosen ratio of fuel injector pressure drop to chamber pressure ($\Delta \bar{P}_{jf}/\bar{P}_c$), the family of curves define the corresponding maximum ratio of fuel to oxidizer injector pressure drops which will barely result in absolute gain stabilization. The shaded region represents physically unrealizable conditions.

C, Volume III, 2, Engine Combustion Stability (cont.)

It should be noted that the system will become more gain stable as the ratio, $\bar{\Delta P}_{jf}/\bar{\Delta P}_{jo}$, is reduced from its maximum value while $\bar{\Delta P}_{jf}/\bar{P}_c$ and \bar{r} are held constant. This is the same as increasing $\bar{\Delta P}_{jo}$ while holding $\bar{\Delta P}_{jf}$ constant.

(2) At a given mixture ratio (\bar{r}) and a chosen ratio of fuel injector pressure drop to oxidizer injector pressure drop ($\bar{\Delta P}_{jf}/\bar{\Delta P}_{jo}$), the family of curves yields a corresponding minimum ratio of fuel injector pressure drop to chamber pressure $\bar{\Delta P}_{jf}/\bar{P}_c$ which will barely result in absolute gain stabilization.

Note that the system becomes more stable as $\bar{\Delta P}_{jf}/\bar{P}_c$ increased above the minimum stabilizing value while $\bar{\Delta P}_{jf}/\bar{\Delta P}_{jo}$ and \bar{r} are held constant. This is the same as increasing $\bar{\Delta P}_{jo}$ while increasing $\bar{\Delta P}_{jf}$.

Use of the data in Figure 55 can be illustrated by the following example:

The present ALRC baseline configuration is a regenerative engine having 1.2 million pounds of thrust and a pressure drop schedule as follows:

	<u>Fuel (RP-1)</u>	<u>Oxidizer (LOX)</u>
ΔP valve, psi	3	6
ΔP regenerative circuit, psi	40	
ΔP injector, psi	<u>52</u>	<u>80</u>

Assume: $\bar{\Delta P}_{jf} = 95$ psi $\bar{\Delta P}_{jo} = 86$ psi

C, Volume III, 2, Engine Combustion Stability (cont.)

chamber pressure, \bar{P}_c , is 250 psia

mixture ratio, \bar{r} , is 2.4

now

$$\frac{\overline{\Delta P}_{jf}}{\bar{P}_c} = \frac{95}{250} = 0.38$$

$$\frac{\overline{\Delta P}_{jf}}{\overline{\Delta P}_{jo}} = \frac{95}{86} = 1.10$$

Plotting the point corresponding to $\overline{\Delta P}_{jf}/\bar{P}_c = 0.38$ and $\bar{r} = 2.4$ on Figure 55 indicates that the maximum acceptable ratio, $\overline{\Delta P}_{jf}/\overline{\Delta P}_{jo}$, for absolute gain stability is equal to 0.625. As noted above, the present ALRC design has $\overline{\Delta P}_{jf}/\overline{\Delta P}_{jo} = 1.10$ and is not absolutely gain stabilized.

c. Feed System Stability (POGO)

(1) Engine Transfer Functions

The analysis of the POGO stability characteristics for a vehicle system requires a knowledge of the engine system transfer functions which relate inlet pressure and flow to engine thrust. The equivalent circuit representation of the pressure fed engine/feedline combination is shown in Figure 56 where:

- $Z_{\ell o}$ is the oxidizer feed system impedance upstream of the engine inlet.
- $Z_{\ell f}$ is the fuel feed system impedance upstream of the engine inlet.
- Z_{io} is the oxidizer circuit impedance between engine inlet and combustion chamber.
- Z_{if} is the fuel circuit impedance between engine inlet and combustion chamber.
- Z_c is the combustion impedance.

C, Volume III, 2, Engine Combustion Stability (cont.)

The engine transfer functions which require evaluation are:

$$\frac{\partial P_c}{\partial P_{inlet}}$$

$$\frac{\partial W}{\partial P_{inlet}}$$

$$\frac{\partial T}{\partial P_c}$$

$$(a) \quad \frac{\partial P_c}{\partial P_{inlet}}$$

For the oxidizer side, the inlet pressure can be designated as P_{io} as shown in Figure 56. Using Millman's network theorem, the following transfer function is obtained:

$$\frac{\partial P_c}{\partial P_{io}} = \frac{1}{1 + \frac{Z_{io}}{Z_c} + \frac{Z_{io}}{Z_{if} + Z_{lf}}}$$

Z_c was defined in the previous section on Feed System Coupled Combustion Stability and can be represented by the equation

$$Z_c = \frac{c^*}{A_{tg}} \frac{e^{-t_1 S}}{1 + t_2 S}$$

The transport time delay, t_1 , has negligible effect in the POGO frequency range. The chamber residence time lag, t_2 , also has a negligible effect for the ALRC baseline configuration.

$$(b) \quad \frac{\partial W}{\partial P_{inlet}}$$

This transfer function is the input admittance for the engine. Referring to the oxidizer side

C, Volume III, 2, Engine Combustion Stability (cont.)

$$\frac{\dot{W}_o}{P_{io}} = \frac{Z_c + Z_{if} + Z_f}{Z_{io} Z_c + (Z_{io} + Z_c) (Z_{if} + Z_f)}$$

where pressure in psi and weight flow in lb/sec.

(c) $\partial T / \partial P_c$

The transfer function relating the perturbations in engine thrust to perturbations in chamber pressure is given by

$$\frac{\partial T}{\partial P_c} = 4800 \quad (\text{Sea Level})$$

$$\frac{\partial T}{\partial P_c} = 6100 \quad (\text{Vacuum})$$

where thrust in pounds and pressure in psi.

C, Volume III, Methodology (cont.)

3. Thermal Analysis

a. Introduction

All passive thrust chamber cooling concepts, regardless of whether supplemental cooling was used or not, were rejected during Phase A of this contract. The actively cooled concepts judged to be worthy of analytical study were full regenerative, ducted film, and a potentially promising combination of the two. With the latter concept, the chamber is regeneratively cooled with a low pressure drop, single forward pass design, and the nozzle entrance is duct cooled.

As discussed Volume I of this report, a fully regeneratively cooled thrust chamber without supplemental fuel film cooling was selected for the engine baseline. The basis for this selection was presented in "Phase A Final Report for Feasibility Study of a Pressure-Fed Engine for a Water Recoverable Space Shuttle Booster," dated 18 January 1972. This section is therefore only concerned with the fully regeneratively cooled baseline design.

Both LOX/RP-1 and LOX/Propane engines were evaluated during Phase A and the results of the thermal analysis are documented in the Phase A final report for this contract. This section is concerned only with the baseline system propellant combination, LOX/RP-1.

Regenerative cooling studies were restricted to the use of fuel (RP-1) because liquid oxygen cooling is inferior. The analyses considered coolant burnout characteristics, gas and coolant side hydrocarbon and carbon deposition and the need for minimizing coolant pressure drop.

C, Volume III, 3, Thermal Analysis (cont.)

b. Analytical Procedure

A parametric study of a regeneratively cooled chamber with fuel film cooling was conducted. The parametric study was conducted utilizing the regeneratively cooled chamber heat transfer computer program developed at Aerojet (Reference 1) and used extensively in the successful design of the Titan II, NERVA, Titan IIIB, and Phoebus chambers to name a few. The combustion gas properties were obtained from the Aerojet developed THERMOCAL computer program (Reference 2) and used in conjunction with the following hot-gas-side heat transfer correlation, a modified form the simplified Bartz (Reference 3) correlation.

$$h_g = C_g \frac{1}{D^{0.2}} \frac{C_p \mu^{0.2}}{Pr^{0.6}} \frac{\dot{W}_T T_\infty}{A T_f}^{0.8} K'$$

Nomenclature is shown on Table II.

The " C_g " is a coefficient which is normally 0.026 but was varied to account for gas-side carbon deposition and " K' " is the correction factor for two-dimensional flow in the nozzle expansion region.⁽¹⁾

The forced-convection correlation for RP-1 was based upon References 4 and 5.

$$h_L = 0.0048 \frac{k_b}{D} \frac{DV \rho_b}{\mu_b}^{0.95} Pr_b^{0.4}$$

(1) The assumed carbon deposition was conservative ($0.7 h_g$) and test data (Reference 6) indicated greater reductions are possible ($0.3 h_g$ to $0.5 h_g$).

TABLE II

THERMAL ANALYSIS NOMENCLATURE

A	=	flow area
C _g	=	multiplier for "hg"
C _p	=	heat capacity
D	=	diameter
H _g	=	gas-side heat transfer coefficient
h _L	=	coolant-side heat transfer coefficient
k	=	thermal conductivity
K'	=	2-D nozzle flow correction factor
Pr	=	Prandtl number
Q _{BO}	=	burnout heat flux
T	=	temperature
V	=	velocity
\dot{W}_T	=	total propellant flow
ρ	=	density
μ	=	viscosity

SUBSCRIPT

b	=	bulk
f	=	film
Sat	=	saturation
∞	=	free stream

C, Volume III, 3, Thermal Analysis (cont.)

The burnout heat flux correlation for RP-1 was derived from Reference 4 and is shown below and on Figure 57.

$$Q_{BO} = 0.9 + 0.000362V\Delta T_{sub}$$

where, $\Delta T_{sub} = (T_{sat} - T_b)$

Soot characteristics on the hot gas side of the thrust chamber tubes were thoroughly investigated to define the most realistic reduction in heat transfer due to the soot. The most pertinent data on soot characteristics is shown in Figure 58 for; (1) the soot layer resistance and (2) local soot flake off phenomena. The soot or carbon layer resistance for the chamber and throat is shown to be approximately 5500 and 4000 in.²-sec-°F/Btu, respectively. Figure 58 also indicates that the soot layer apparently builds up and flakes off continuously during a firing. These soot characteristics were incorporated into the Phase B thermal analysis.

Thermal radiation from the LO₂/RP-1 combustion gases was also incorporated in the Phase B heat transfer analysis. The quantity of heat transferred by radiation was varied with thrust chamber location and the condition of the tube wall, i.e., clean or sooted. The heat fluxes from convection and radiation for the chamber and throat are shown in Figure 59 for clean wall, soot, and soot flaked off conditions. Heat flux due to radiation in the chamber for a clean wall is 1.4 Btu/in.²-sec-°F out of a total of 3.7 Btu/in.²-sec-°F. With a sooted wall the radiation is 0.1 Btu/in.²-sec-°F out of a total of 0.8 Btu/in.²-sec-°F.

For the parametric analysis, round cross section, constant diameter wall thickness tubes were assumed throughout. A two pass chamber was also used to conduct the parametric studies and the total number of

C, Volume III, 3, Thermal Analysis (cont.)

tubes was varied from 150 to 300 with tube wall thicknesses of 0.05, 0.03, and 0.02 inches. The analysis was conducted initially assuming no carbon deposit and then with carbon deposition in the hot-gas side of the tubes. The results of the LOX/RP-1 regenerative coolant study is shown on Figures 45 and 18.

Total chamber coolant pressure drop and coolant bulk temperature rise is shown versus number of tubes (Figure 45) for 0.050, 0.030 and 0.020 in. tube wall thicknesses. For any wall thickness pressure drop (ΔP) increases for increasing number of tubes. The noted ΔP increases are due to the decreasing flow areas as the number of circular tubes is increased.

The study indicates that tube burnout is not a design problem with RP-1 coolant. Burnout is not the only limiting factor on the coolant-side; a slow buildup of varnish or tar accumulates over the total period of run time. A literature search was conducted, and this buildup rate was interpreted (Reference 7) in terms of wall temperature rise per flight (160 sec) and shown in Figure 45.

Studies involving the relative merits of single pass, pass and a half, and two pass designs were also conducted. Factors common to the three designs are that (1) coolant is available at the forward end of the engine, (2) coolant must be fed the entire engine length and back, a 180° turn necessarily being made by the coolant at the nozzle exit, and (3) the coolant bulk temperature rise through the chamber wall is so low that cooling considerations need not enter into flow scheme determination. Table III summarizes the advantages and disadvantages for the three concepts. The selected flow scheme is the double pass design, because the tube bifurcation technique is well developed, and the hot gas sealing problem of the pass and a half design is recognized to be quite difficult. As noted from the table, there is little difference in the required coolant jacket ΔP for the three cooling methods.

TABLE III

REGENERATIVE COOLANT FLOW SCHEMES - ADVANTAGES AND DISADVANTAGES

<u>Coolant Flow Scheme</u>	<u>Advantages</u>	<u>Disadvantages</u>
Single Pass ($\Delta P = 39$ psi)	None of Significance	Largest nozzle exit outside diameter Heaviest coolant inlet manifold Longest inlet line Largest gimballing moment Large tube taper, bifurcation, or tapered tube walls required
Pass and a Half ($\Delta P = 38$ psi)	No bifurcations, excessive tube taper, or tapered walls needed Small nozzle outside exit diameter small coolant inlet manifold weight Small gimbal moment	Difficult hot gas sealing problem at coolant inlet joint
Two Pass ($\Delta P = 40$ psi)	Small nozzle exit outside diameter Small gimbal moment Shortest inlet line length and volume Small coolant inlet manifold weight	Large tube taper, bifurcation, or tapered tube walls required

REFERENCES

1. Daily, J., "Heat II - Final Report", Aerojet Liquid Rocket Company, TCER 9641:0119, June 18, 1971
2. Hester, J. N. and Chan, J., "Thermocal - Phase I, Vol. I and II", Aerojet Liquid Rocket Company, Report No. 9600:M014, 1 September 1969
3. Bartz, D. R., "A Simple Equation for Rapid Estimation of Rocket Nozzle Convective Heat Transfer Coefficients", Jet Propulsion, January 1959, p 59
4. Dean, L. E. and Thompson, W. R., "Heat Transfer Characteristics of RP-1", Aerojet Liquid Rocket Company, TCD 9650-010, October 1964
5. Hines, W. S., "Turbulent Forced Convection Heat Transfer to Liquids at Very High Heat Fluxes and Flow Rates, Research Report 61-14, Rocketdyne Division of North American Aviation, Canoga Park, California, 30 November 1961
6. Masters, A. I., "Investigation of Light Hydrocarbon Fuels with Flox Mixtures as Liquid Rocket Propellants", NASA CR-54445, 1 September 1965
7. Thompson, R. J., "Investigation of Cooling Problems at High Chamber Pressures", Rocketdyne Report R-3999, May 1963

BASELINE PROGRAM SCHEDULE (NASA PRESSURE-FED BOOSTER ENGINE)

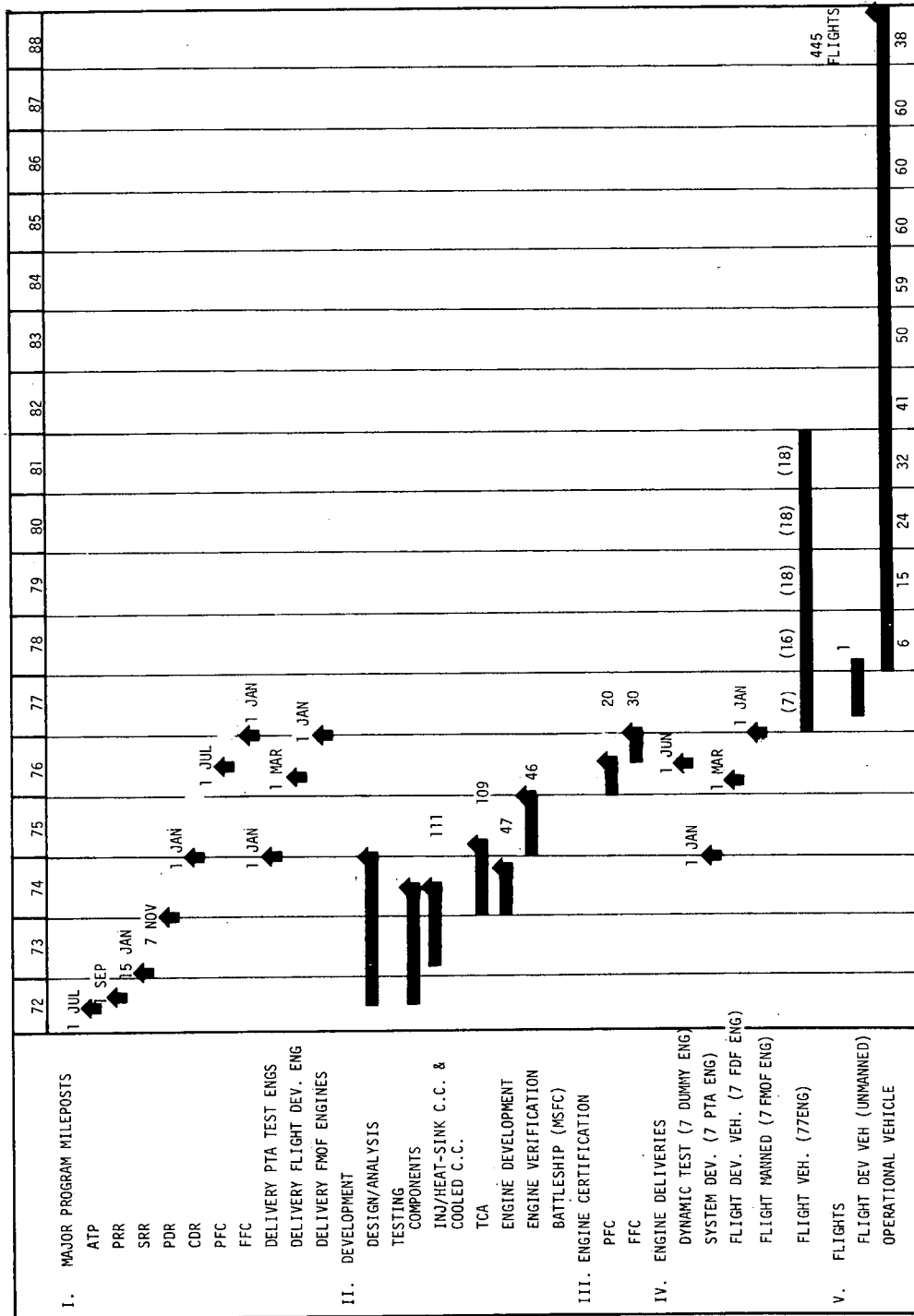
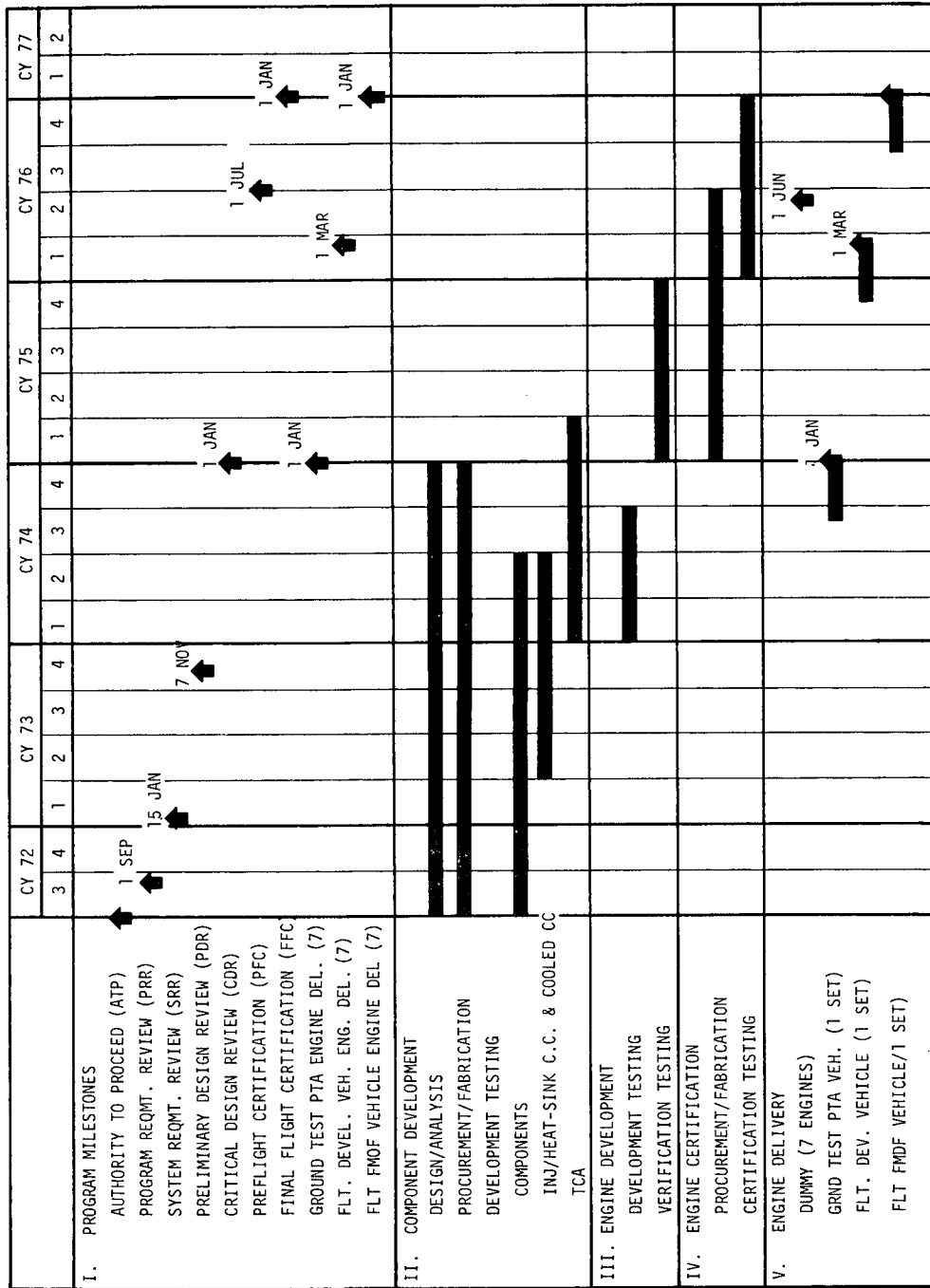


Figure 1



24 FEB 1972

BASELINE DEVELOPMENT PROGRAM SCHEDULE (NASA PRESSURE-FED BOOSTER ENGINE)



1 JAN 1972

Figure 2

TEST PROGRAM	CY '72								CY '73								CY '74								CY '75								CY '76								TOTAL NO. TEST																				
	3	4	1	2	3	4	1	2	3	4	1	2	3	4	1	2	3	4	1	2	3	4	1	2	3	4																																			
PROGRAM MILESTONES.	<div style="text-align: center;">△ ATP</div>																												△	<div style="text-align: center;">CDR</div>																												△	PFC	△	PFC
<u>ALRC-SACTO-COMPONENTS</u>																																																													
• INJECTOR MODULE																																																													
• BEARINGS / SEALS																																																													
• VALVES / LINES																																																													
• TVC																																																													
<u>EAFB-COMBUSTION ASSY</u>																																																													
• INJECTOR/HEAT SINK C.C.																																																													
• INJECTOR/C.C.																																																													
• TCA																																																													
* • TCA - R & D																																																													
• TCA VERIF.																																																													
<u>EAFB - ENGINE</u>																																																													
• ENG. DEV																																																													
• 2 ENG.LIMITS & VERIF.																																																													
• PFC																																																													
• FFC																																																													
• DEL. ENG'S.																																																													

TOTAL	391
-------	-----



24 FEB 1972



Figure 3

BASELINE HARDWARE DEMAND (NASA PRESSURE-FED BOOSTER ENGINE)

	72	1973				1974				1975				1976				Totals	
		1	2	3	4	1	2	3	4	1	2	3	4	1	2	3	4		
ATP	Δ	4																	

DEVELOPMENT PROGRAM PHASE



24 FEB 1972

Figure 4

[illegible][illegible]
$$\vdots$$

NASA - MSFC PRESSURE-FED ENGINE NEED DATES BASED ON BOOSTER ATP 7-1-72

(11 VEHICLE SYSTEM FLIGHT PROGRAM)

	Schedule Date (On Dock at ALRC)	Engines Delivered
	Baseline	
SYSTEM DEV VEH - PTA (R&D)	1-1-75	7
FLT DEV VEH - FLT ENG	3-1-76	7
DYNAMIC TEST VEH (DUMMY ENGINES)	6-1-76	7
FLT TEST VEH #2	1-1-77	7
	FMOF VEH	
#3	7-1-77	7
#4	1-1-78	7
#5	1-1-79	7
#6	7-1-79	7
#7	1-1-80	7
#8	7-1-80	7
#9	1-1-81	7
#10	7-1-81	7
Spares Engines (2)	3-1-78	2
Spares Engines (12)	None	12
		<u>105 Total Engines</u>

Note: Support 11 Boosters - 1 Unmanned plus 10 Manned
 77 Flt Engines, plus 14 Spares = 91 Engines
 445 Flights - 2 Sets Flight Engines/Year



Figure 6

24 FEB 1972

SPACE SHUTTLE VEHICLE FLIGHT SCHEDULE (NASA PRESSURE-FED BOOSTER ENGINE)

VEHICLE SYSTEM NUMBER*	78	79	80	81	82	83	84	85	86	87	88	Totals
2	3	10	12	12	3							40
3	3	5	12	12	8							40
4				8	12	12	8					40
1					12	12	12	4				40
5					6	12	12	10				40
6						12	12	12	4			40
7						2	12	12	12	2		40
8							3	12	12	12	1	40
9								10	12	12	6	40
10									12	12	12	36
OVERHAUL ENG.									8	12	12	32
OVERHAUL ENG.										10	7	17
FLIGHTS	6	15	24	32	41	50	59	60	60	60	38	445

*Synthetic

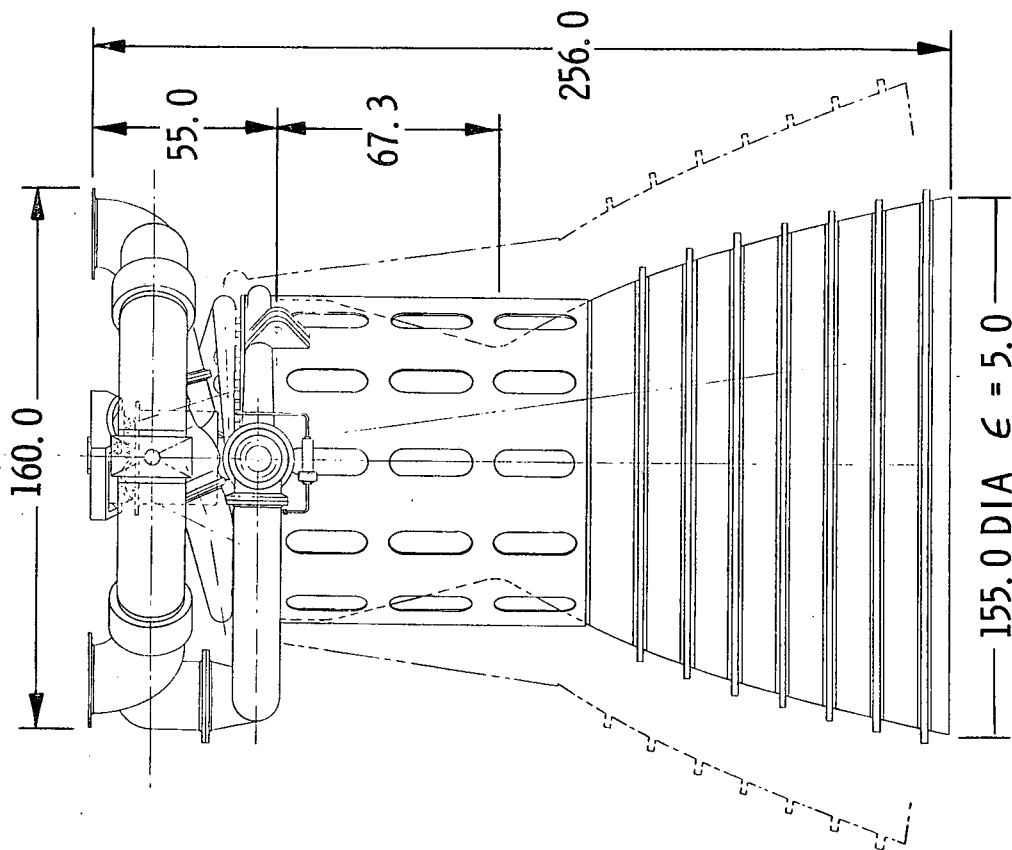
Note: Max of 6 engines in the loop/4years with 14 engines being overhauled.



Figure 7

24 FEB 1972

PRESSURE-FED BOOSTER ENGINE CHARACTERISTICS (NASA PRESSURE-FED BOOSTER ENGINE)



- PROPELLANTS = LOX/RP-1
- THRUST = 1, 200, 000 LB
- CHAMBER PRESSURE = 250 PSIA
- MIXTURE RATIO = 2.4:1
- EXPANSION RATIO = 5:1
- DIMENSIONS
 - 256 IN. LONG
 - 155 IN. DIAM.
- SPECIFIC IMPULSE
 - 237.8 SEC S.L.
 - 289.8 SEC VAC

Figure 8



24 FEB 1972

PRESSURE-FED ENGINE SCHEMATIC (NASA PRESSURE-FED BOOSTER ENGINE)

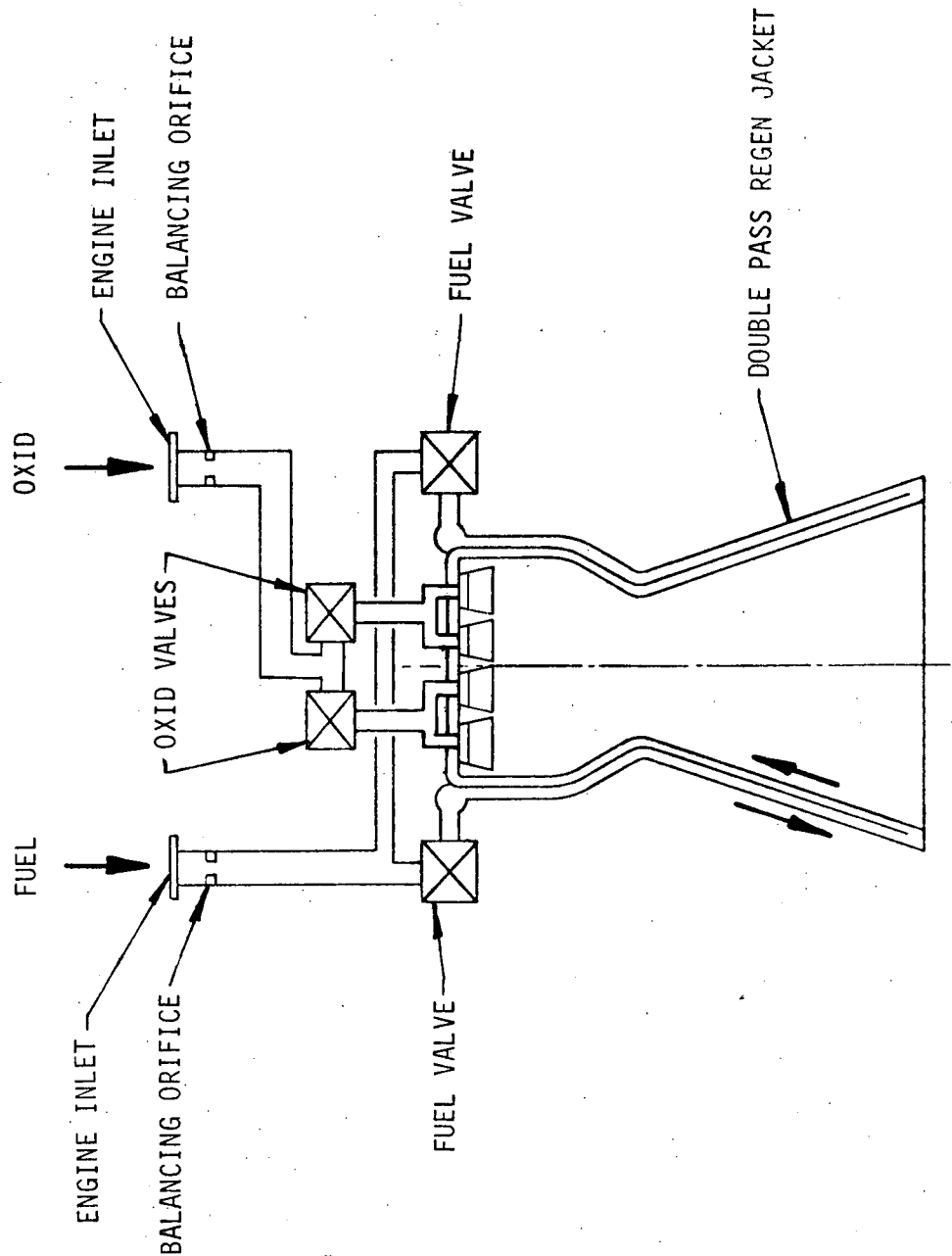


Figure 9



24 FEB 1972

HYPERGOL IGNITER CARTRIDGE

THRUST CHAMBER

INJECTOR ASSEMBLY

GIMBAL ASSEMBLY

GIMBAL POINT

ENGINE INTERFACE

GIMBAL ENVELOPE

FUEL INLET GIMBAL MANIFOLD

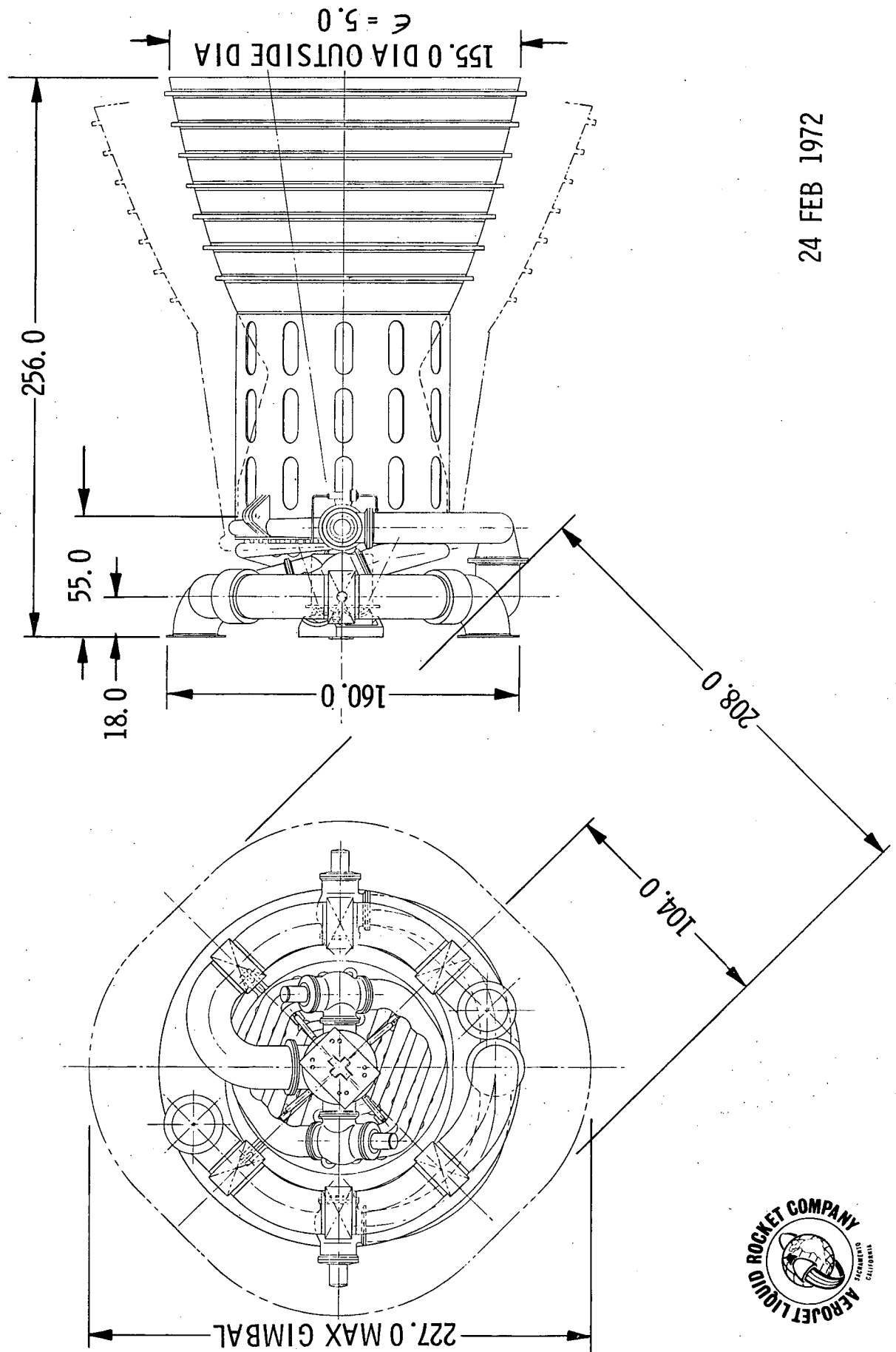
FUEL VALVE (2 PLACES)

OXIDIZER INLET GIMBAL MANIFOLD

OXIDIZER VALVE (2 PLACES)

Figure 10

PRESSURE-FED ENGINE DESIGN (Page 2 of 2)
(NASA PRESSURE-FED BOOSTER ENGINE)



24 FEB 1972



Figure 10

SUMMARY OF KEY DESIGN PARAMETERS (NASA PRESSURE-FED BOOSTER ENGINE)

<u>PARAMETERS</u>	<u>VALUE</u>
SEA LEVEL THRUST	1,200,000 LB
PROPELLANTS	LOX/RP-1
MIXTURE RATIO	2.4
NOZZLE AREA RATIO	5.0
NOZZLE CONTOUR LENGTH	86%
CHAMBER PRESSURE	250 PSIA
CONTRACTION AREA RATIO	1.8
CHAMBER LENGTH	70 IN.
THROTTLING RANGE	70% OF P_c



24 FEB 1972

Figure 11

SUMMARY OF DESIGN FEATURES (NASA PRESSURE-FED BOOSTER ENGINE)

ITEM	DESIGN FEATURE
STABILITY CONTROL (HIGH FREQUENCY)	MODULAR POCKETS
STABILITY CONTROL (CHUGGING)	FILTER
VALVE TYPE	<ul style="list-style-type: none"> • RIGHT ANGLE POPPET • 2 PER PROPELLANT
VALVE INLET	13.5 IN. (RP-1)
DIAMETER	13.5 IN. (LOX)
MISSION BEFORE OVERHAUL	40
DESIGN LIFE	100
FAILURE CRITERIA	FO/FS (ELECT.) FO (MECH.)



Figure 12

2-2

SUMMARY OF DESIGN FEATURES (Cont.) (NASA PRESSURE-FED BOOSTER ENGINE)

ITEMS	DESIGN FEATURES
THRUST VECTOR CONTROL	$\pm 6^{\circ}$
TVC METHOD	HEAD-END GIMBAL
INJECTOR TYPE	MODULAR
INJECTOR THRUST PER ELEMENT	1000 LB
INJECTION ELEMENT TYPE	LIKE-ON-LIKE
IGNITION METHOD	HYPERGOL
CHAMBER/NOZZLE	FULL REGEN.
COOLING METHOD	2 PASS NO FILM
ENGINE INLET PRESSURE	380 (RP-1) 380 (LOX)



Figure 12

MODULAR INJECTOR DESIGN
(NASA PRESSURE-FED BOOSTER ENGINE)

SEPARATED INDIVIDUAL COMBUSTION COMPARTMENTS

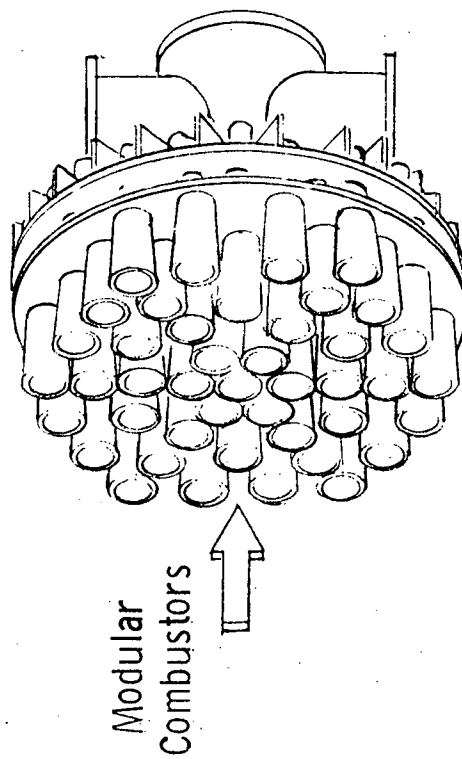
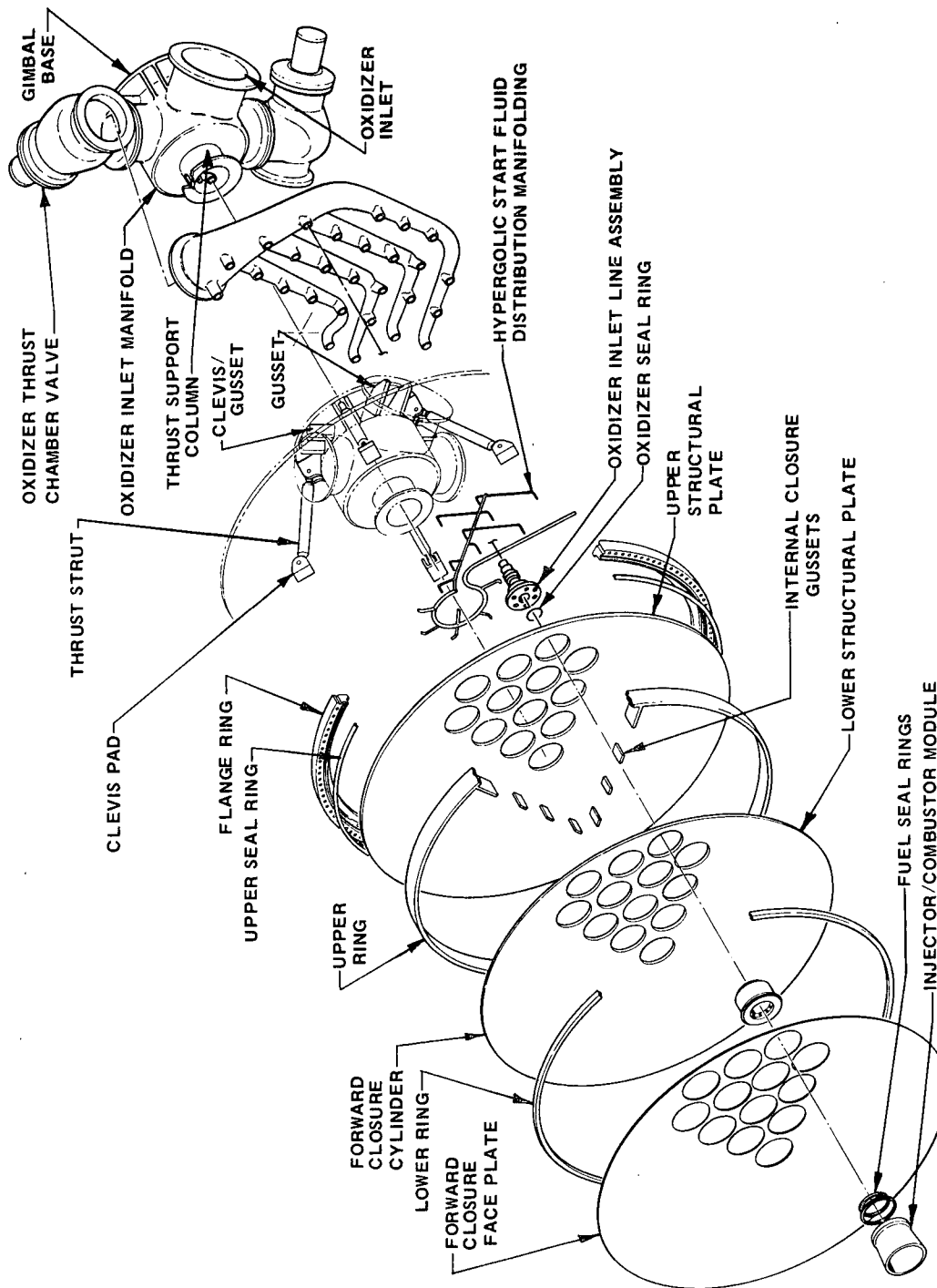


Figure 13



24 FEB 1972

MODULAR INJECTOR CONSTRUCTION (NASA PRESSURE-FED BOOSTER ENGINE)



24 FEB 1972



Figure 14

PFE MODULAR COMBUSTOR - HIGH THRUST PER ELEMENT
(NASA PRESSURE-FED BOOSTER ENGINE)

THRUST = 21.8×10^3 LB/MODULE

THRUST/ELEMENT = 1090 LB

$\dot{W}_O = 66$ LB/SEC

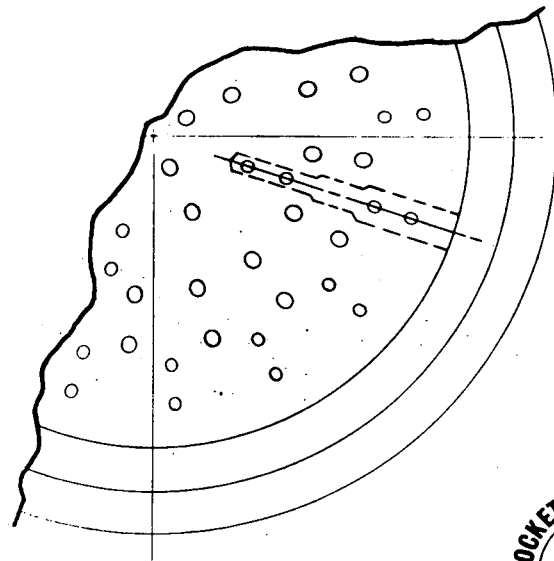
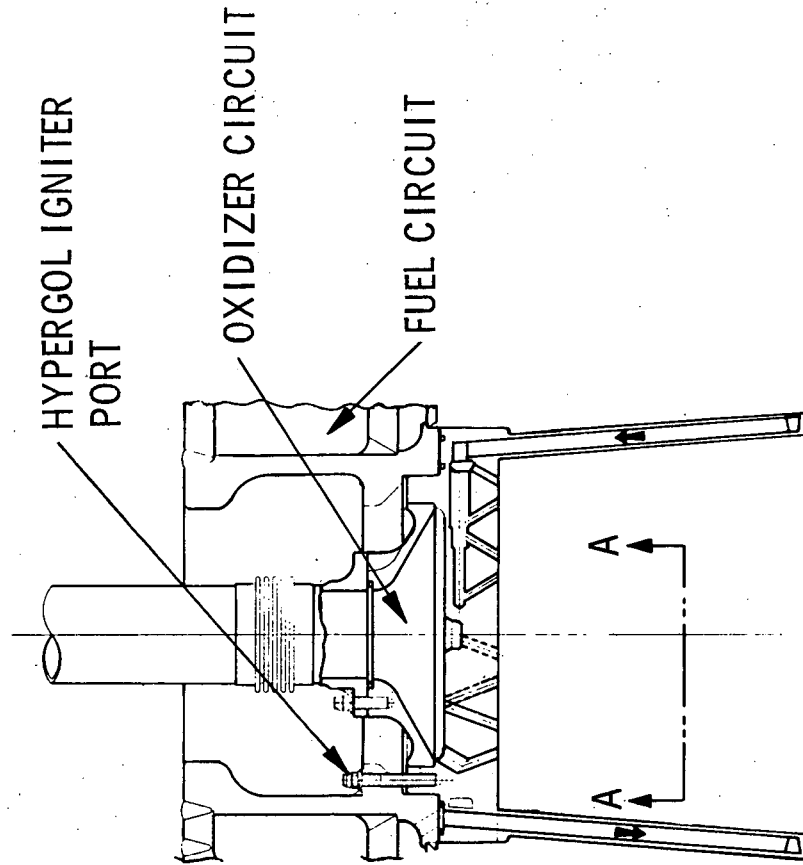
$\dot{W}_f = 27$ LB/SEC

MR = 2.4

INJECTOR DIA = 9.0 IN.

COMB. DIA = 10.25 IN.

COMB. LENGTH = 8.0 IN.



VIEW A-A

24 FEB 1972



Figure 15

MODULAR INJECTION/THRUST CHAMBER INTERFACE (NASA PRESSURE-FED BOOSTER ENGINE)

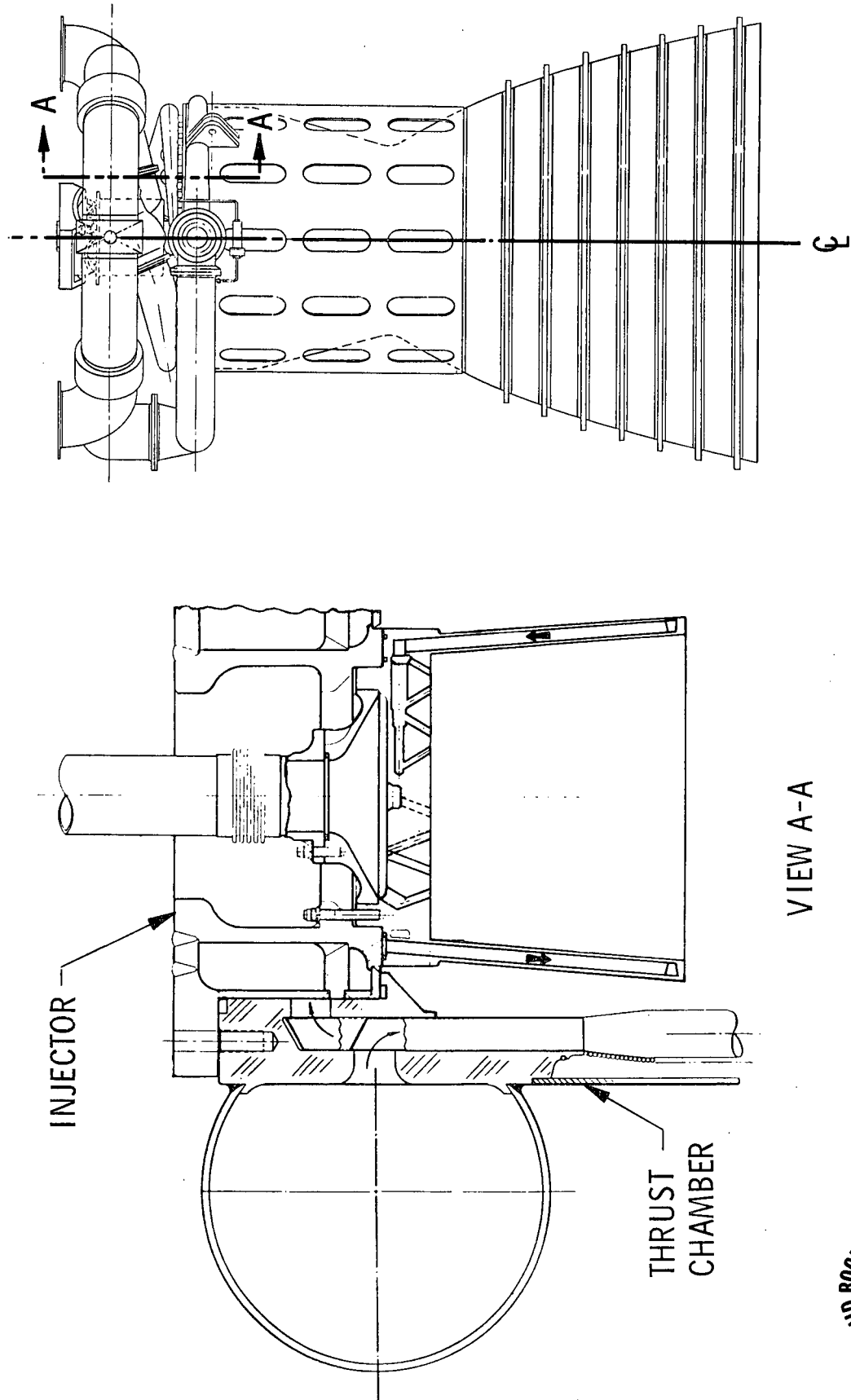


Figure 16



24 FEB 1972

REGENERATIVE THRUST CHAMBER (NASA PRESSURE-FED BOOSTER ENGINE)

FEATURES

- RP-1 COOLED 2 PASS
- NO SUPPLEMENTAL COOLING
- CONSTANT TUBE DIA. (SQUASHED AT THROAT)
- CONSTANT TUBE WALL
- WELDED CONSTRUCTION
- CHAMBER DIA. 91 IN.
- CONTRACTION RATIO 1.8
- CHAMBER L' 70 IN.
- STRESSED FOR INERTIAL LOADING AT 200 FT/SEC SPLASHDOWN VELOCITY

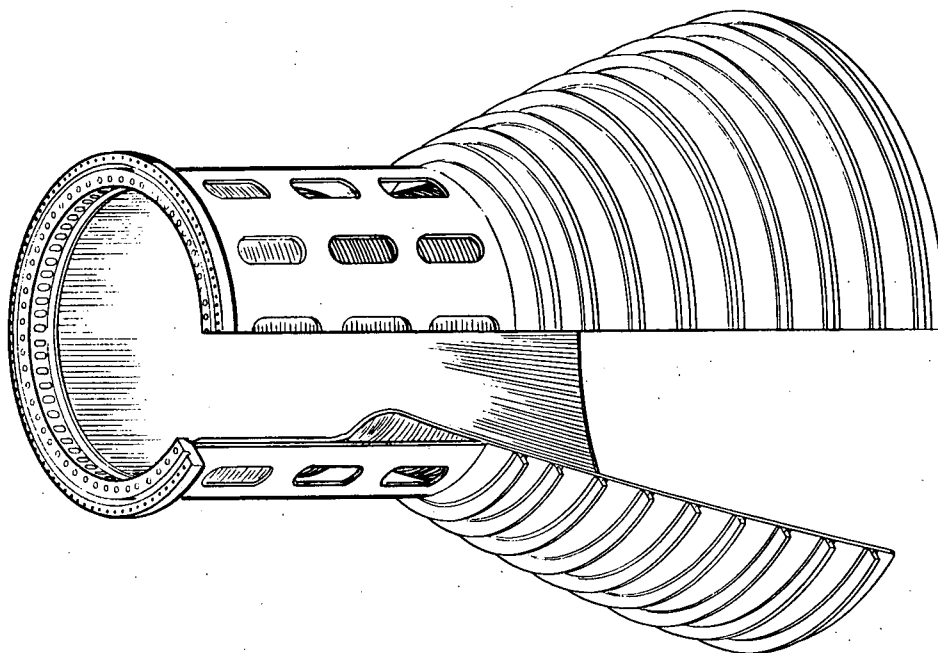


Figure 17



24 FEB 1972

TUBE BUNDLE THERMAL DESIGN - 2 PASS (NASA PRESSURE-FED BOOSTER ENGINE)

• $P_c = 250$ PSIA (100% THRUST)

	<u>SOOT FLAKED OFF</u>		<u>NOMINAL SOOT</u>	
	T WALL (°F)	RBO	T WALL (°F)	RBO
THROAT	1350	0.47	680	0.12
CHAMBER	1220	0.38	525	0.11

• $P_c = 150$ PSIA (60% THRUST)

	<u>SOOT FLAKED OFF</u>	
	T WALL (°F)	RBO
THROAT	1190	0.73
CHAMBER	1110	0.67

• $P_c = 250$ PSIA

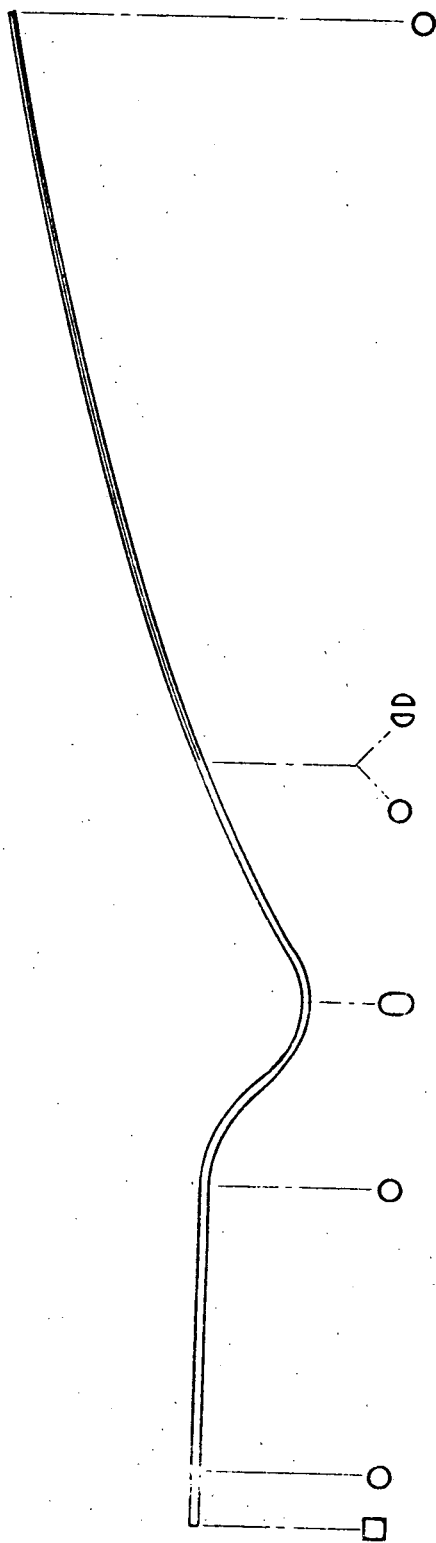
TUBE BUNDLE AND TURN AROUND	30 PSI
MANIFOLDING, INLETS ETC	10 PSI
TOTAL ΔP	<u>40 PSI</u>



24 FEB 1972

Figure 18

THRUST CHAMBER TUBE DESIGN DETAILS (NASA PRESSURE-FED BOOSTER ENGINE)



TUBE FEATURES

- MATERIAL: _____ INCONEL 625 ANNEALED
- TYPE: _____ CONSTANT WALL, CONSTANT DIA WITH BIFURCATION
- ORIGINAL TUBE _____ FORWARD SECTION _____ 1.30 DIA _____ .036 WALL
CONFIGURATION: _____ AFT SECTION (After Bifurcation) _____ 1.20 DIA _____ .036 WALL
- CONSTRUCTION _____ BEND TO SHAPE, FLATTEN IN PRESS, FORM ENDS FOR MANIFOLDS
SEQUENCE: _____ AND BIFURCATION
- STATE OF THE ART _____ ALL FAB METHODS PROPOSED HAVE BEEN IN USE 10 YEARS OR MORE
FABRICATION

Figure 19



24 FEB 1972

GIMBALLING CHARACTERISTICS (NASA PRESSURE-FED BOOSTER ENGINE)

- MAX. GIMBAL ANGLE = $\pm 6^{\circ}$
- MAX. GIMBAL RATE = $5.76^{\circ} / \text{SEC}$
- MIN. ACCELERATION RATE = 2.2 RAD/SEC^2
- BIAS LOAD = 0 - 319,000 FT-LB ESTIMATE
- ENGINE MOMENT OF INERTIA ABOUT GIMBAL POINT = $43,150 \text{ SLUG} - \text{FT}^2$
- COMBINED STRUCTURAL SPRING RATE = 250,000 LB/IN
- GIMBAL MOMENT ARM = 65.75-IN.
- MIN. NATURAL FREQUENCY (SINGLE PLANE) = 7.3 HZ

Figure 20



24 FEB 1972

PRESSURE SCHEDULE
(NASA PRESSURE-FED BOOSTER ENGINE)

LOCATION	PRESSURE, PSI	
	RP-1 CIRCUIT	LOX CIRCUIT
ENGINE INLET	380	380
Δ P ORIFICE	(5)	(7)
Δ P LINES	(3)	(10)
VALVE INLET	372	363
Δ P VALVE	(3)	(6)
REGEN. CHAMBER INLET	369	—
Δ P REGEN. CHAMBER	(40)	—
INJ. MODULE INLET	329	357
Δ P MODULE	(52)	(80)
CHAMBER PRESSURE, FACE	277	277
CHAMBER PRESSURE, PLENUM	250	250



24 FEB 1972

Figure 21

PERFORMANCE AND WEIGHT SUMMARY (NASA PRESSURE-FED BOOSTER ENGINE)

<u>PERFORMANCE</u>	<u>ALRC</u> <u>DESIGN</u>	<u>NASA</u> <u>BASELINE</u>	<u>CONTINGENCY</u>
I _S SEA LEVEL (NOMINAL), SEC	237.8	227.0	+ 10.8
I _S SEA LEVEL (MINIMUM), SEC	235.8	225.0	+ 10.8
I _S VACUUM (NOMINAL), SEC	289.8	277.5	+ 12.3
I _S VACUUM (MINIMUM), SEC	287.3	275	+ 12.3
<u>WEIGHT</u>			
*TOTAL DRY WEIGHT, LB	17,484	18,000	- 516
*TOTAL WET BURNOUT WEIGHT, LB	21,344	-	-

*W/O GIMBAL ACTUATORS



24 FEB 1972

Figure 22

PERFORMANCE SUMMARY (NASA PRESSURE-FED BOOSTER ENGINE)

THEORETICAL SPECIFIC IMPULSE (ODE), SEC _____ 303.6

REGENERATED COOLING ENERGY _____ 0.7

PERFORMANCE LOSSES, SEC

ERL _____ 5.9

FCL - CHAMBER _____ 0.0

FCL - BAFFLES _____ 0.0

BLL _____ 1.6

DL _____ 3.6

KL _____ 0.6

CONTAMINANTS (ARGON) _____ 0.4

MRD _____ 2.4

TOTAL - 14.5

DELIVERED PERFORMANCE, VACUUM SPECIFIC IMPULSE, SEC 289.8

SEA LEVEL SPECIFIC IMPULSE 237.8 (95% Theor.)

24 FEB 1972



Figure 23

VEHICLE EXCHANGE RATIOS (NASA PRESSURE-FED BOOSTER ENGINE)

	CHRYSLER	GDC	MDAC	MMC	TBC ⁽³⁾
1. GROSS LIFTOFF WEIGHT/SPECIFIC IMPULSE $\Delta GLOW/\Delta I_s$, LB/SEC		41,750	28,860*	43,100	80,000
2. GROSS LIFTOFF WEIGHT/INERT WEIGHT ⁽¹⁾ $\Delta GLOW/\Delta W_I$, LB/LB		3.25	3.2 ⁽²⁾	2.94	3.2
3. INERT WEIGHT ⁽¹⁾ /SPECIFIC IMPULSE, $\Delta W/\Delta I_s$, LB/SEC		12,850*	9,020*	14,700	25,000
4. GROSS LIFTOFF WEIGHT/TANK PRESSURE (BOTH TANKS), $\Delta GLOW/\Delta P_T$, LB/PSI		2,951	3,674*		4,737
5. GROSS LIFTOFF WEIGHT/FUEL TANK PRESSURE, $\Delta GLOW/\Delta P_{FT}$, LB/PSI		1,115	1,388*		2019
6. GROSS LIFTOFF WEIGHT/OX TANK PRESSURE, $\Delta GLOW/\Delta P_{OT}$, LB/PSI		1,836	2,286*		2,718
7. GROSS LIFTOFF WEIGHT/AFT SKIRT BASE DIAMETER, $\Delta GLOW/\Delta D_{AFT}$, LB/FT		12,650*			31,320
8. GROSS-LIFTOFF WEIGHT/AFT SKIRT LENGTH, $\Delta GLOW/\Delta L_{AFT}$, LB/FT		3,032*			17,510*
(1) DRY INERTS (2) ASSUMED (3) VEHICLE 979-150A *DATA DERIVED FROM OTHER EXCHANGE RATIOS OR INFORMATION SUPPLIED					

19 JAN 1972



Figure 24

VEHICLE EXCHANGE RATIOS (SERIES BURN VEHICLES)

	CHRYSLER	GDC	MDAC	MMC	TBC ⁽³⁾
1. GROSS LIFTOFF WEIGHT/SPECIFIC IMPULSE $\Delta GLOW/\Delta I_s$, LB/SEC	29,400	41,750	29,490*	43,100	40,000
2. GROSS LIFTOFF WEIGHT/ENGINE SYSTEM INERT ⁽¹⁾ WEIGHT, $\Delta GLOW/\Delta W_E$, LB/LB	3,914	5.0	3.63*	4.5 ⁽²⁾	4.46
3. GROSS LIFTOFF WEIGHT/TANK PRESSURE (BOTH TANKS), $\Delta GLOW/\Delta P_T$, LB/PSI	2770	4540	4167*	—	3174
4. GROSS LIFTOFF WEIGHT/FUEL TANK PRESSURE $\Delta GLOW/\Delta P_{FT}$, LB/PSI	920	1715	1574*	—	1148
5. GROSS LIFTOFF WEIGHT/OXID TANK PRESSURE, $\Delta GLOW/\Delta P_{OT}$, LB/PSI	1850	2825	2593*	—	2026
6. GROSS LIFTOFF WEIGHT/AFT SKIRT BASE DIAMETER, $\Delta GLOW/\Delta D_{AFT}$, LB/FT	7000*	12,530*	—	—	5160
7. GROSS LIFTOFF WEIGHT/AFT SKIRT LENGTH, $\Delta GLOW/\Delta L_{AFT}$, LB/FT	5620*	3000*	—	—	9928
(1) DRY INERTS (2) ASSUMED (3) VEHICLE 979-176					
*Data Derived From Other Exchange Ratios or Information Supplied					



3 MAR 1972

Figure 25

CHAMBER PRESSURE OPTIMIZATION (NASA PRESSURE-FED BOOSTER ENGINE)

LOX/RP-1
 $F_{SL} = 1.2 \text{ MLB}$
 $MR = 2.4$
 $\epsilon = 5.0$
 $\text{CHAMBER } L' = 70 \text{ IN.}$
 $C.R. = 1.8$
 $\% \text{ BELL} = 86$
 $\text{THRUST/EL} = 1000$

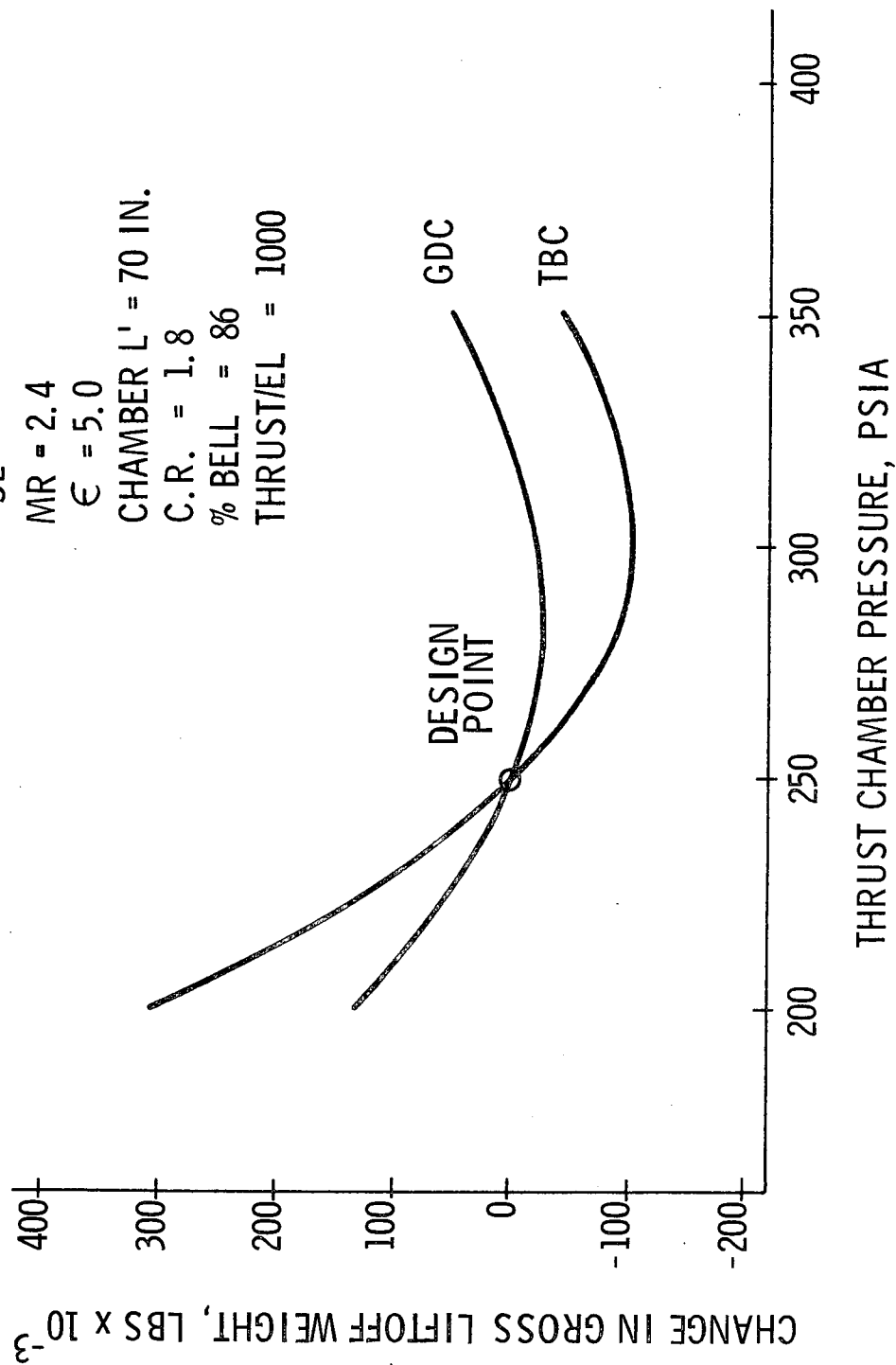


Figure 26



24 FEB 1972

SPECIFIC IMPULSE VS MR FOR LOX/RP-1 (NASA PRESSURE-FED BOOSTER ENGINE)

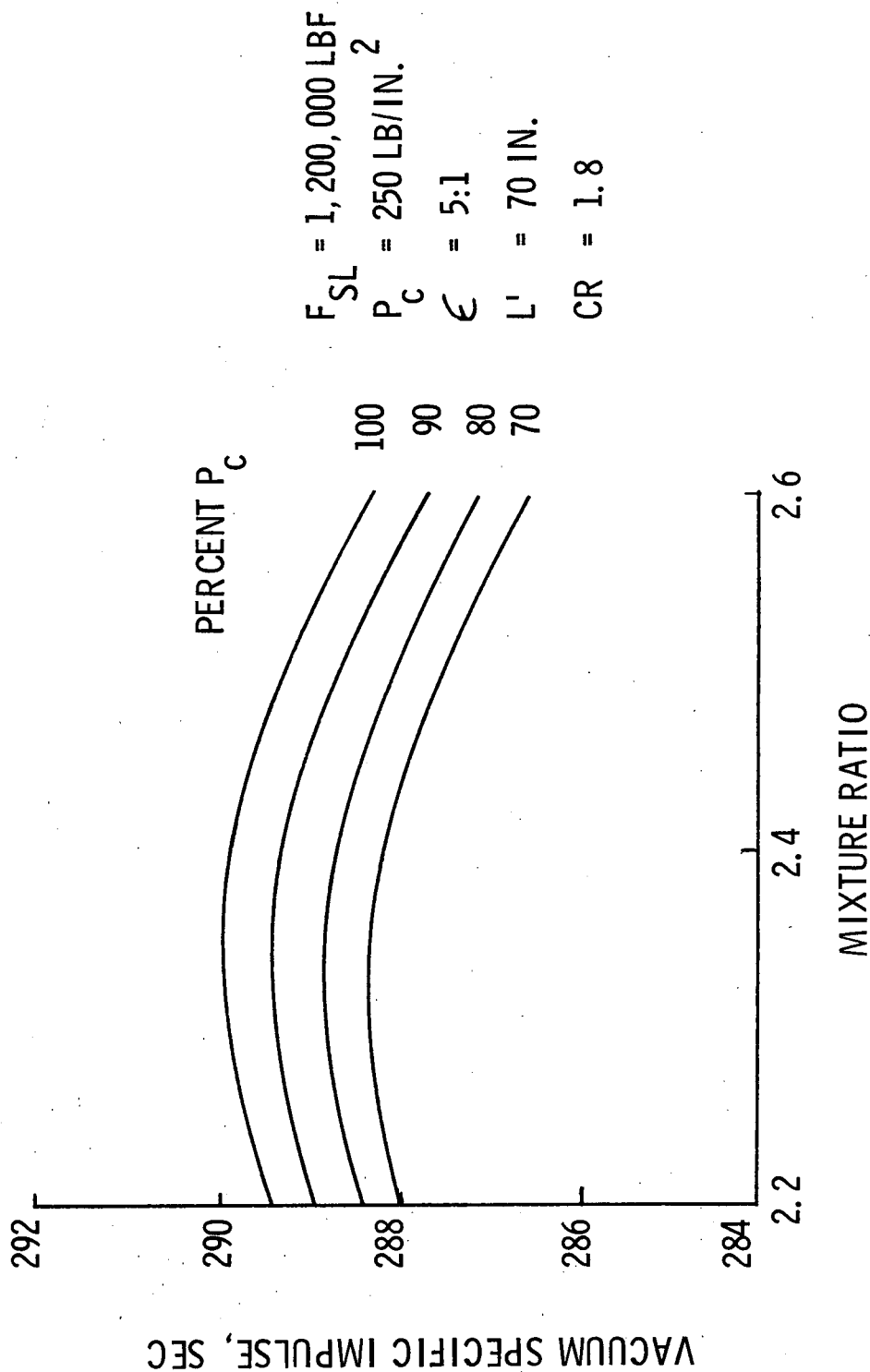


Figure 27



24 FEB 1972

MIXTURE RATIO OPTIMIZATION (NASA PRESSURE-FED BOOSTER ENGINE)

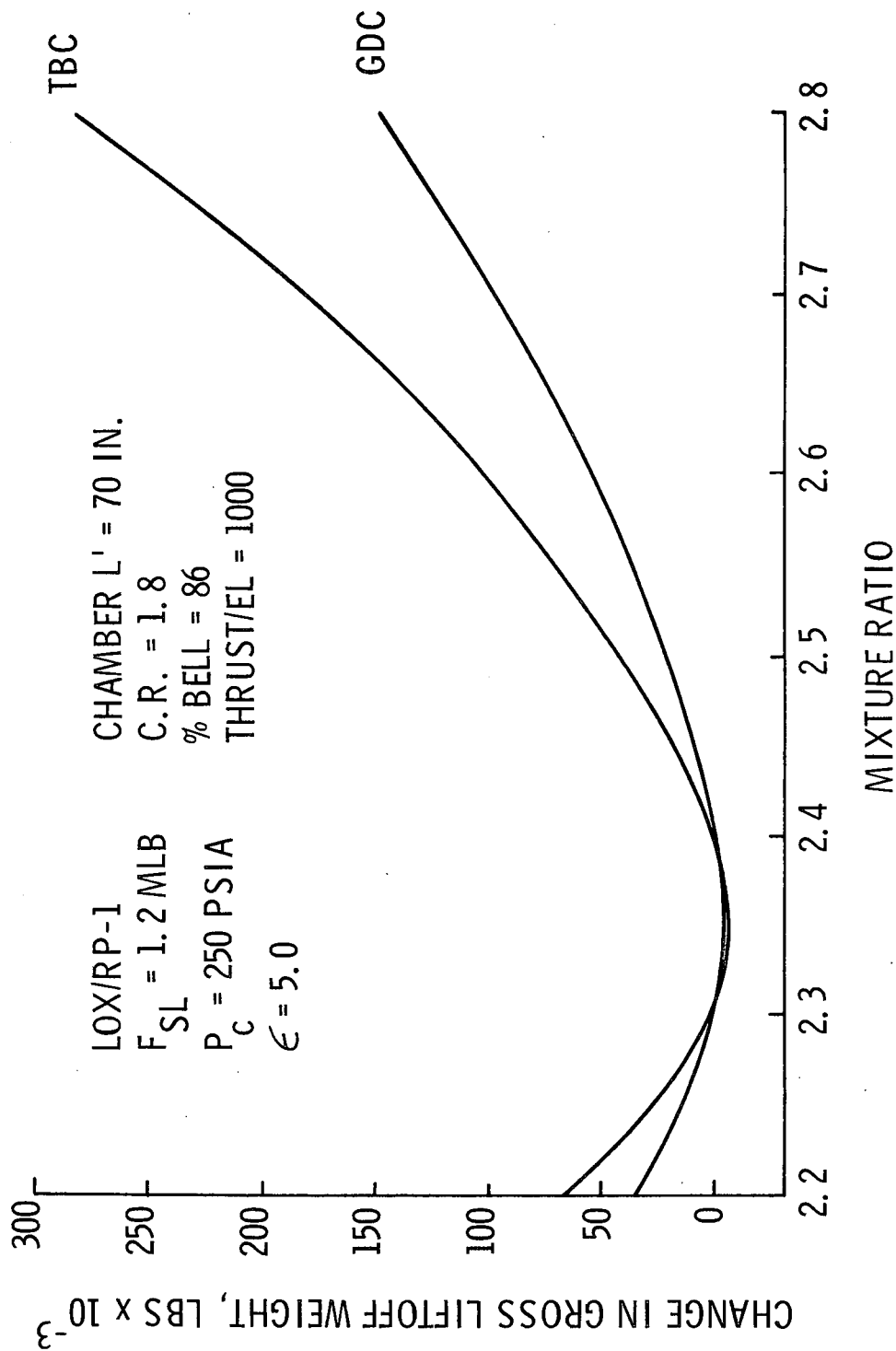


Figure 28



24 FEB 1972

CHAMBER LENGTH OPTIMIZATION (CURRENT EXCHANGE RATIOS TYPICAL OF CHRYSLER AND MDAC)

LOX/RP-1
 $F_{SL} = 1.2 \text{ M-LB}$
 $MR = 2.4$
 $P_c = 250 \text{ PSIA}$
 $\epsilon = 5.0$
 $C.R = 1.8$
 $\% \text{ BELL} = 86$

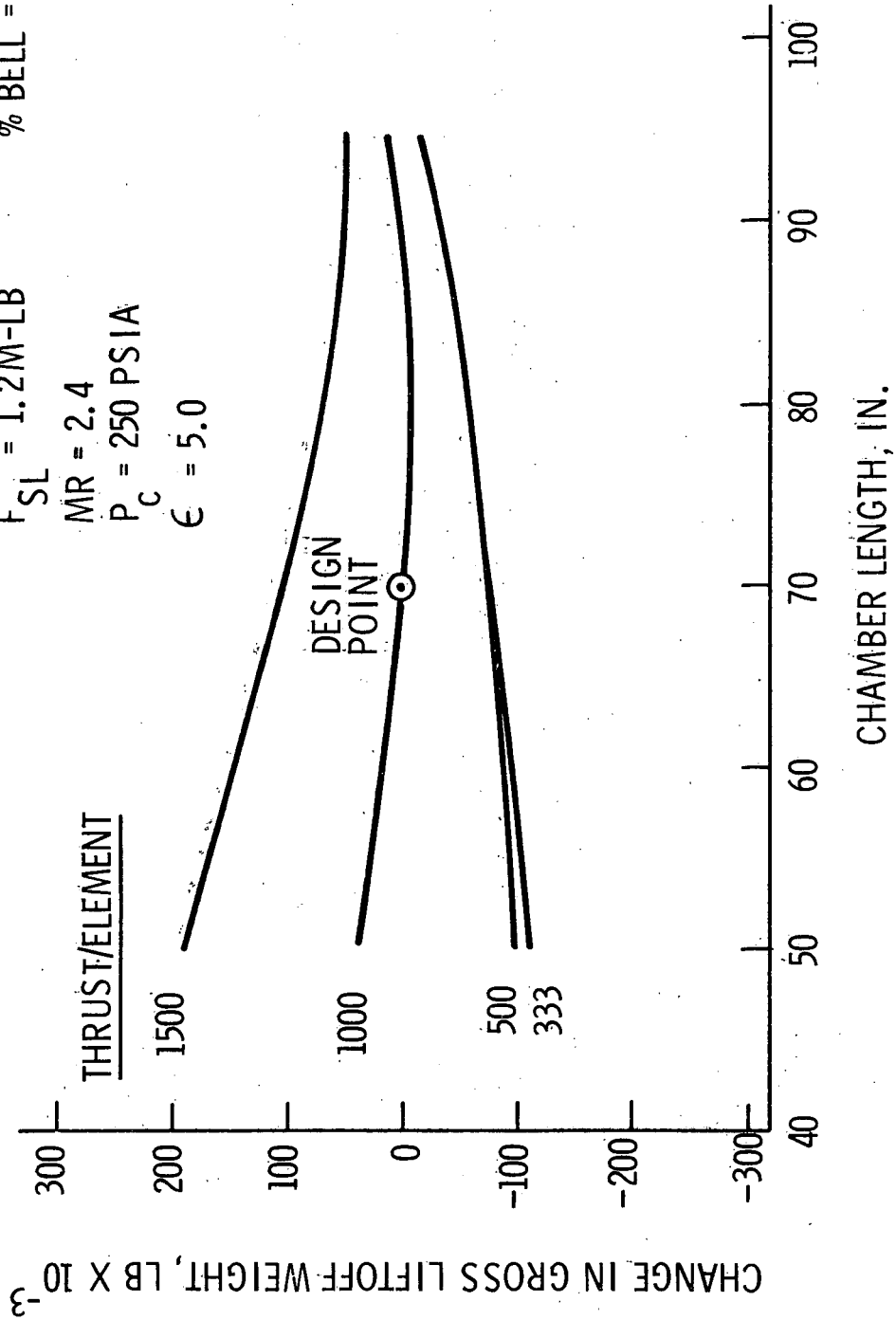


Figure 29



24 FEB 1972

CHAMBER LENGTH OPTIMIZATION (CURRENT EXCHANGE RATIOS TYPICAL OF GDC, MMC AND TBC)

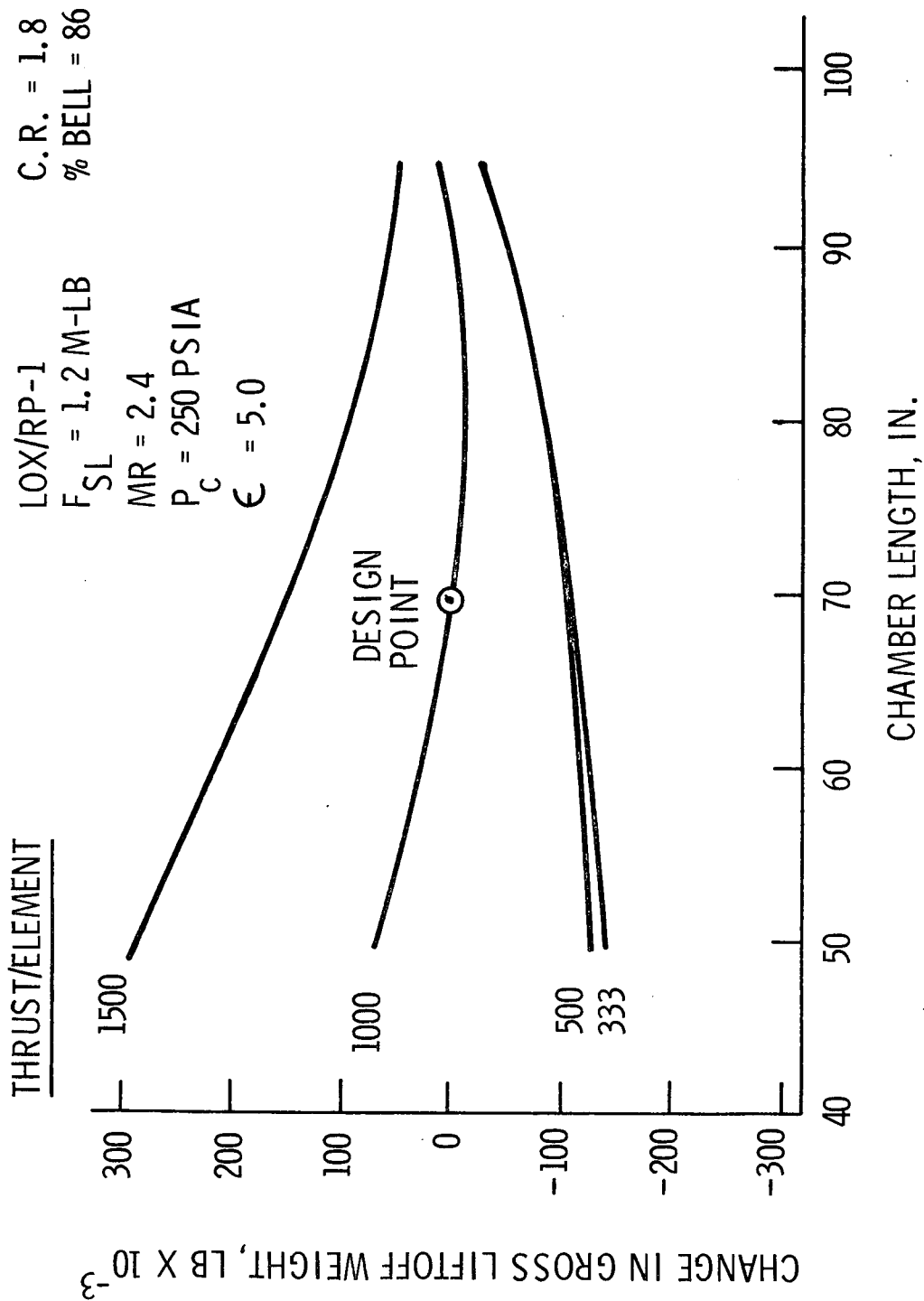


Figure 30



24 FEB 1972

NOZZLE SEPARATION DATA (NASA PRESSURE-FED BOOSTER ENGINE)

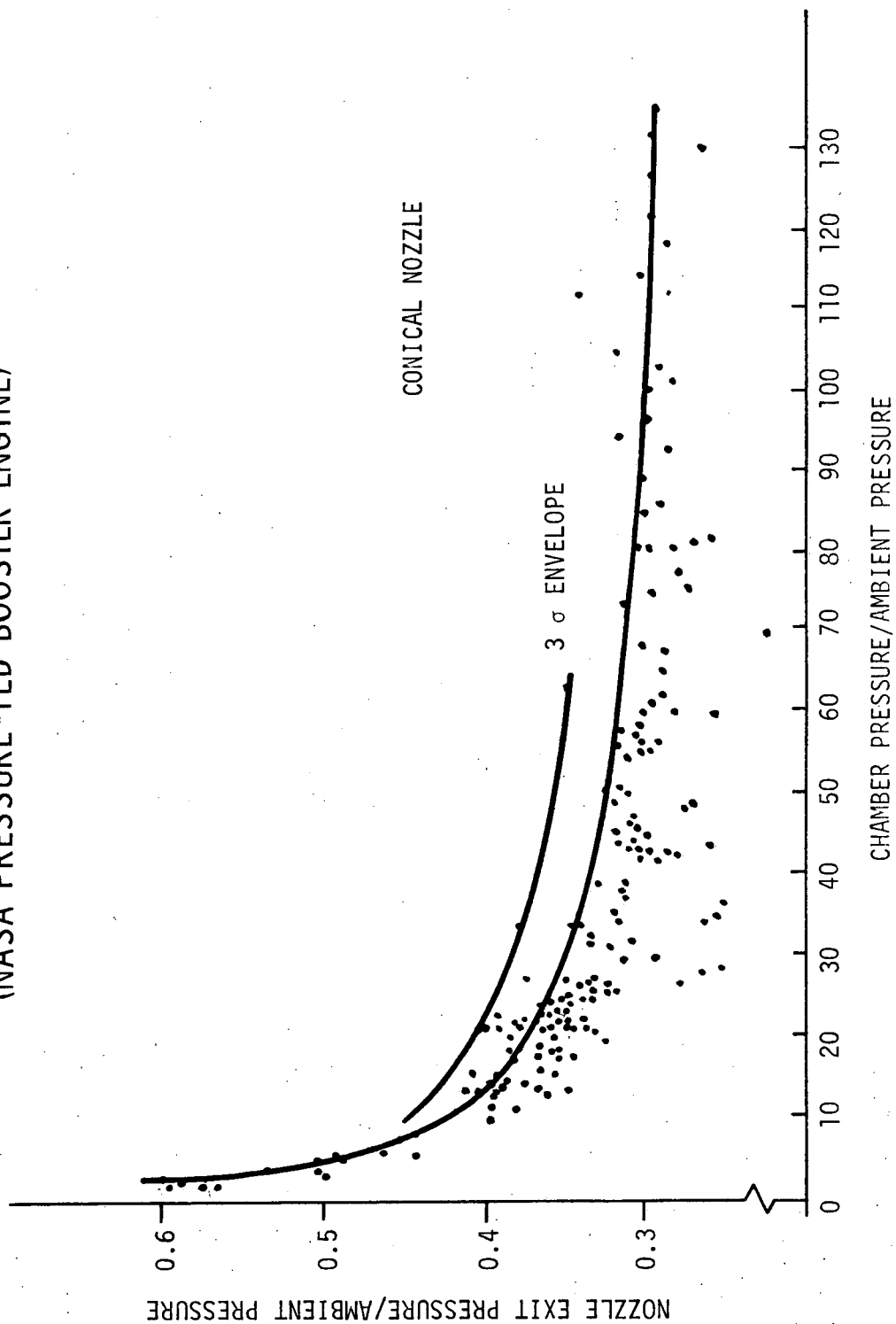


Figure 31



NOZZLE EXIT PRESSURE VARIATION WITH AREA RATIO (NASA PRESSURE-FED BOOSTER ENGINE)

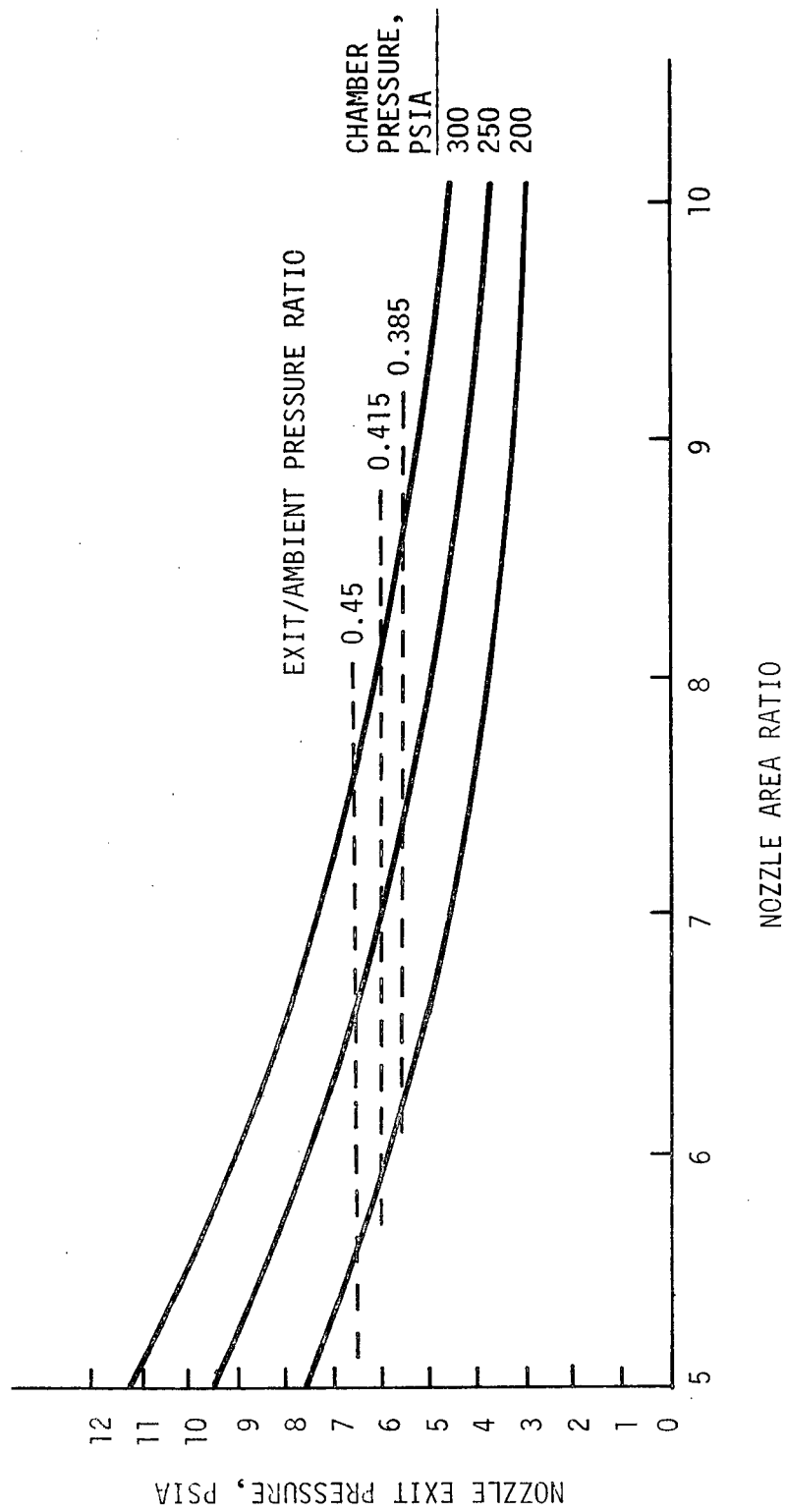


Figure 32



24 FEB 1972

AREA RATIO FOR NOZZLE SEPARATION AS FUNCTION OF THROTTLING CAPABILITY (NASA PRESSURE-FED BOOSTER ENGINE)

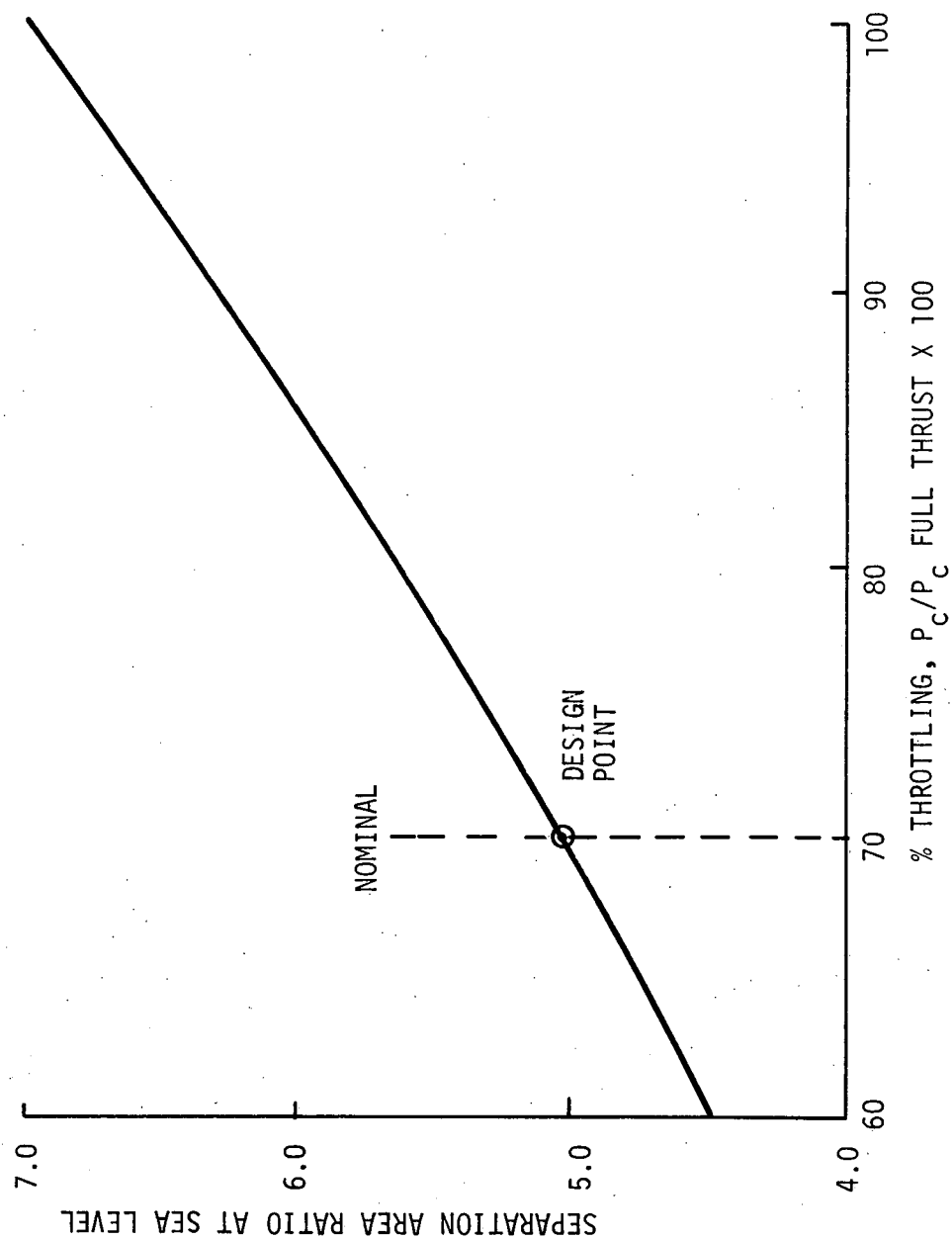


Figure 33



24 FEB 1972

NOZZLE AREA RATIO IMPACT ON GROSS LIFTOFF WEIGHT (NASA PRESSURE-FED BOOSTER ENGINE)

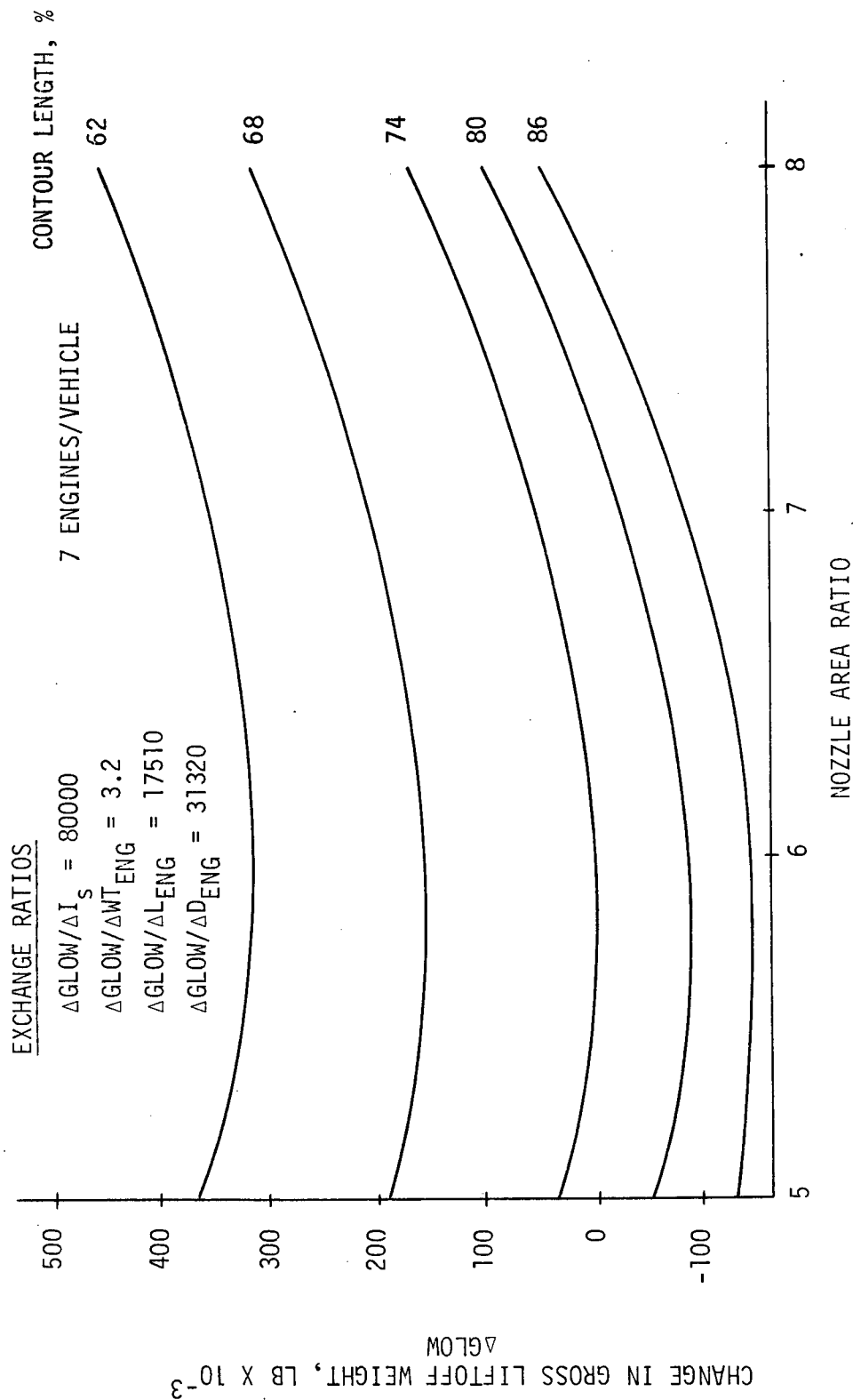


Figure 34



24 FEB 1972

NOZZLE CONTOUR LENGTH OPTIMIZATION (NASA PRESSURE-FED BOOSTER ENGINE)

LOX/RP-1
 $F_{SL} = 1.2M \text{ LB}$
 $P_C = 250 \text{ PSIA}$
 $MR = 2.4$
 $\epsilon = 5.0$
 CONTRACTION RATIO = 1.8
 CHAMBER LENGTH = 70 IN.
 THRUST/ELEMENT = 1000 LB

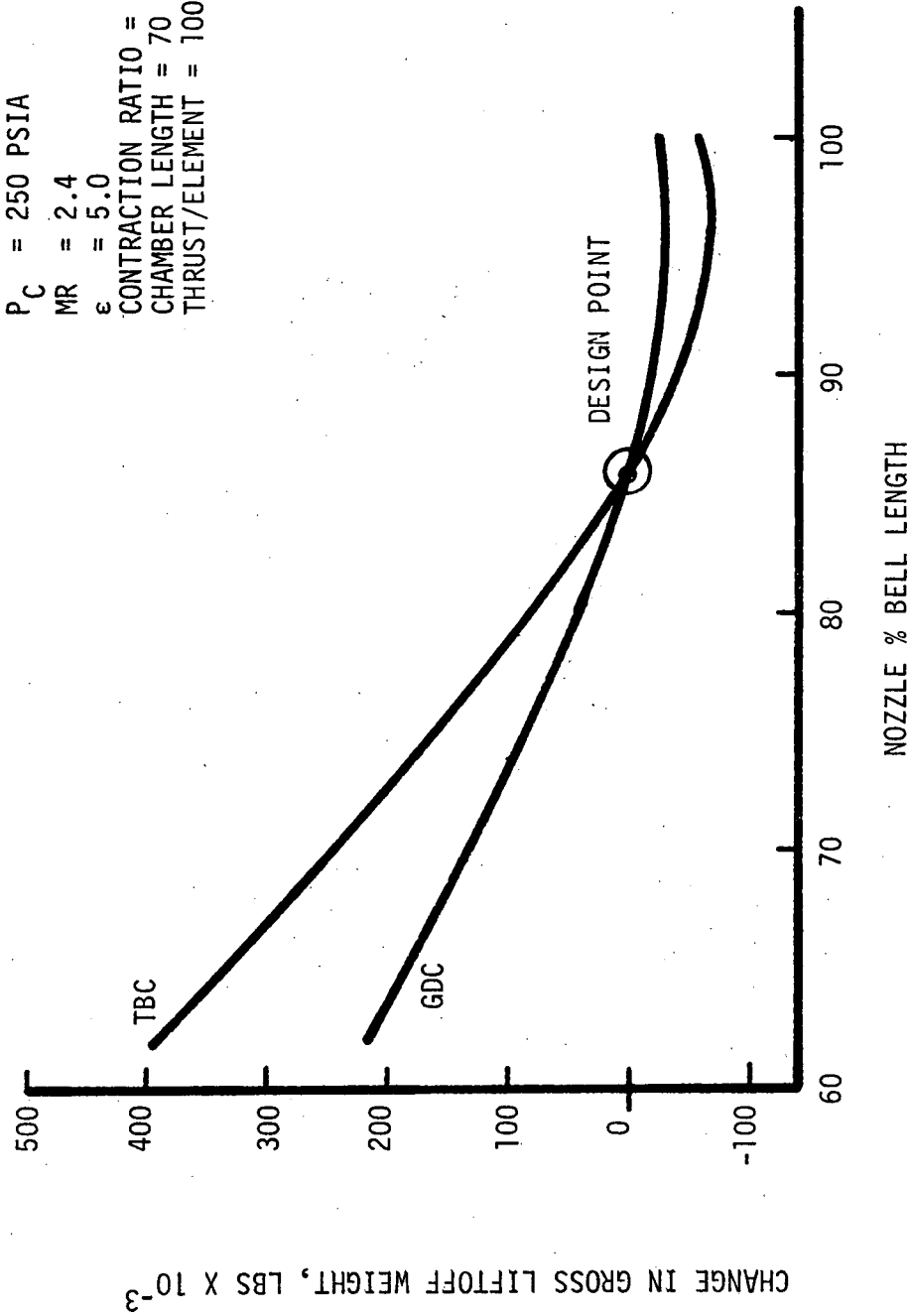


Figure 35



24 FEB 1972

VARIATION IN SPECIFIC IMPULSE WITH NOZZLE AREA RATIO (NASA PRESSURE-FED BOOSTER ENGINE)

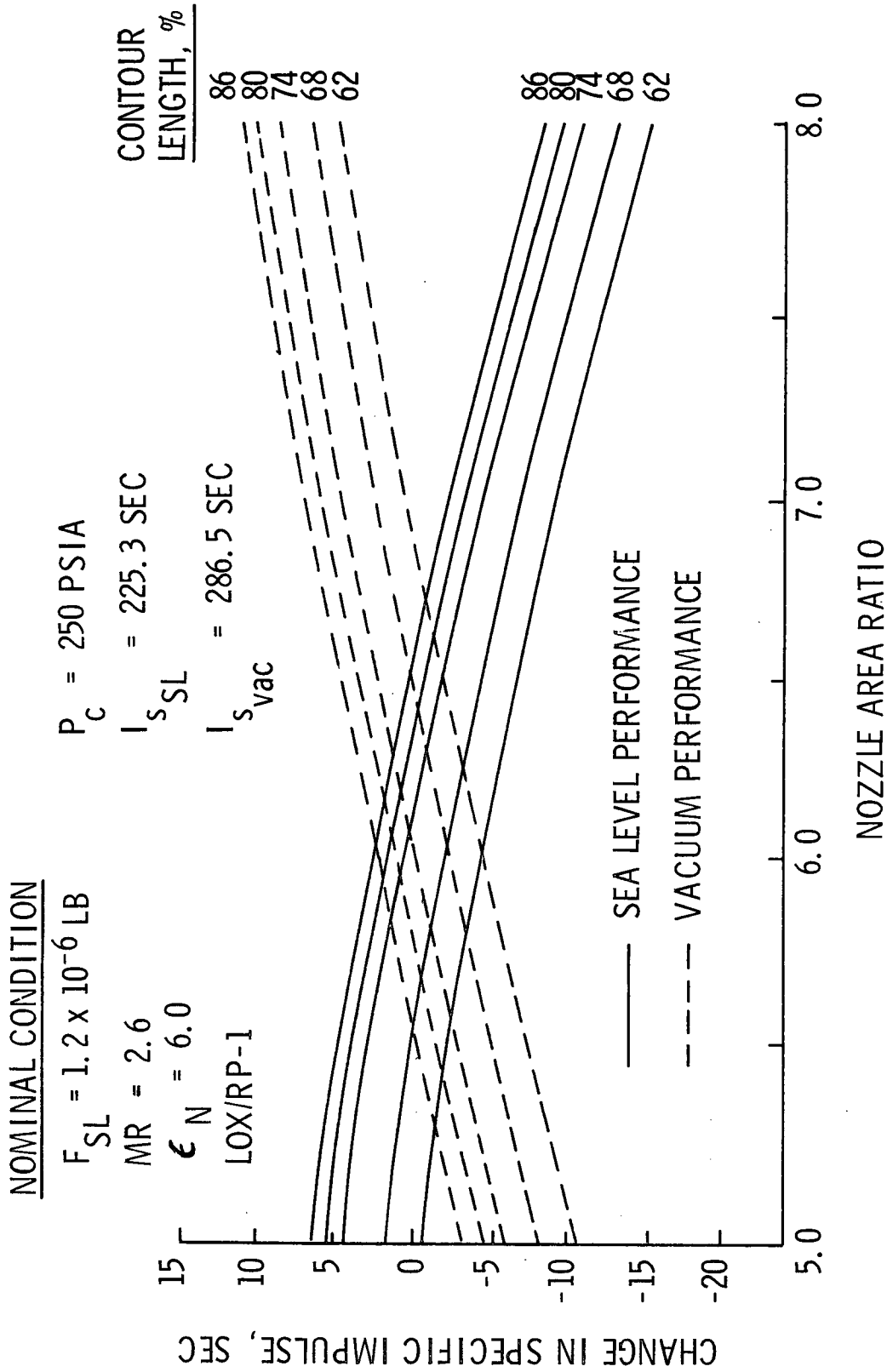


Figure 36



24 FEB 1972

VARIATION IN ENGINE WEIGHT WITH NOZZLE AREA RATIO (NASA PRESSURE-FED BOOSTER ENGINE)

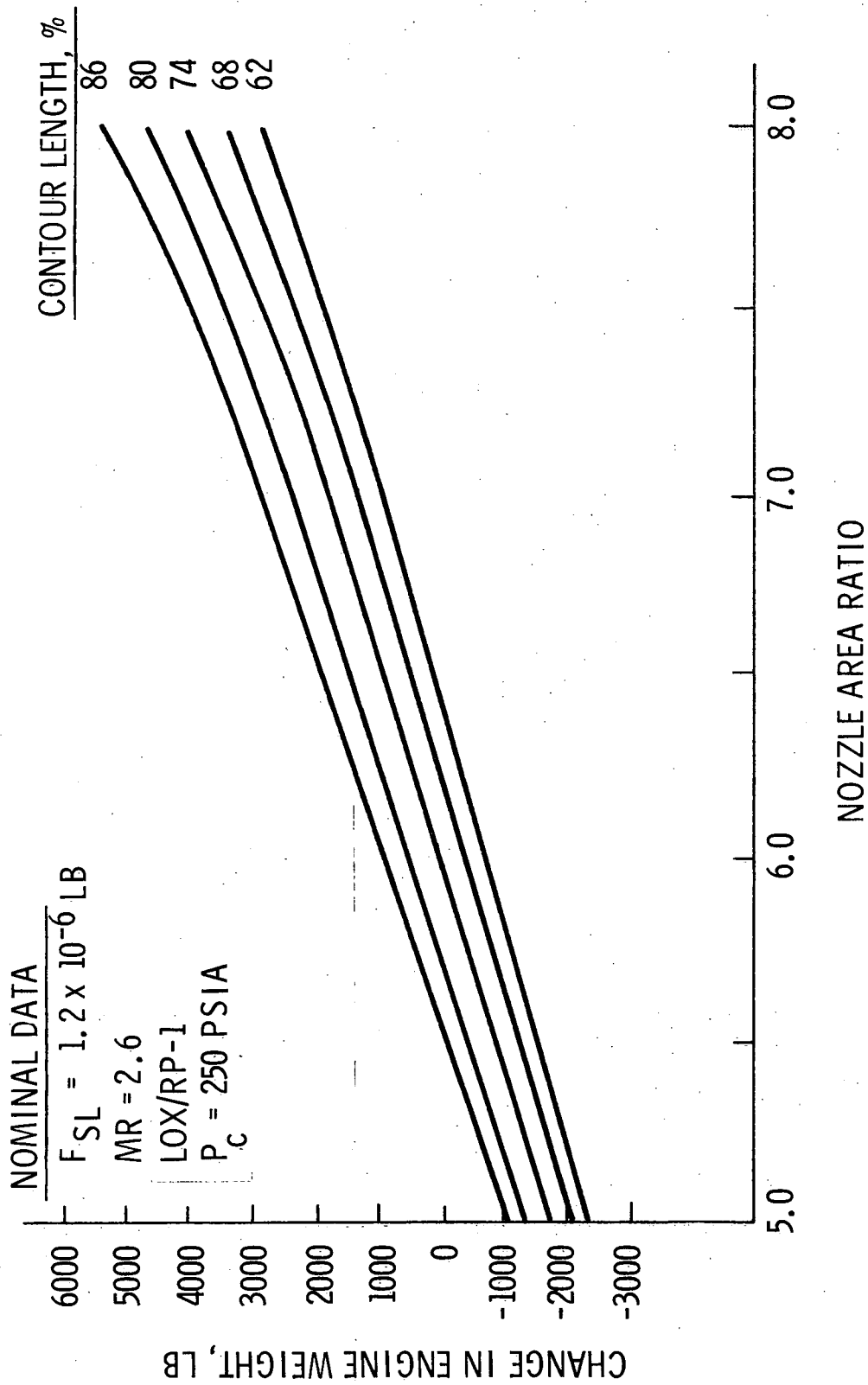
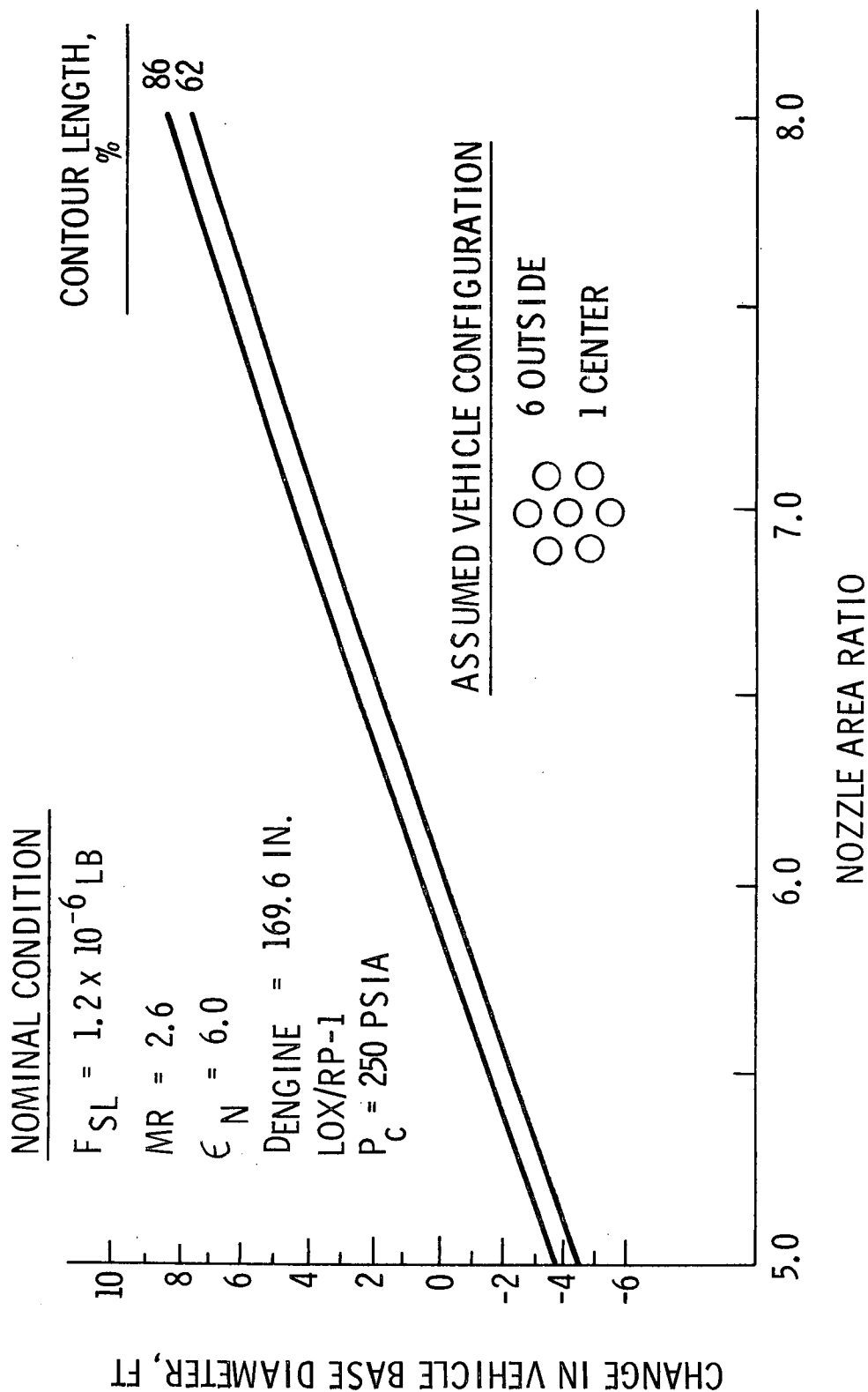


Figure 37



24 FEB 1972

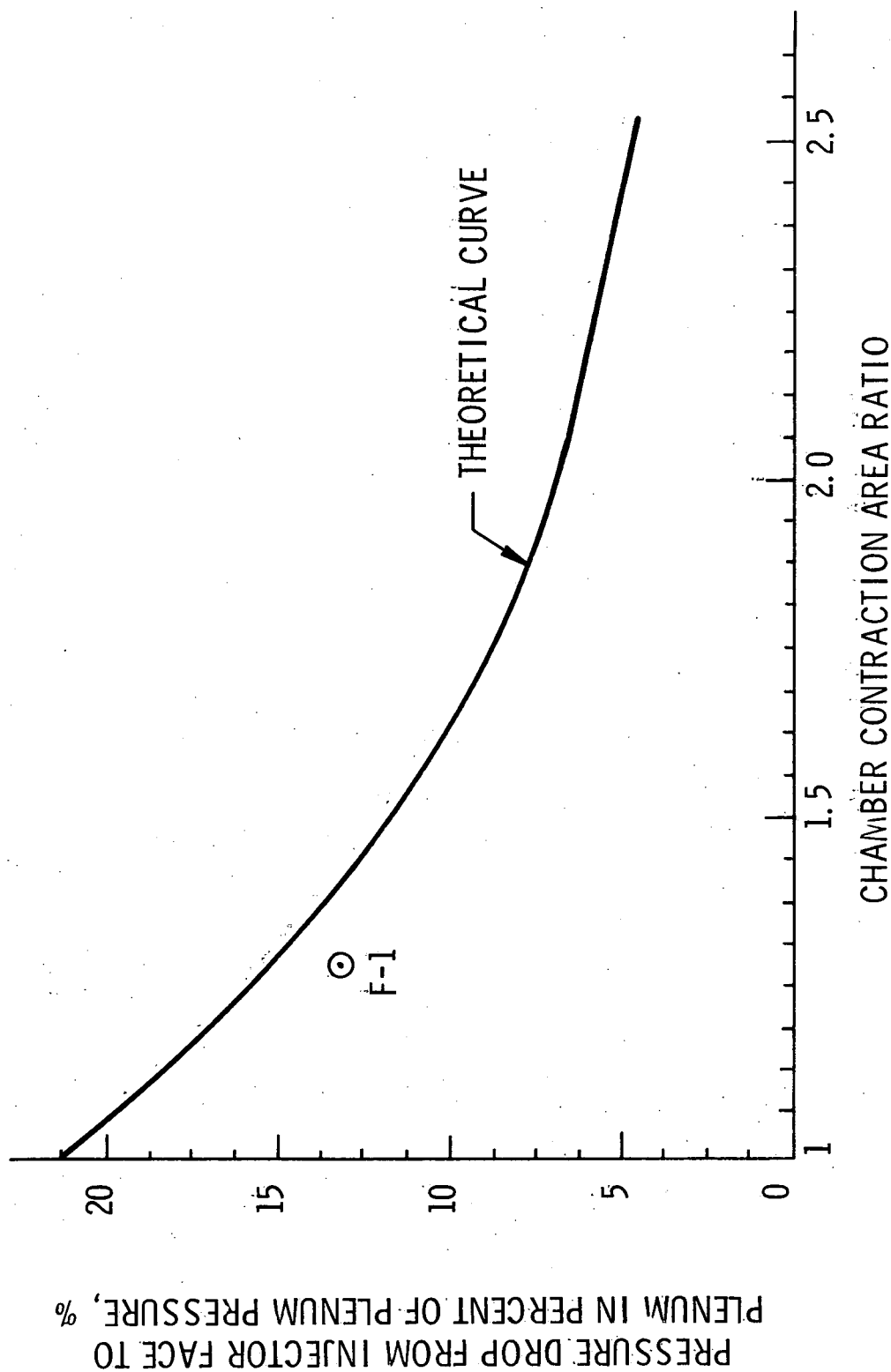
STAGE DIAMETER VARIATION WITH NOZZLE AREA RATIO (NASA PRESSURE-FED BOOSTER ENGINE)



24 FEB 1972

Figure 38

CHAMBER PRESSURE DROP DUE TO COMBUSTION (NASA PRESSURE-FED BOOSTER ENGINE)



24 FEB 1972



Figure 39

VARIATION IN INLET PRESSURE WITH CONTRACTION RATIO
(NASA PRESSURE-FED BOOSTER ENGINE)
FUEL AND OXIDIZER CIRCUITS

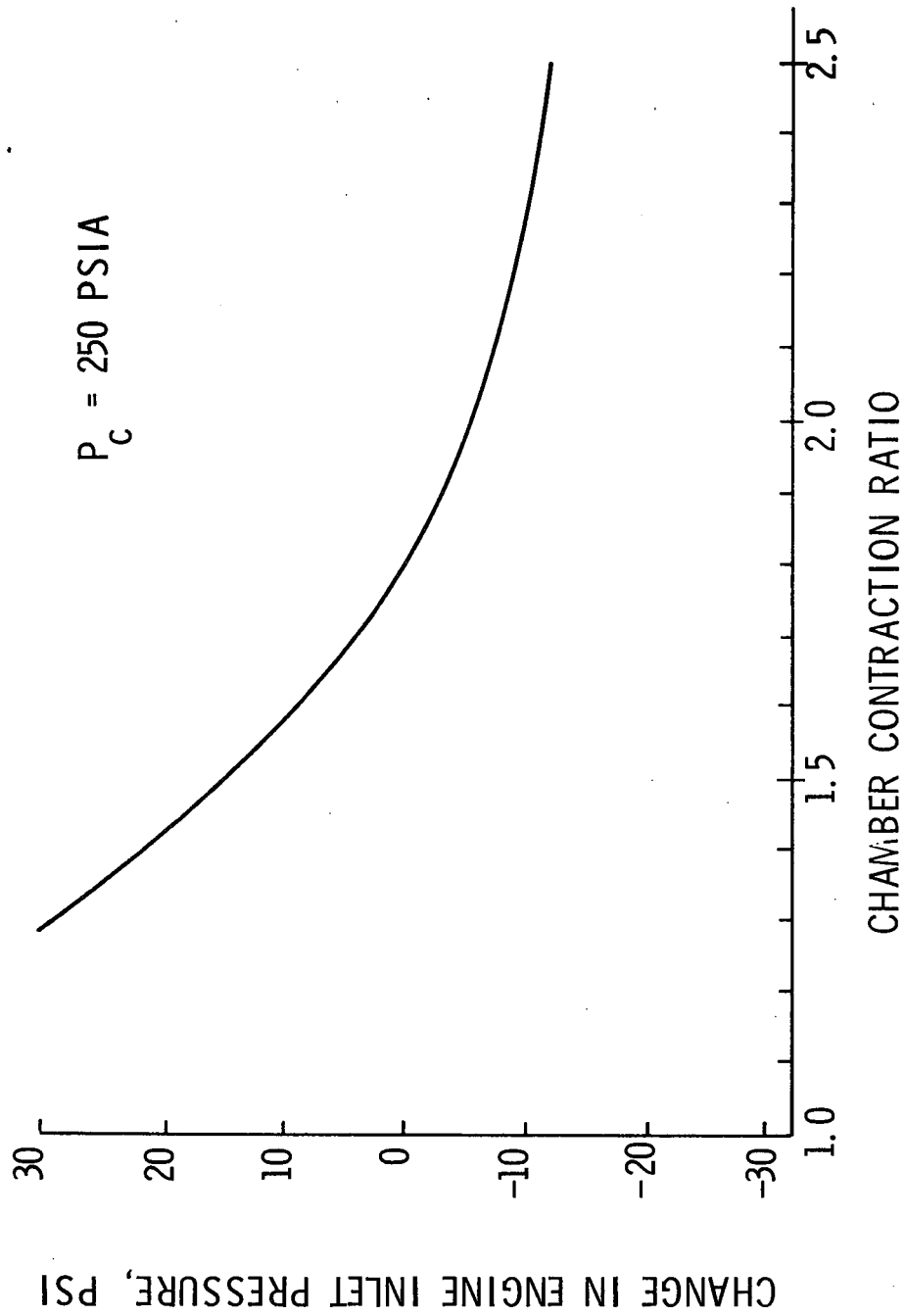
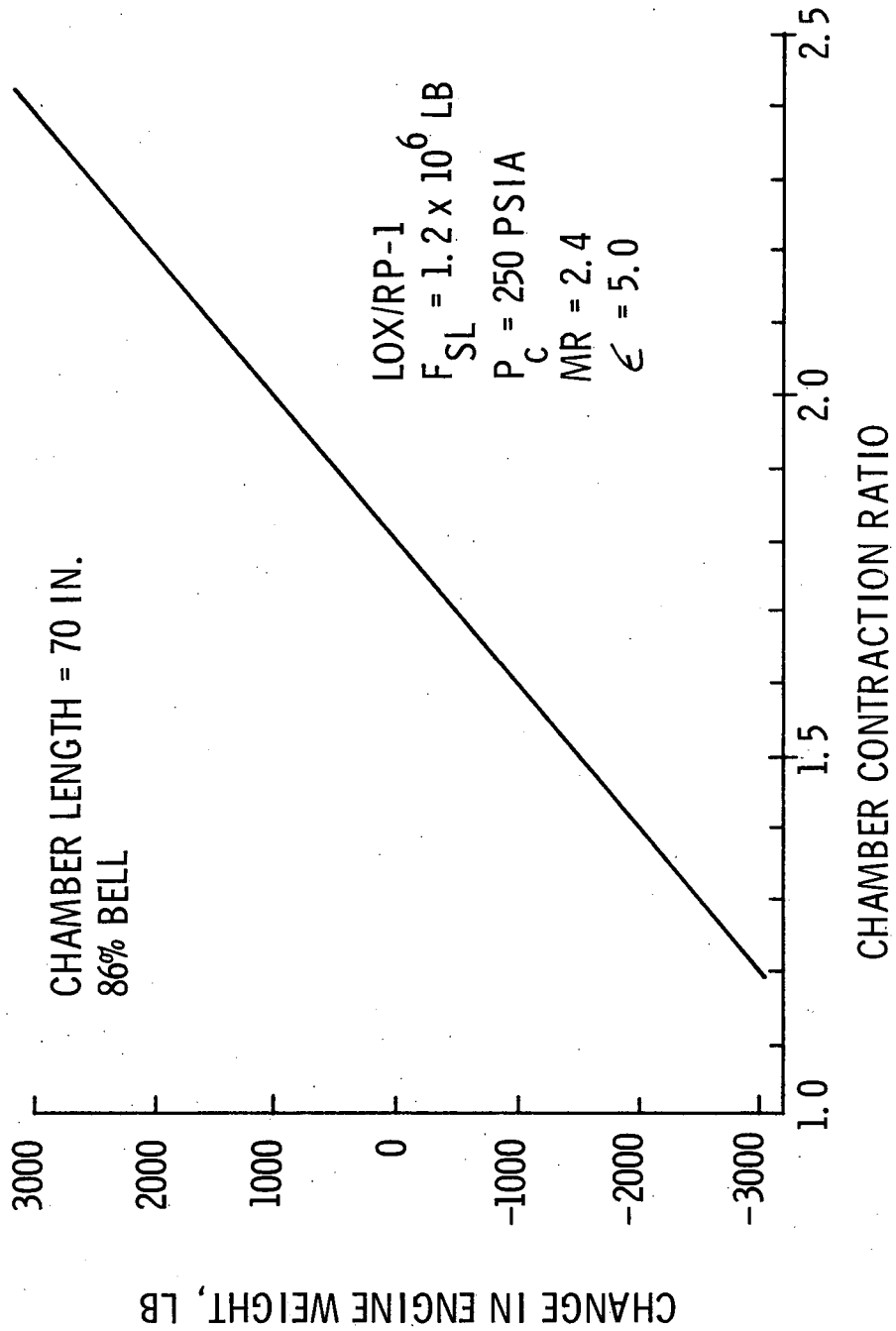


Figure 40



24 FEB 1972

ENGINE WEIGHT VARIATION WITH CONTRACTION RATIO (NASA PRESSURE-FED BOOSTER ENGINE)



24 FEB 1972

Figure 41

CONTRACTION RATIO OPTIMIZATION (NASA PRESSURE-FED BOOSTER ENGINE)

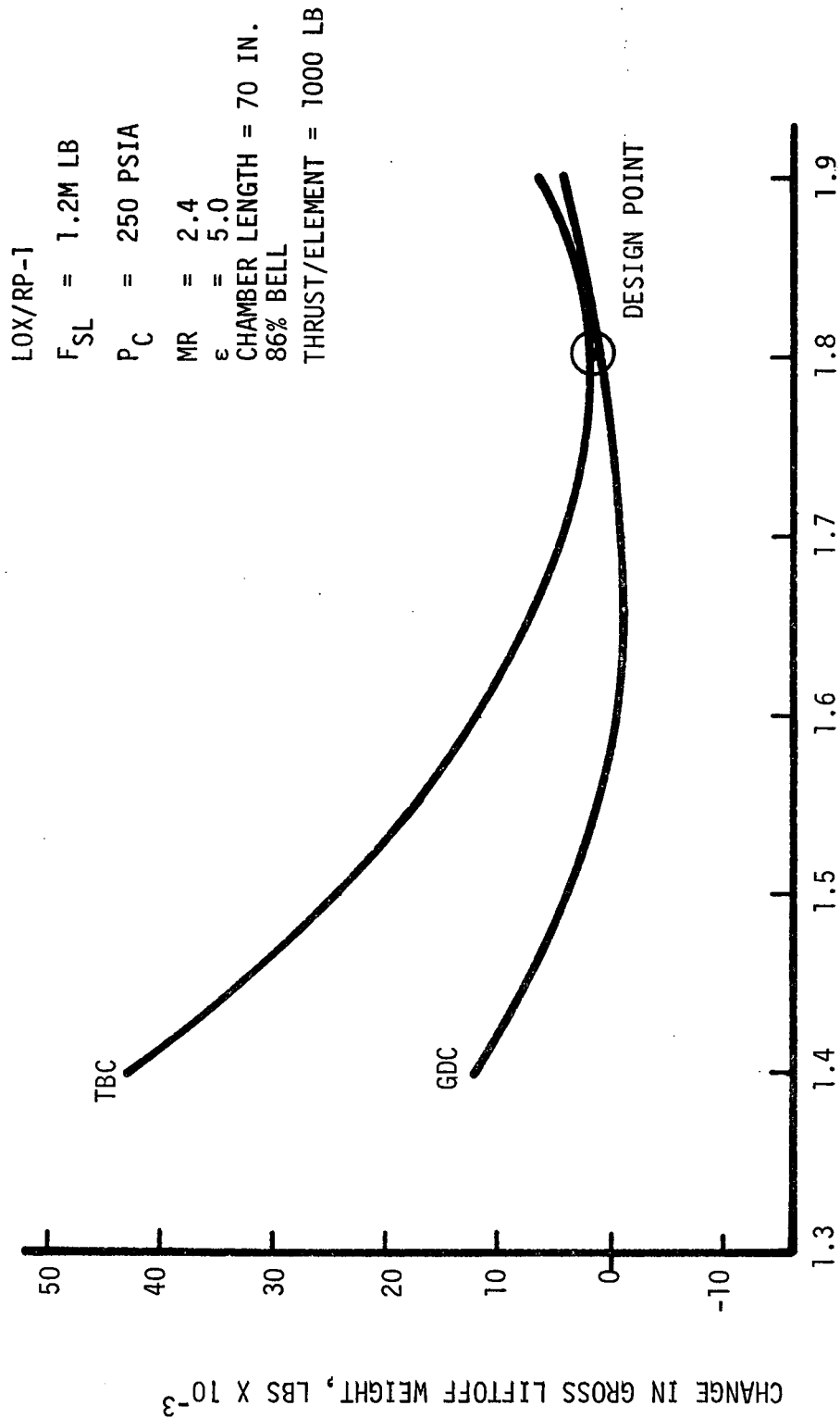


Figure 42



24 FEB 1972

PROPELLANT LINE VELOCITY EFFECTS ON VEHICLE LIFTOFF WEIGHT (NASA PRESSURE-FED BOOSTER ENGINE)

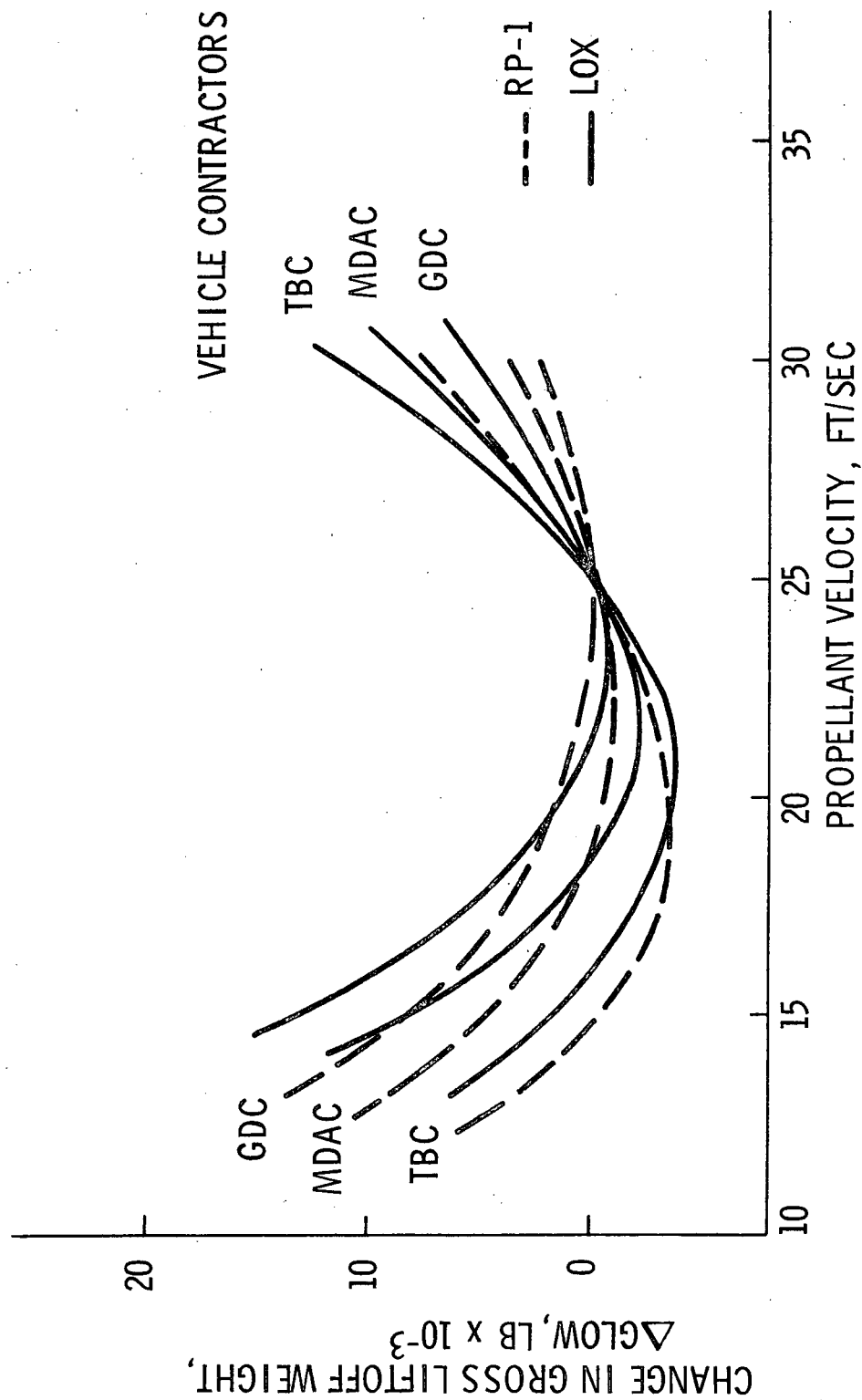


Figure 43



24 FEB 1972

PROPELLANT LINE VELOCITY OPTIMIZATION (NASA PRESSURE-FED BOOSTER ENGINE)

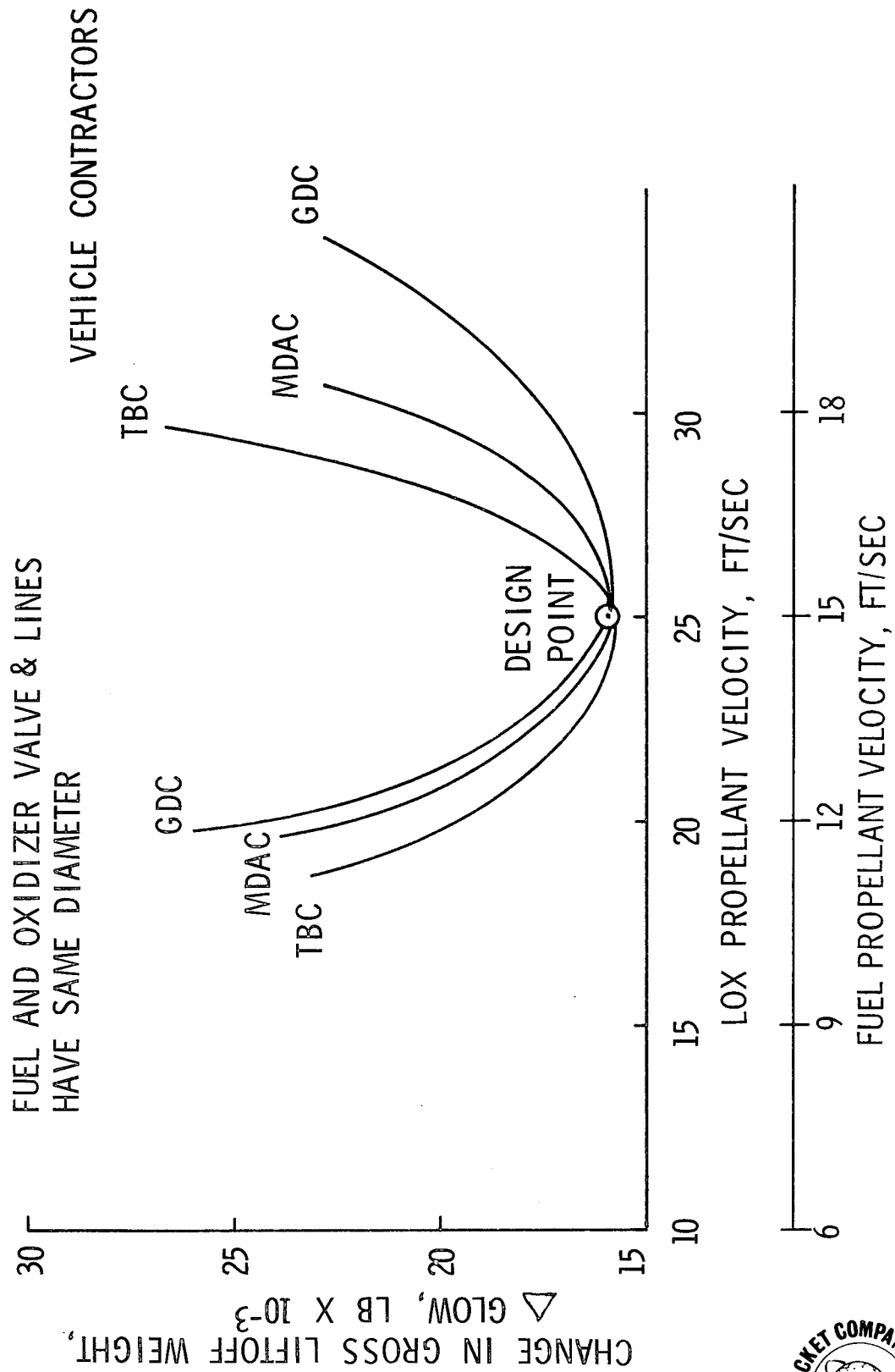


Figure 44

24 FEB 1972

PRESSURE-FED ENGINE REGENERATIVELY-COOLED CHAMBER (NASA PRESSURE-FED BOOSTER ENGINE)

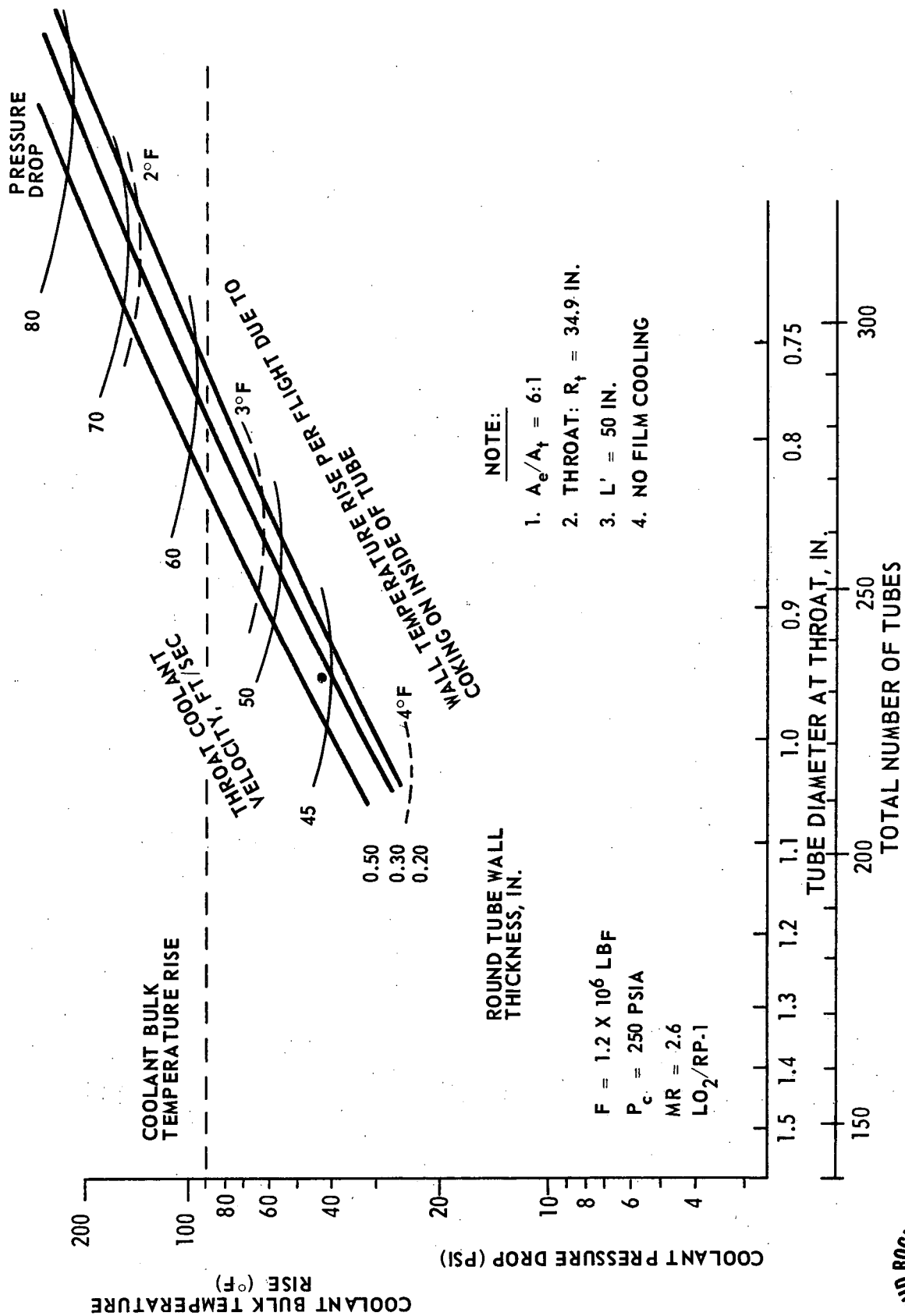
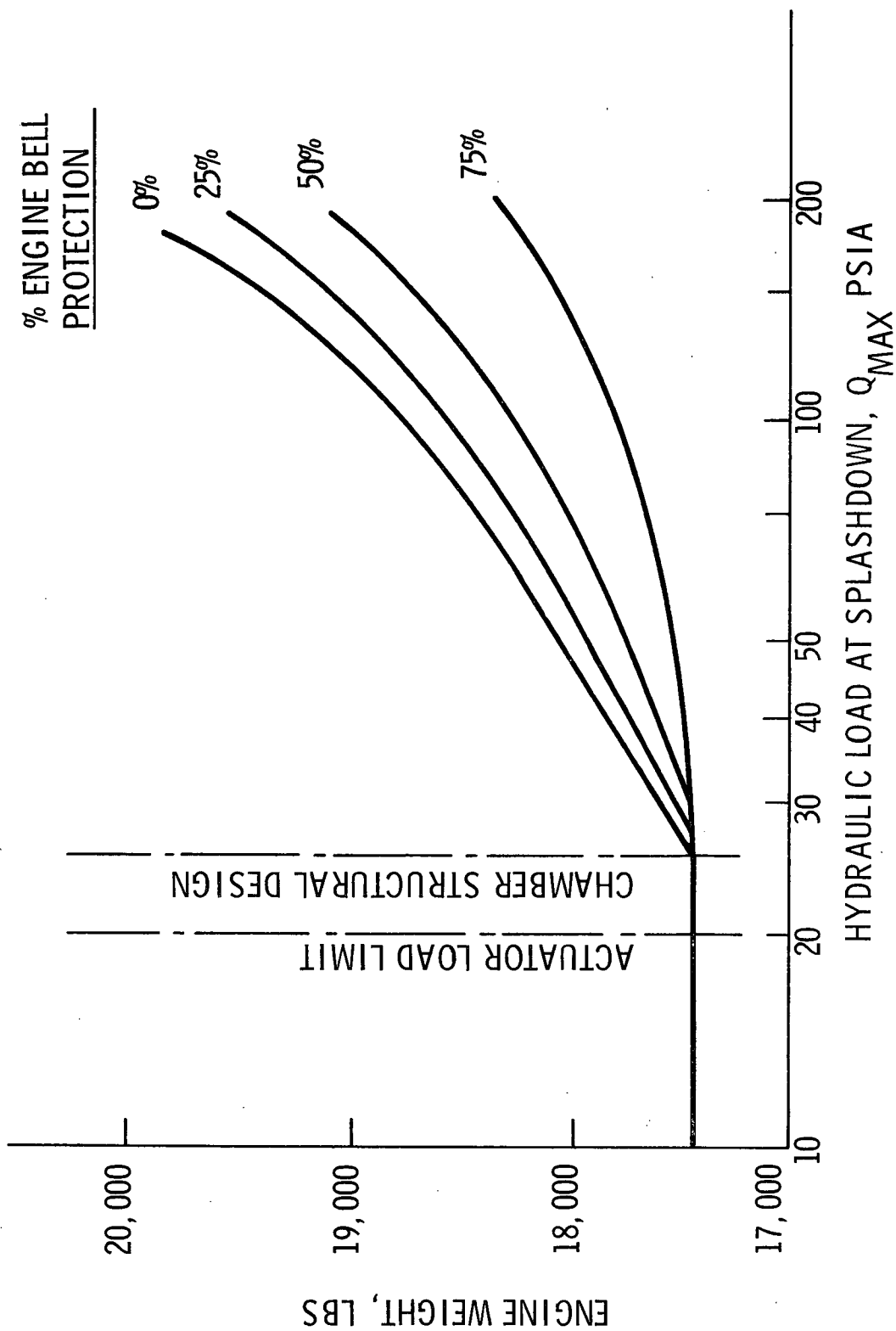


Figure 45



HYDRAULIC LOAD INFLUENCE ON ENGINE WEIGHT (NASA PRESSURE-FED BOOSTER ENGINE)



24 FEB 1972

Figure 46

EFFECTS OF VEHICLE RECOVERY IMPACT ON ENGINE & ACTUATOR (NASA PRESSURE-FED BOOSTER ENGINE)

BASED ON BOEING IMPACT DECELERATION DATA

ENGINE CHARACTERISTICS

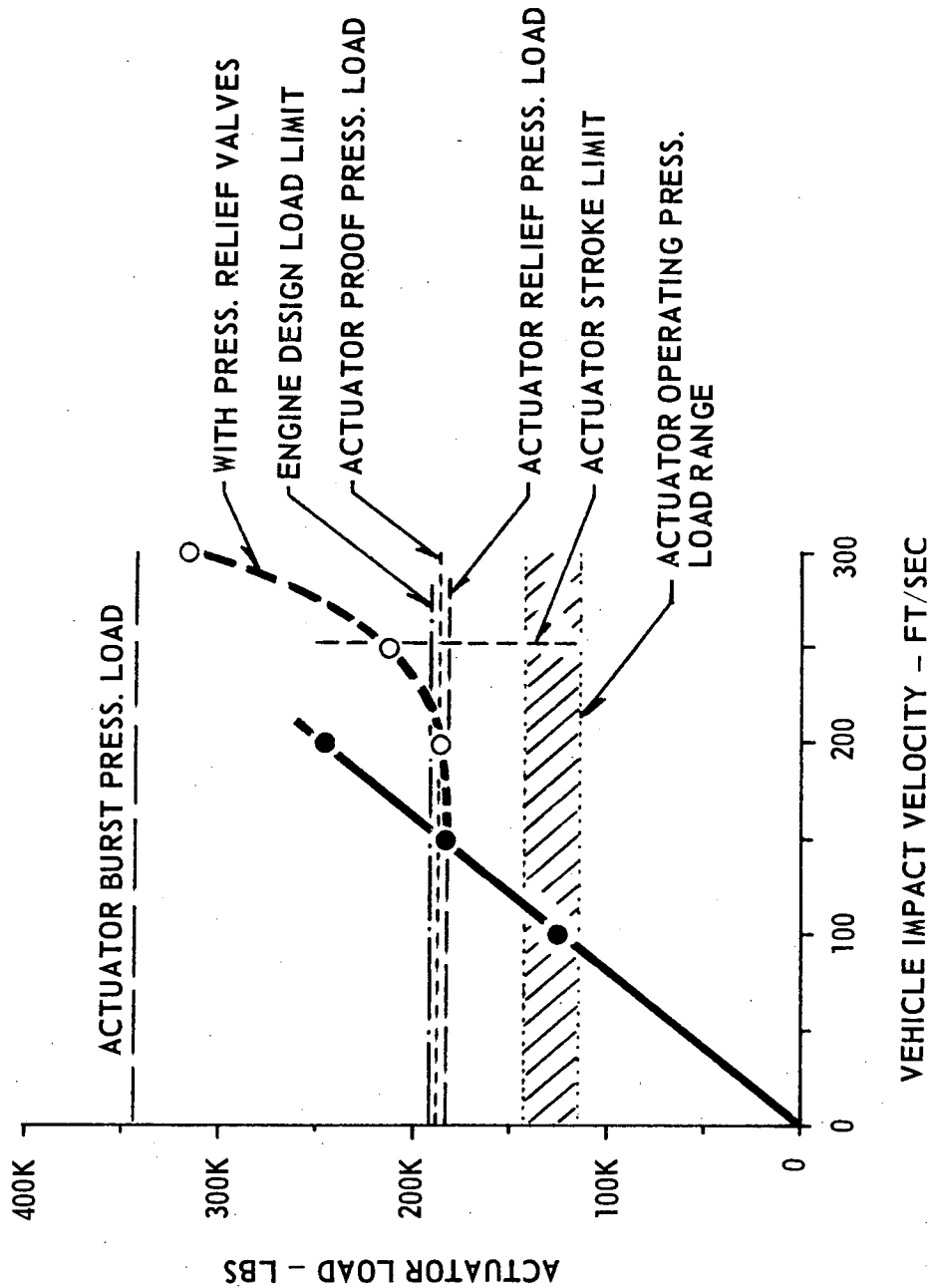
$L' = 70$ INCHES

$I_{GP} = 41,042$ SLUG-FT²
(ENGINE DRY)

PORTING CHARACTERISTICS

PRESSURE = 3250 PSI

ORIFICE = 0.7500 DIA.



24 FEB 1972

Figure 47

DESIGN CONDITIONS CORRELATED WITH VAPORIZATION MODEL
(NASA PRESSURE-FED BOOSTER ENGINE)

PROPELLANT COMB.:

CRYOGENIC
EARTH STORABLE
SPACE STORABLE

INJECTOR ELEMENT TYPES:

DOUBLETS
TRIPLETS
QUADLETS
PENTADS
MICRO ORIFICE (HIPERTHIN)
CO-AXIAL
VORTEX
SHOWERHEAD

THRUST / ELEMENT:

< 0.1 TO 40,000 LB

PROPELLANT STATE:

LIQUID / LIQUID
LIQUID / GAS



24 FEB 1972

PERFORMANCE LOSS EVALUATION

$$\boxed{\text{DELIVERED VACUUM } I_{SP}} = \boxed{(I_{SP}^{ODE})_{O/F}} - \boxed{I_{SP}^{LOSSES}}$$

PERFORMANCE LOSSES

MATHEMATICAL REPRESENTATION**

$$\boxed{\text{ENERGY RELEASE LOSS, ERL}} = \sum_i^n \left[I_{spODE(O/F)_i} \dot{m}_i - I_{spODE(O/F)_{Vi}} \dot{m}_{Vi} \right] \frac{1}{\dot{m}_T}$$

$$\boxed{\text{MIXTURE RATIO MAL-DISTRIBUTION LOSS, MRDL}} = I_{spODE(O/F)_{OA}} - \sum_i^n \left(I_{spODE(O/F)_i} \cdot \frac{\dot{m}_i}{\dot{m}_T} \right)$$

$$\boxed{\text{FILM COOLING LOSS}} = I_{spODE(O/F)_{OA}} \dot{m}_{core} I_{sp(O/F)_{core H}} + \dot{m}_{coolant}$$

$$\boxed{\text{KINETIC LOSS, KL}^*} = \sum_i^n \left[I_{spODE(O/F)_{Vi}} - I_{spODK(O/F)_{Vi}} \right] \frac{\dot{m}_{Vi}}{\dot{m}_T}$$

$$\boxed{\text{BOUNDARY LAYER LOSS (BLL)}} = \frac{(\Delta F_{BLL}^{(O/F)})_v}{\dot{m}_T}$$

$$\boxed{\text{DIVERGENCE LOSS, DL}} = I_{sp_{del}} \frac{1 - \eta_{DIV}}{\eta_{DIV}}$$

Figure 49

* Loss estimated to be less than 0.3% for pressure fed booster engines
 ** See list of symbols in text

JANNAF PROCEDURE
SEA LEVEL SPECIFIC IMPULSE CALCULATION
(NASA PRESSURE-FED BOOSTER ENGINE)

$$I_{spSL} = I_{spvac} - ERL - DL - KL - MRDL - BLL - FCL - PA + A_e \dot{W}_T$$

WHERE:

PA = SEA LEVEL BAROMETRIC PRESSURE, PSIA

A_e = EXIT AREA, IN.²

\dot{W}_T = TOTAL ENGINE FLOW RATE, LBS/SEC



24 FEB 1972

Figure 50

SENSITIVE TIME LAG CHARACTERISTICS (NASA PRESSURE-FED BOOSTER ENGINE)

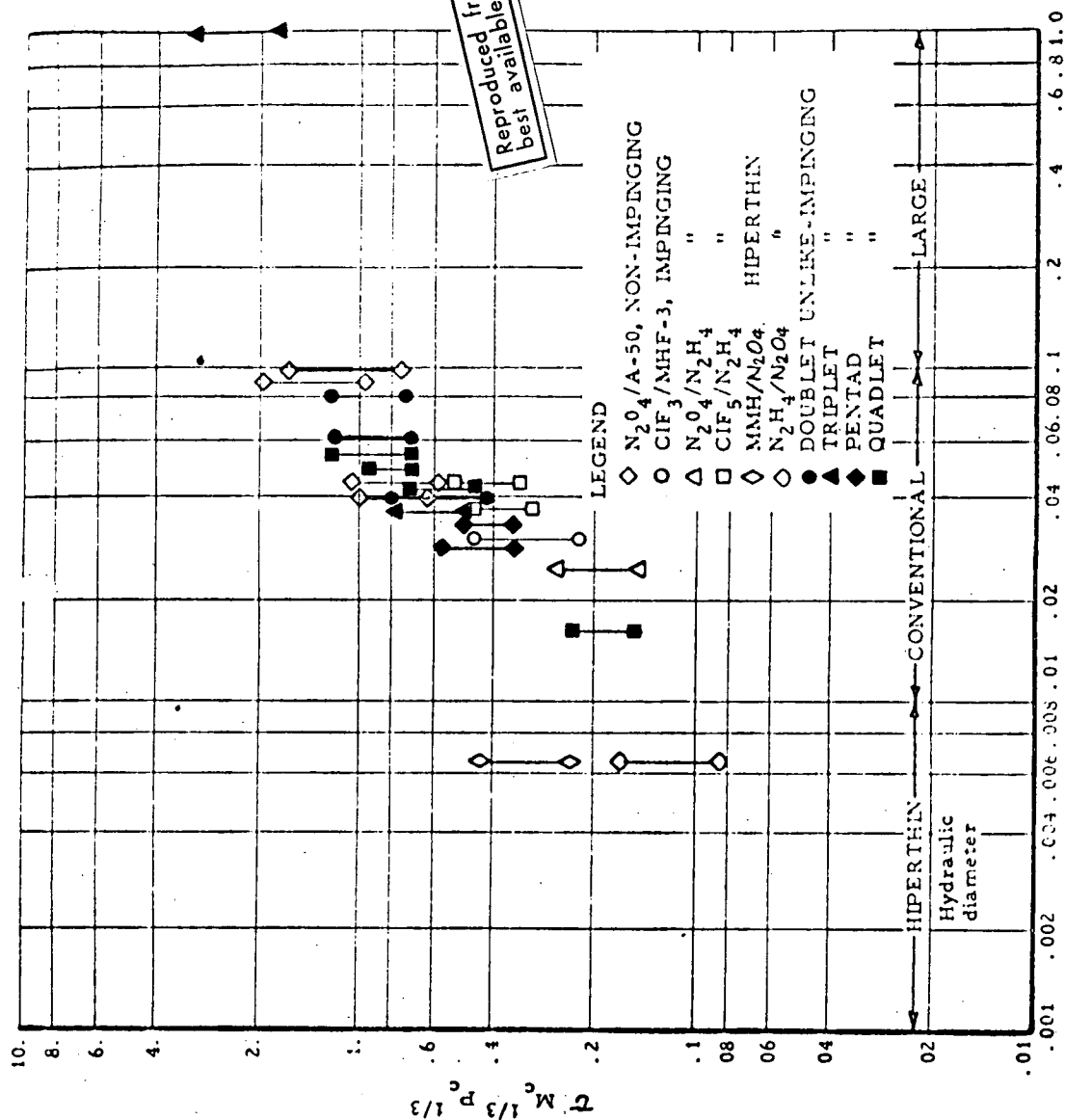


Figure 51



24 FEB 1972

PRESSURE-FED ENGINE (STABILITY) (NASA PRESSURE-FED BOOSTER ENGINE) RELATIONSHIP

- NOTE:
1. 1000 LB THRUST / ELEMENT INJECTOR
 2. 92 IN. DIAMETER CHAMBER

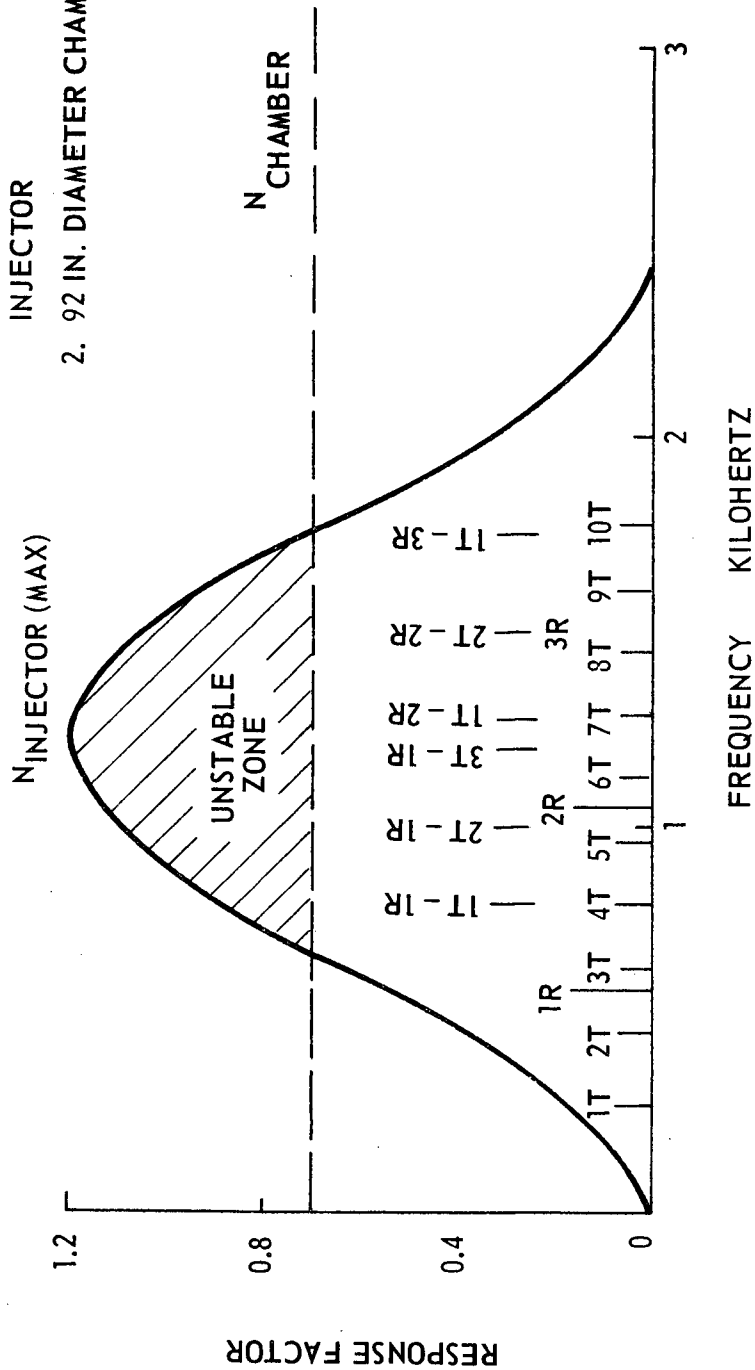


Figure 52



24 FEB 1972

BLOCK DIAGRAM OF LOW-FREQUENCY COMBUSTION INSTABILITY (NASA PRESSURE-FED BOOSTER ENGINE)

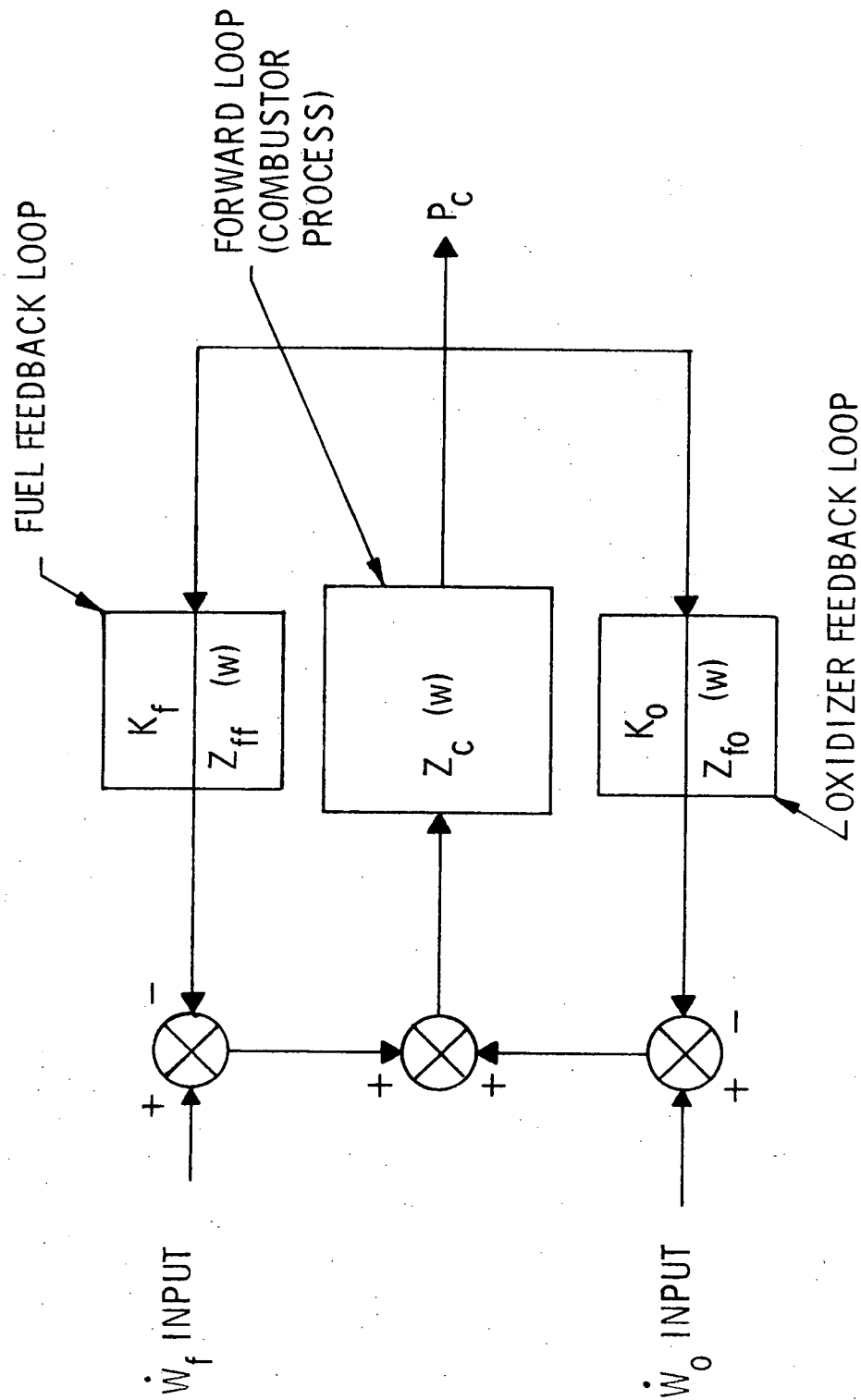


Figure 53



24 FEB 1972

NYQUIST DIAGRAM FOR TYPICAL ENGINE WITH
FEED SYSTEM RESONANCES
(NASA PRESSURE-FED BOOSTER ENGINE)

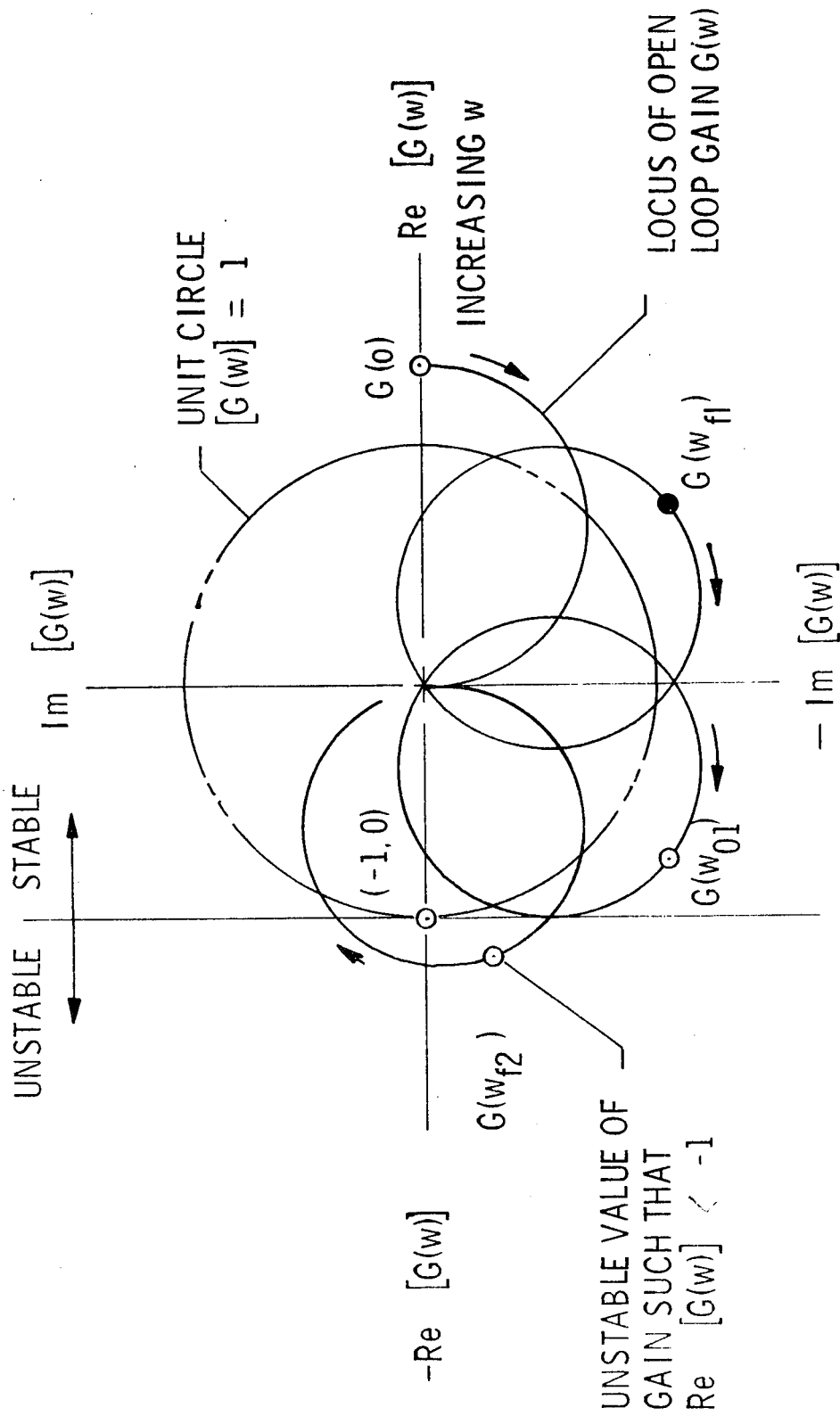


Figure 54



24 FEB 1972

FEED SYSTEM COUPLED STABILITY GAIN STABILIZING PRESSURE DROPS FOR LOX AND RP-1

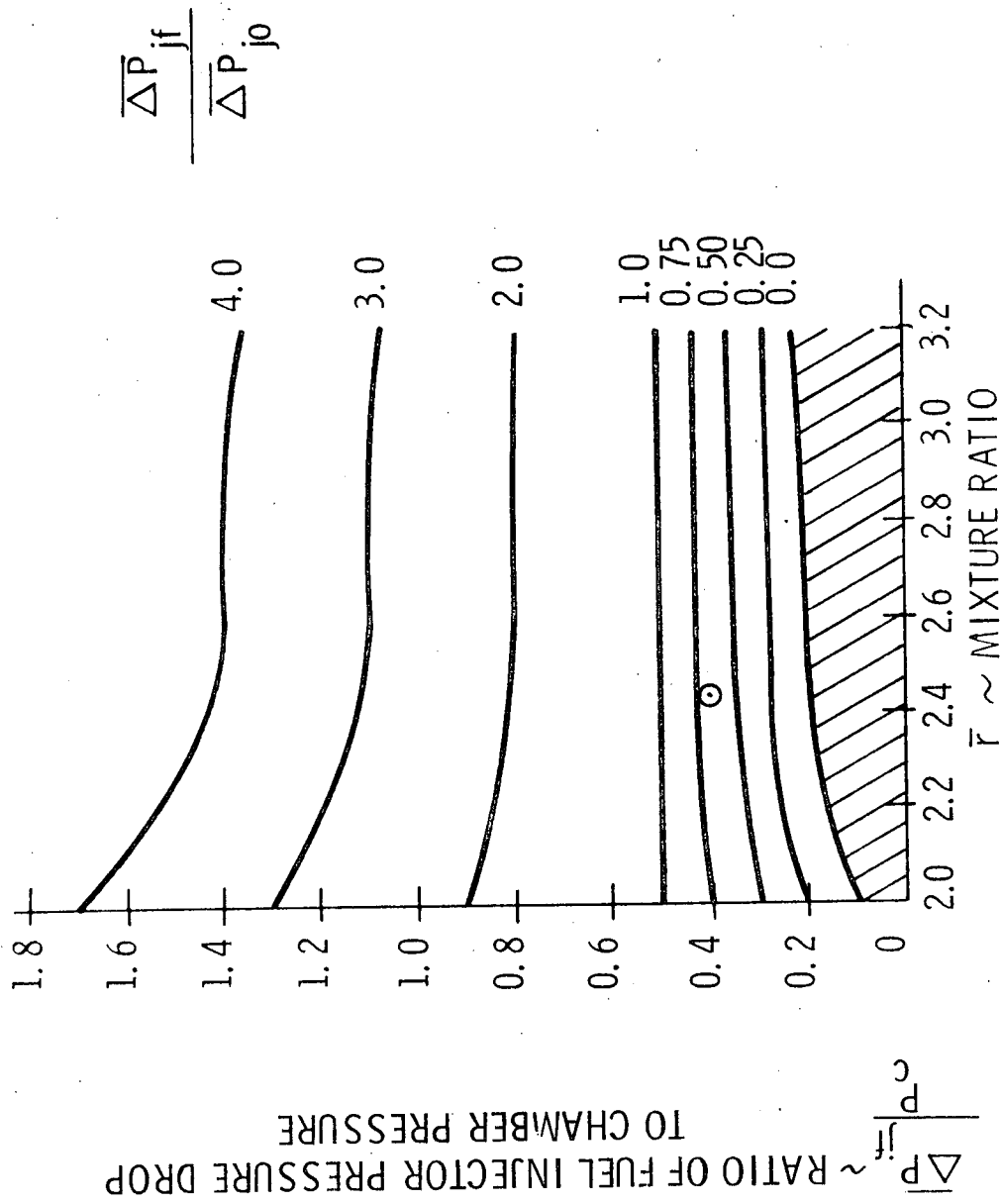


Figure 55



24 FEB 1972

EQUIVALENT CIRCUIT FOR ENGINE/FEED SYSTEM (NASA PRESSURE-FED BOOSTER ENGINE)

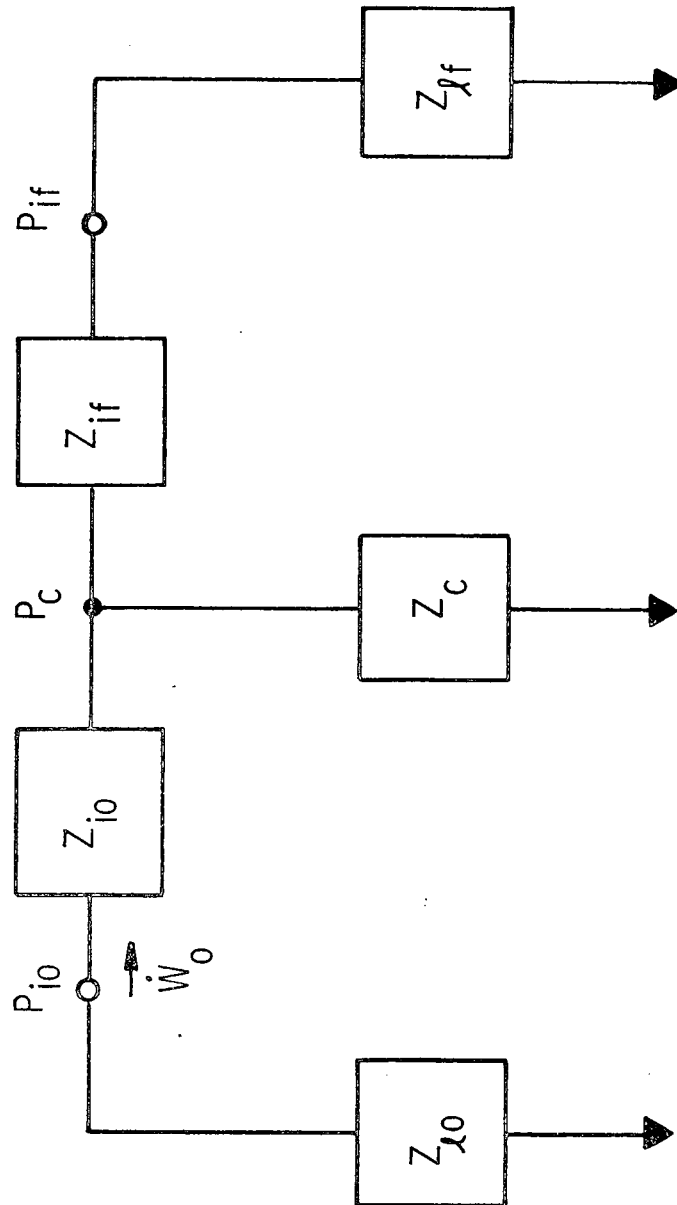


Figure 56



24 FEB 1972

RP-1 BURNOUT CHARACTERISTICS (NASA PRESSURE-FED BOOSTER ENGINE)

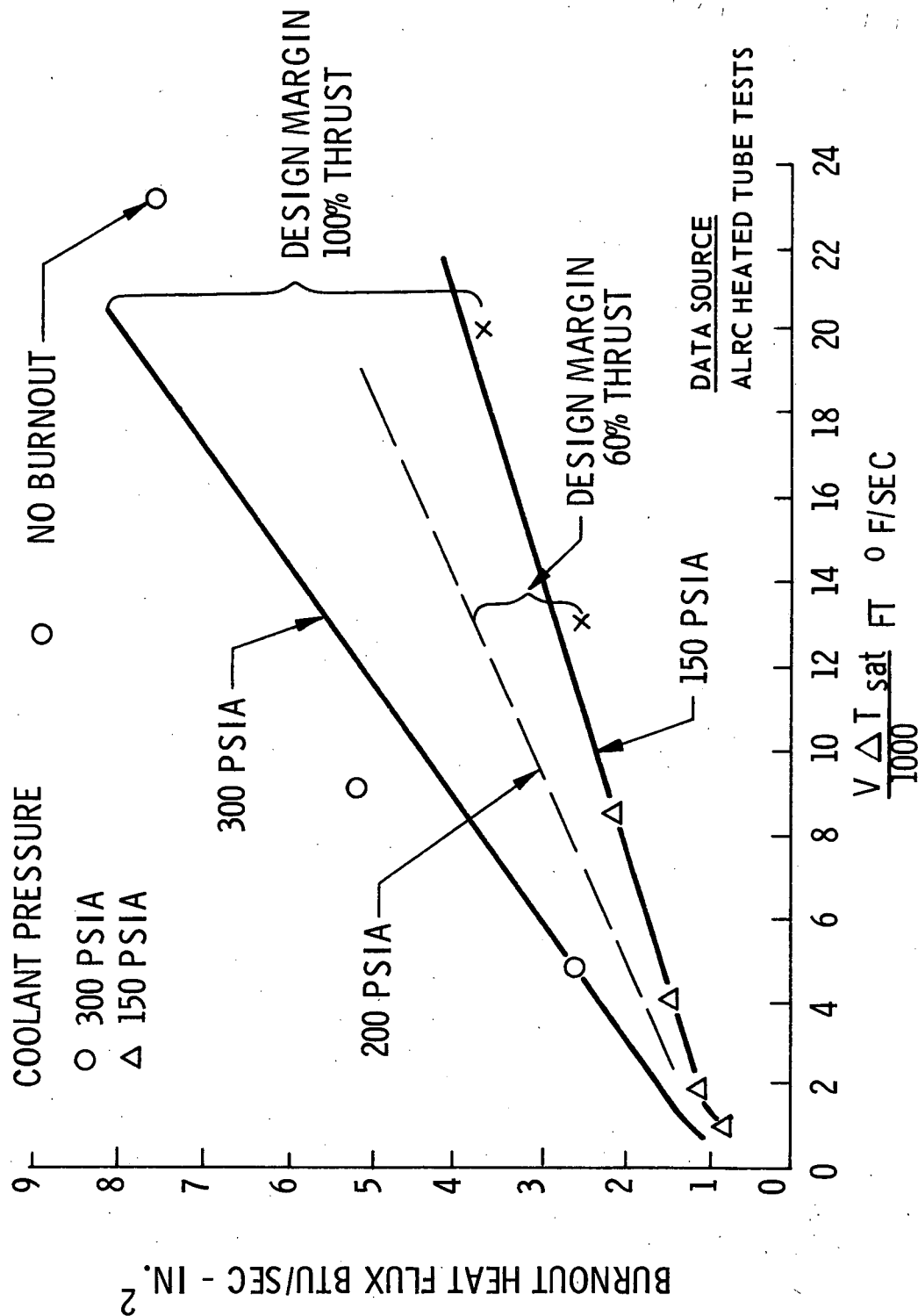


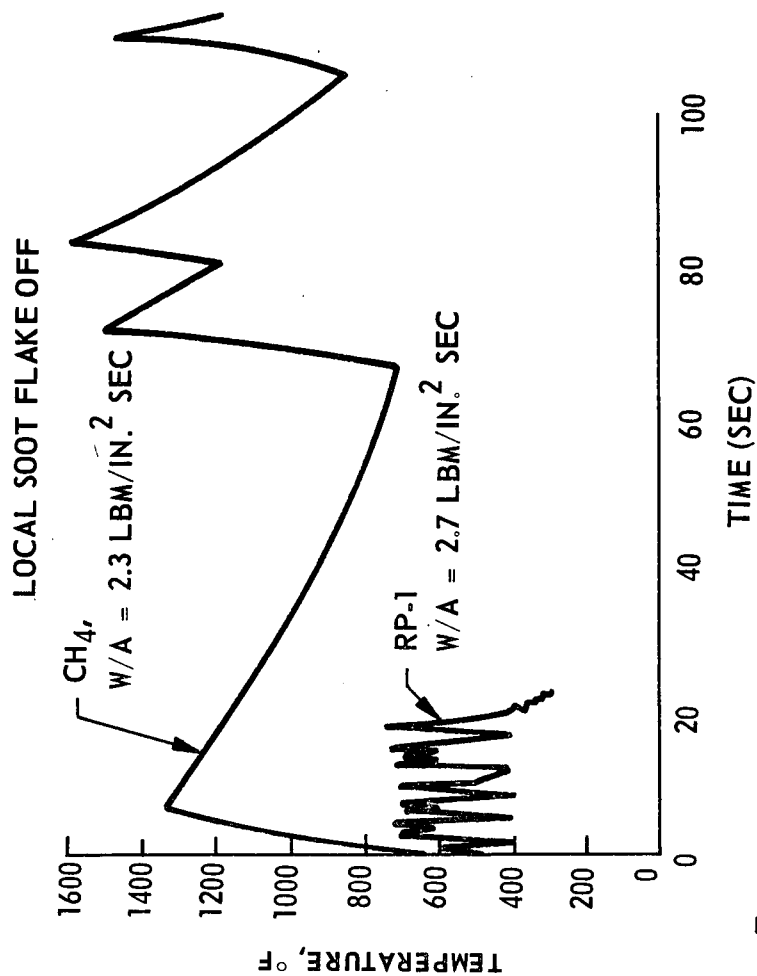
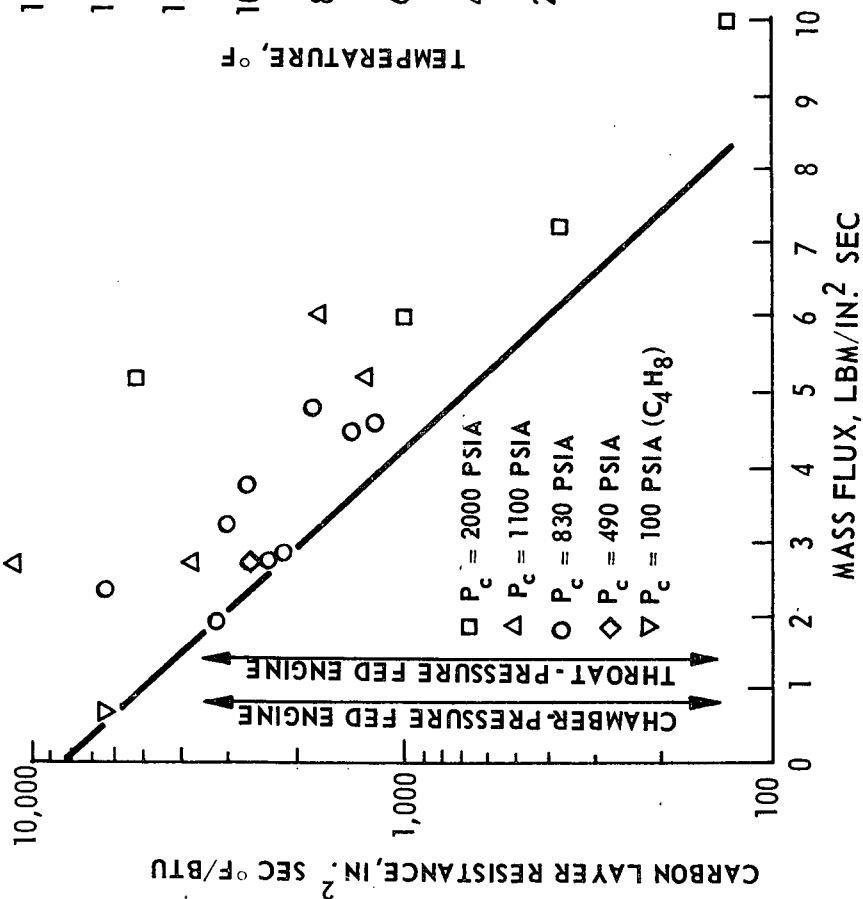
Figure 57



24 FEB 1972

SOOT CHARACTERISTICS

SOOT LAYER RESISTANCE - RP-1 COMBUSTORS



- Apparently insensitive to MR below $MR \approx 2.7$ with RP-1
- Initial buildup very rapid ($< 0.10 \text{ sec}$, Titan I)
- Coking inside tubes not significant for P.F.E. conditions (full regen.)



24 FEB 1972

Figure 58

RADIATION HEAT TRANSFER EFFECTS

THERMAL ENVIRONMENT $P_c = 250$ PSIA MR = 2.4

<u>CHAMBER (INJECTOR)</u>	<u>HEAT FLUX (BTU/IN.² SEC)</u>		
	<u>CLEAN WALL</u>	<u>SOOT</u>	<u>SOOT FLAKED OFF</u>
q conv	2.3	0.7	1.7
q rad	1.4	0.1	1.0
q total	3.7	0.8	2.7
<u>THROAT</u>			
q conv	3.5	1.0	3.0
q rad	1.0	0.0	0.5
q total	4.5	1.0	3.5

Clean Wall - Initial condition of new engine - normally will operate only momentarily (<1.0 sec) in this condition

Soot/Soot Flaked Off - Engine can be expected to oscillate between these two conditions as soot builds up and flakes off. Represents thermal cycling on tubes.



24 FEB 1972

Figure 59